Publications of the Astronomical Society of Australia (PASA), Vol. 31, e043, 36 pages (2014).

doi:10.1017/pasa.2014.38

The Dawes Review 3: The Atmospheres of Extrasolar Planets and Brown Dwarfs

Jeremy Bailey[1,2]

[1]School of Physics, University of New South Wales, NSW, 2052, Australia
[2]Email: j.bailey@unsw.edu.au

(Received January 10, 2014; Accepted September 20, 2014)

Abstract

The last few years has seen a dramatic increase in the number of exoplanets known and in the range of methods for characterising their atmospheric properties. At the same time, new discoveries of increasingly cooler brown dwarfs have pushed down their temperature range which now extends down to Y-dwarfs of <300 K. Modelling of these atmospheres has required the development of new techniques to deal with the molecular chemistry and clouds in these objects. The atmospheres of brown dwarfs are relatively well understood, but some problems remain, in particular the behavior of clouds at the L/T transition. Observational data for exoplanet atmosphere characterisation is largely limited to giant exoplanets that are hot because they are near to their star (hot Jupiters) or because they are young and still cooling. For these planets there is good evidence for the presence of CO and H_2O absorptions in the IR. Sodium absorption is observed in a number of objects. Reflected light measurements show that some giant exoplanets are very dark, indicating a cloud free atmosphere. However, there is also good evidence for clouds and haze in some other planets. It is also well established that some highly irradiated planets have inflated radii, though the mechanism for this inflation is not yet clear. Some other issues in the composition and structure of giant exoplanet atmospheres such as the occurrence of inverted temperature structures, the presence or absence of CO_2 and CH_4, and the occurrence of high C/O ratios are still the subject of investigation and debate.

Keywords: planets and satellites: atmospheres – brown dwarfs – planetary systems – techniques: spectroscopic

The Dawes Reviews are substantial reviews of topical areas in astronomy, published by authors of international standing at the invitation of the PASA Editorial Board. The reviews recognise William Dawes (1762–1836), second lieutenant in the Royal Marines and the astronomer on the First Fleet. Dawes was not only an accomplished astronomer, but spoke five languages, had a keen interest in botany, mineralogy, engineering, cartography and music, compiled the first Aboriginal-English dictionary, and was an outspoken opponent of slavery.

1 INTRODUCTION

It is appropriate to consider the properties of extrasolar planet and brown dwarf atmospheres together because they have many similarities. Planets and brown dwarfs cover similar temperature ranges and have similar radii. Planets extend up from very low temperatures (such as those of the ice giants Uranus and Neptune in our Solar system) to effective temperatures of ∼3 000 K in hot Jupiters, while new discoveries are continually pushing down the temperature of the coolest known brown dwarfs. The recently discovered Y dwarf class have temperatures as low as ∼300 K (Cushing et al. 2011).

The important processes that occur in these atmospheres are also similar as these are determined primarily by effective temperature. Molecules, chemistry and clouds are important in determining the opacities and hence structure of all these objects. At any temperature below about ∼2 000 K, solid and liquid condensates can start to form, resulting in considerable complications compared with higher temperatures where only gas phase processes need to be considered. More complex molecules such as methane (CH_4) become important and the excitation of high vibrational and rotational levels mean that vast numbers of spectral lines are needed to model the opacity. The modelling of these atmospheres thus presents new challenges compared with those encountered in conventional stellar atmosphere models, and these challenges are largely common to the modeling of both exoplanets and brown dwarfs. The differences between giant exoplanets and brown dwarfs include the generally lower mass (and hence gravity) in exoplanets, and the difference in environment. An exoplanet orbits a star, and the stellar illumination can have a

significant influence on its structure and properties, particularly for close in planets such as hot Jupiters. The presence of the host star also impacts on our ability to observe the planet. While some observations can be easier for planets than brown dwarfs (e.g. determining mass and radius), spectroscopy to characterise the atmospheres is usually extremely challenging for exoplanets while relatively straightforward for brown dwarfs.

The structure of this review will be to begin with looking at brown dwarf atmospheres. This reflects the fact that these are better observed and understood objects, without the complications that are introduced by the presence of the host star in exoplanet systems, but nevertheless illustrate many of the processes that are also important in giant exoplanets. Exoplanet atmospheres will be considered next, with a brief look at the giant planets in our own solar system as a guide. Observations relevant to atmospheric structure and composition are now being obtained by a number of methods primarily for giant exoplanets. These will be outlined and the results of these methods discussed.

The next section will look at the modelling of brown dwarf and exoplanet atmospheres. The techniques are very similar for both classes of objects. A final section will look at the possibilities of detecting extrasolar habitable planets and searching for signatures of life on such planets.

2 BROWN DWARFS

2.1 History and properties

The existence of brown dwarfs was predicted long before they were recognised observationally. Kumar (1963) and Hayashi & Nakano (1963) showed that there was a lower limit to the mass of a main-sequence star below which hydrogen burning could not occur. Kumar referred to the objects below this limit as 'black' dwarfs, but the name 'brown dwarf' proposed by Tarter (1975) is the one that has been adopted. More recent models set the hydrogen burning mass limit at 0.072–0.075 $M_\odot$ for a solar composition and somewhat higher for lower metallicities (Chabrier & Baraffe 1997; Burrows et al. 2001).

Because brown dwarfs do not have a continuing nuclear energy source, their evolution is a process of cooling and decreasing luminosity with age. Unlike stars on the main sequence whose properties are determined primarily by their mass, the temperature and luminosity of a brown dwarf are determined by both mass and age. This is illustrated in Figure 1 where the effective temperatures of low mass objects with masses between 0.0005 and 0.1 $M_\odot$ are plotted as a function of age. The evolutionary models used here are those of Baraffe et al. (2003) but similar general trends would be obtained with other recent models (e.g Chabrier et al. 2000a; Burrows et al. 2001; Baraffe et al. 2002; Saumon & Marley 2008).

The four tracks at the top of Figure 1 are for objects massive enough to be stars, so their effective temperature even-

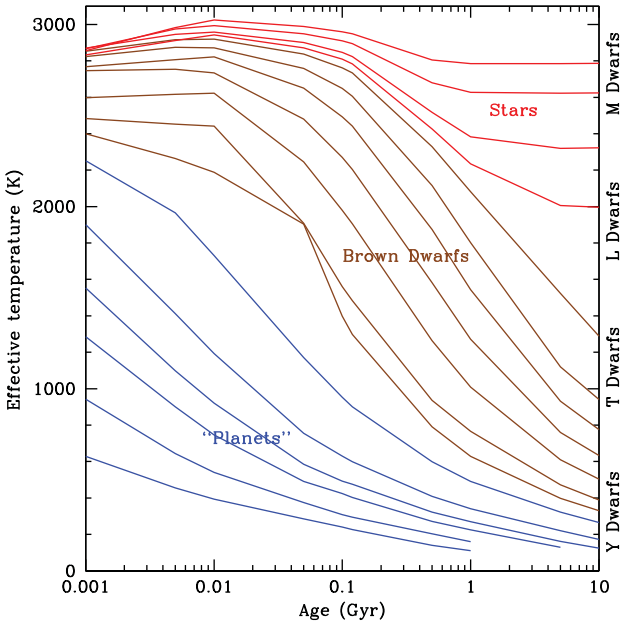

Figure 1. Evolution of effective temperature for objects from 0.0005 to 0.1 $M_\odot$ based on the models of Baraffe et al. (2003). The red tracks are for stars with masses above the hydrogen burning limit. The magenta tracks are for brown dwarfs, and the blue tracks are for objects below the deuterium burning limit (planets or sub brown dwarfs) The tracks plotted from top to bottom are masses of (Stars: 0.1, 0.09, 0.08, 0.075 $M_\odot$) (Brown Dwarfs: 0.07, 0.06, 0.05, 0.04, 0.03, 0.02, 0.015 $M_\odot$), (Planets: 0.01, 0.005, 0.003, 0.002, 0.001, 0.0005 $M_\odot$).

tually stabilises to a near constant value. However, for brown dwarfs the effective temperature continues to decrease with increasing age. It can be seen from this diagram that a determination of effective temperature alone is not sufficient to determine whether an object is a star or a brown dwarf. An object with $T_{eff} = 2\ 200$ K, for example, can be a young brown dwarf or an older star.

This age-mass degeneracy complicated the early observational search for brown dwarfs, and while several candidates were found (e.g. GD165b Becklin & Zuckerman 1988) it was not possible to confirm them as brown dwarfs. That changed in 1995 with the discovery of Gl 229b (Nakajima et al. 1995; Oppenheimer et al. 1995), an object sufficiently cool to be unambiguosly a brown dwarf, and with the use of the lithium test to confirm the brown dwarf nature of several objects in the Pleiades cluster (Rebolo, Zapatero-Osorio, & Martin 1995; Rebolo et al. 1996; Basri, Marcy, & Graham 1996). The lithium test (Rebolo, Martín, & Magazzu 1992) relies on the fact that lithium is destroyed by nuclear reactions down to masses just below the hydrogen burning limit. Since cool dwarfs are fully convective, lithium would be removed from the photosphere if these reactions occurred. Hence the presence of lithium in the spectrum can be used to confirm that an object is a brown dwarf.

The deuterium burning mass limit which is at about 13 M_J or 0.0125 $M_\odot$ (Saumon et al. 1996; Burrows et al. 1997; Chabrier et al. 2000b) is usually considered to be the lower mass limit for brown dwarfs. Objects below this mass limit

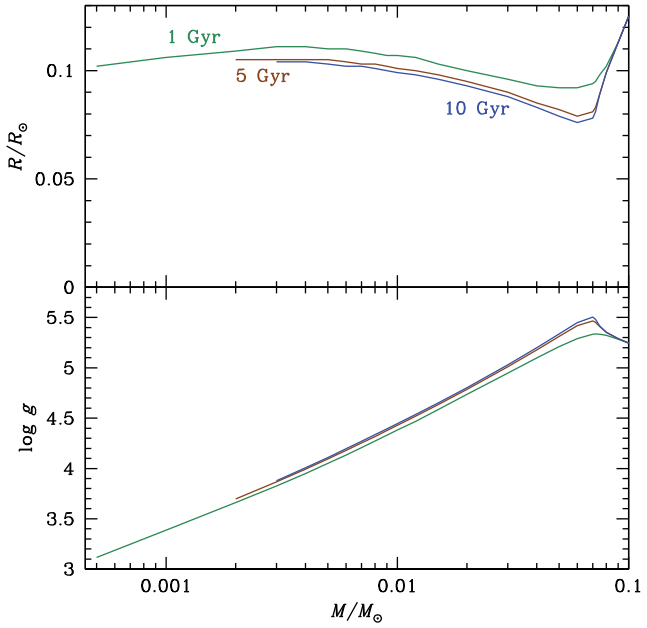

Figure 2. Radius and surface gravity (log g in cgs units) as function of mass for the models of Baraffe et al. (2003) at ages of 1 Gyr, 5 GYr and 10 Gyr.

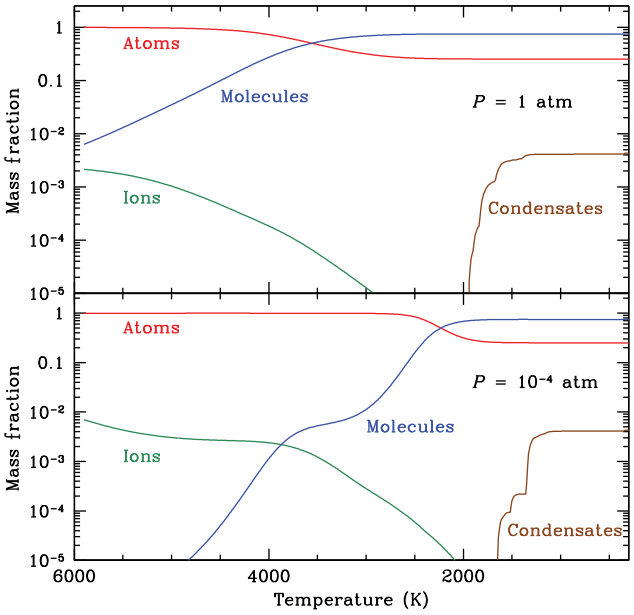

Figure 3. Equilibrium composition of a gas with solar elemental abundances as a function of temperature at two different pressures using the chemical model of Bailey & Kedziora-Chudczer (2012).

that orbit stars are generally agreed to be designated as planets. There is less consensus on how to refer to object below this mass limit that do not orbit a star. While these are sometimes referred to as 'free-floating planets' (Lucas & Roche 2000; Delorme et al. 2012) it has also been argued that such objects should not be referred to as planets but as 'sub-brown dwarfs' or some other designation (see Boss et al. 2003; Basri & Brown 2006, for a discussion of the issues involved in this controversy).

The electron degeneracy in the cores of brown dwarfs results in their radius varying little with mass as can be seen in Figure 2. All brown dwarfs (except at very young ages) have radii not far from 0.1 $R_\odot$ or about 1 Jupiter radius. A consequence of this is that surface gravity ($g = GM/R^2$) varies with mass from more than 1 000 m s^{-2} (log $g = 5$ in cgs units) to around 30 m s^{-2} for Jupiter mass objects as shown in the lower panel of Figure 2.

Brown dwarfs are objects whose atmospheric composition is dominated by molecular gas, as opposed to atoms and ions in the case of hotter stars. This is apparent from Figure 3 which shows the chemical equilibrium composition of a solar composition gas (using the abundances of Grevesse, Asplund & Sauval 2007). It shows the division of the material by mass fraction into ions, atoms, gas-phase molecules and solid or liquid condensates as calculated by the chemical model of Bailey & Kedziora-Chudczer (2012). It can be seen that molecules become dominant over atoms for temperatures below about 3 500 K. Helium and other noble gases persist as atoms at all temperatures, but other elements are mostly in the form of molecules. Below about 2 000 K condensed phases start to appear, and become a significant fraction of the material. At lower pressures, as shown in the lower panel, the pattern is similar but shifted to lower temperatures.

The number of ultracool dwarfs[1] has increased rapidly over the years since the recognition of the first brown dwarfs in 1995. Most of the objects have come from deep surveys such as the Sloan Digital Sky Survey (SDSS — Fan et al 2000; Hawley et al. 2002) and the Canada-France Brown Dwarfs Survey (CFBDS — Delorme et al. 2008a; Albert et al. 2011) and particularly from infrared surveys such as the Deep Near-Infrared Sky Survey (DENIS — Delfosse et al. 1997; Martín, Delfosse, & Guieu 2004), the 2 Micron All Sky Survey (2MASS — Kirkpatrick et al. 2000; Burgasser et al. 2002, 2004), and the UKIRT Infrared Deep Sky Survey (UKIDSS — Pinfield et al. 2008; Burningham et al. 2010, 2013).

The most recent additions have come from the Wide-field Infrared Survey Explorer (WISE — Wright et al. 2010). This Earth orbiting NASA mission surveyed the entire sky at four wavelengths (3.4, 4.6, 12 and 22 μm). The first of these wavelengths probes a deep CH_4 absorption band in brown dwarfs. WISE has proved effective in identifying the coolest brown dwarfs. It has led to the discovery of many T dwarfs (Kirkpatrick et al. 2011; Mace et al. 2013) and to the first Y dwarfs (Cushing et al. 2011; Kirkpatrick et al. 2012; Tinney et al. 2012).

Other recent discoveries from WISE are that of a binary brown dwarf (Luhman 2013) and an extremely cool brown dwarf (Luhman 2014) both at distances of around 2pc. WISE J104915.57−531906.1 (also known as Luhman 16) consists of an L7.5–L8 primary and T0.5–T1.5 secondary (Burgasser,

[1] Ultracool dwarf is a name normally used for objects with spectral type later than about M7, which could potentially be brown dwarfs, but could also be stars

Sheppard, & Luhman 2013; Kniazev et al. 2013). Its brightness and proximity are likely to make it an important object for future detailed studies. WISE J088510.83−071442.5 (Luhman 2014) appears to be the coldest brown dwarf known based on its absolute magnitude and colours. These two systems are the closest brown dwarf systems, and the third and fourth closest systems to the Earth (after the α Centauri system and Barnard's star).

2.2 Brown dwarf spectral sequence

The study of brown dwarfs has led to a significant extension of the traditional spectral sequence from O-M that was adopted more than 100 years ago (Cannon & Pickering 1901). Objects such as GD 165B and Gl 229B clearly had quite different spectra and were cooler objects than any M dwarfs. This was recognised by the adoption of the new spectral classes L and T. The motivation for this and the reasons for the choice of those letters are described by Kirkpatrick et al. (1999). The sequence has been further extended by the recent recognition of even cooler objects that have been assigned to the new spectral class Y (Cushing et al. 2011).

Figure 4 shows the main features of the spectral sequence from M9 to T7.5 with the main absorbing species indicated.

2.2.1 M dwarfs

The M spectral classification has been recognised from the early days of astronomical spectroscopy. While most M dwarfs are stars, young objects of late M spectral types can be brown dwarfs (as shown in Figure 1). The modern classification scheme for M-dwarfs is based on that of Boeshaar (1976) extended by Boeshaar & Tyson (1985) and Kirkpatrick, Henry & McCarthy (1991) to spectral type M9.5. The Kirkpatrick et al. (1991) spectral classification is based on the spectral region from 630–900 nm. The spectral standards chosen for late M types are listed in Table 1.

The M spectral class is characterised by the presence of bands of TiO and VO. TiO bands increase in strength up to spectral type M6, and VO becomes strong in the latest types.

In the near infrared (near-IR) M dwarfs show broad absorptions due to H_2O centred around 1.4 and 1.9 μm increasing in strength with later spectral types. Late M dwarfs also show Na I and K I absorptions in the 1.15–1.25 μm region. FeH absorption is present in the Wing-Ford band at 1 μm as well as the E-A band in the 1.6 μm region (Hargreaves et al. 2010). CO absorption is present at 2.3 μm.

2.2.2 L dwarfs

The L dwarf class is disinguished by the weakening and disappearance of the TiO and VO bands that are distinctive of M dwarfs. TiO has disappeared by L6 and VO by L4. A classification scheme for L dwarfs based on the optical spectral region (630–1000 nm) is described by Kirkpatrick et al. (1999). It lists spectral standards for classes L0 to L8 (see Table 1) and classification is based on the weakening TiO and VO bands, changes in CrH and FeH bands (CrH is strongest at L5) and the alkali metals, with Cs I and Rb I lines increasing in strength to later types.

Spectral classification of L dwarfs in the near-IR is discussed by Reid et al. (2001), Geballe et al. (2002) and Nakajima, Tsuji, & Yanagisawa (2004). Kirkpatrick et al. (2010) defined a set of spectral standards for the near-IR for spectral types M0 – L9. The near-IR region shows broad absorption bands of H_2O increasing in strength towards later spectral types.

While methane in the 1–2.5 μm region is not seen until spectral type T, the stronger methane ν_3 band in the 3.3 μm region is observable in late L dwarfs (Noll et al. 2000; Schweitzer et al. 2002; Stephens et al. 2009).

The physical basis for the M-L transition is thought to be the formation of condensates. At temperatures just below 2000 K the condensation of Ti bearing species such as $CaTiO_3$ (perskovite) and Ti_2O_3 removes TiO from the gas phase, and at slightly lower temperatures VO condenses as solid VO (Burrows & Sharp 1999; Lodders 2002). Species such as enstatite ($MgSiO_3$), forsterite (Mg_2SiO_4), spinel ($MgAl_2O_4$) and solid iron also condense and these produce the dust clouds that are necessary to explain the spectra and colours of L dwarfs (Allard et al. 2001; Marley et al. 2002; Tsuji 2002)

2.2.3 T dwarfs

The T dwarf class is characterised by the appearance of methane (CH_4) absorption features in the near-IR region (1–2.5 μm) . Methane first becomes apparent in early T dwarfs due to features at 1.67 and 2.2 μm which represent the Q-branches of the strongest methane bands $2\nu_3$ at 1.67 μm and $\nu_2 + \nu_3$ at 2.2 μm. This is accompanied by weakening of the CO absorption at 2.3 μm.

At later types broad methane absorptions develop due to the complex methane band systems, the octad (8 ground-state bands in the 2.1–2.4 μm region; Hilico et al. 2001) and the tetradecad (14 ground-state bands in the 1.6–2.0 μm region; Nikitin et al. 2013a). These ground-state bands are associated with large numbers of hot bands. Methane absorption is also present at around 1.4 μm (the icosad – 20 ground-state bands) and 1.15 μm (the triacontad – 30 ground-state bands). Bailey, Ahlsved, & Meadows (2011) provides a more detailed description of the methane spectrum.

In late T dwarfs the broad CH_4 and H_2O absorptions deepen and combine to leave a spectrum defined by approximately triangular peaks at 1.08 μm, 1.27 μm and 1.58 μ (the 'windows' between the deep absorptions), as well as a weaker peak at about 2.1 μm. T dwarf spectra are also shaped by the collision-induced absorption due to $H_2 - H_2$ pairs (Borysow 2002; Abel et al. 2011) which depresses the 2 μm peak, and by the far wings of very strong Na I and K I lines in the optical (Burrows & Volobuyev 2003; Allard et al. 2003) which absorb at wavelengths up to $\sim$1 μm.

Classification schemes for T dwarfs based on near-IR spectra, were developed by Burgasser et al. (2002) and Geballe

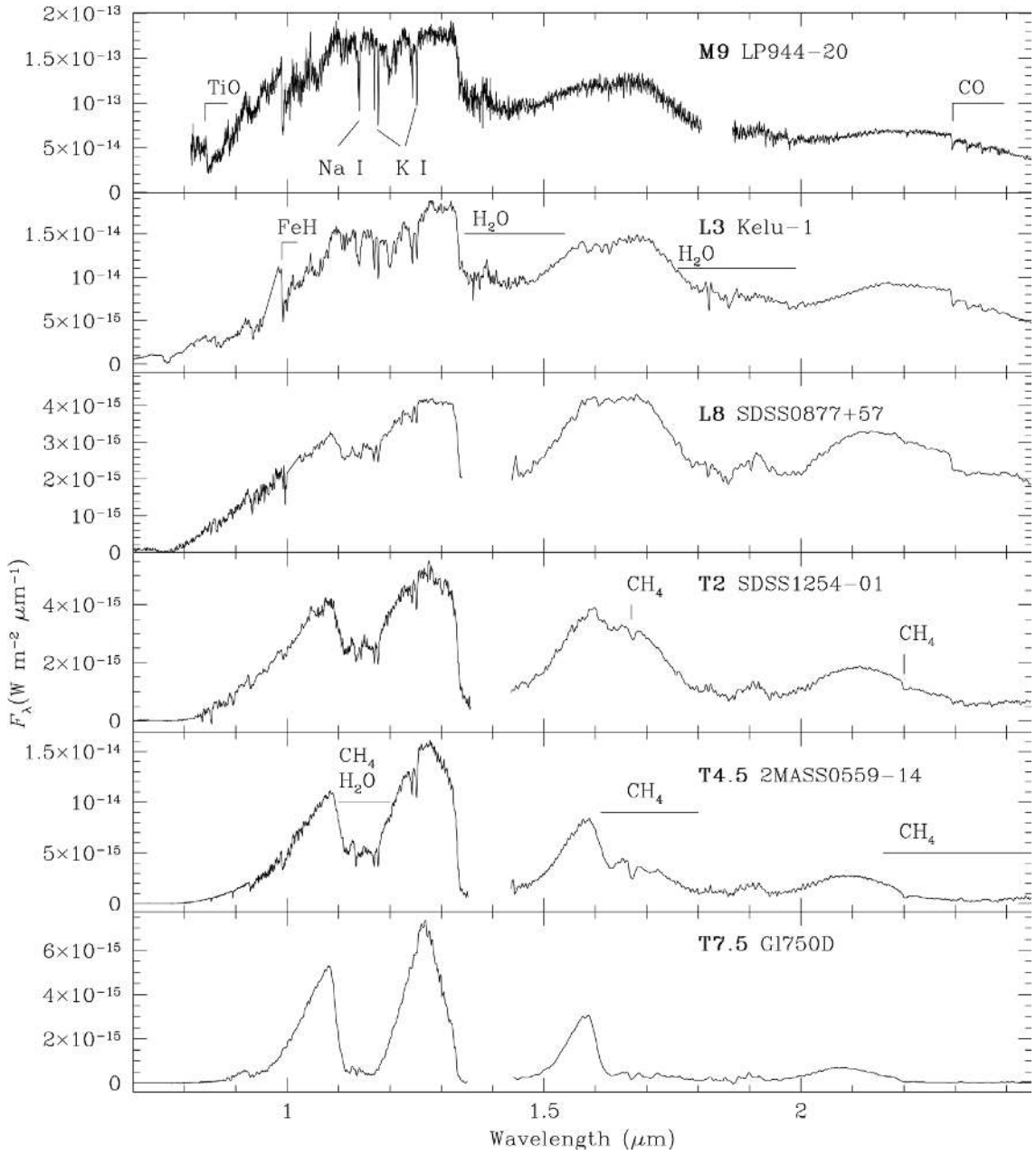

Figure 4. Spectra of ultracool dwarfs from M9 to T7.5. The species responsible for the main absorption features are indicated. Spectral data is from Burgasser et al. (2003), Cushing, Rayner, & Vacca (2005), Geballe et al. (2001), Geballe et al. (2002), Leggett et al. (2000), Leggett et al. (2001), Leggett et al. (2002), Rayner, Cushing, & Vacca (2009), Ruiz, Leggett, & Allard (1997)

et al. (2002) and the two schemes were unified in Burgasser et al. (2006a). That work gives a set of spectral standards for T0–T8 (see Table 1). The main features used for classification are the increasing depths of the H_2O and CH_4 bands towards later classes. A parallel optical classification scheme based on the 630–1010 nm region is described by Burgasser et al. (2003) and is based on some of the same spectral standards used in the near-IR.

The transition from L to T is associated with the switch in chemical equlibirum between CO and CH_4 (Lodders 2002; Burrows & Sharp 1999) that occurs at about 1400 K at 1 bar pressure, with CO being more stable above this temperature, and CH_4 being favoured at lower temperatures. However, the transition is also associated with a clearing of the dust clouds that are important in L dwarfs (Allard et al. 2001; Burgasser et al. 2002).

2.2.4 Y dwarfs

The possible existence of objects even cooler than the T dwarfs was investigated in models by Burrows, Sudarsky, & Lunine (2003). Among the features suggested as marking the transition to a new spectral class, were the appearance

Table 1. Mean properties and spectral standards for late M to Y dwarfs

	T_{eff}	M_J	M_H	M_K	Spectral standard	Refs
M7	2 633	10.31	9.94	9.50	2MASS J16 553 529−0 823 401 (Gl 644C, vB8)	1, 7
M8	2 520	10.99	10.40	9.88	2MASS J19 165 762+0 509 021 (Gl 752B, vB10)	1, 7
M9	2 465	11.80	11.15	10.62	2MASS J14 284 323+3 310 391 (LHS 2924)	1, 7
L0	2 438	11.69	11.04	10.46	2MASS J03 454 316+2 540 233	2, 7
L1	2 329	11.87	11.26	10.66	2MASS J07 464 256+2 000 321	2, 7
L2		12.18	11.45	10.82	2MASS J13 054 019−2 541 059 (Kelu-1)	2, 7
L3	1 948	12.81	11.97	11.26	2MASS J1 1463 449+2 230 527	2, 7
L4	1 801	12.83	12.14	11.25	2MASS J11 550 087+2 307 058	2, 7
L5	1 686	13.44	12.61	11.96	2MASS J12 281 523−1 547 342	2, 7
L6	1 501	14.12	13.05	12.00	2MASS J08 503 593+1 057 156	2, 7
L7	1 446	14.67	13.70	12.89	2MASS J02 059 240−1 159 296	2, 7
L8	1 445	14.68	13.77	13.05	2MASS J16 322 911−1 904 407	2, 7
L9		14.33	13.48	12.73	2MASS J02 550 327−4 700 509	3, 7
T0	1 370	14.24	13.52	13.17	SDSS J120 747.17+024 424.8	4, 7
T1		14.37	13.81	13.62	SDSS J083 717.21−000 018.0	4, 7
T2	1 328	14.43	13.88	13.58	SDSS J125 453.90−012 247.4	4, 7
T3					2MASS J12 095 613−1004 008	4, 7
T4	1 251	15.04	14.41	14.13	2MASS J22 541 892+3 123 498	4, 7
T5	1 185	14.43	14.66	14.81	2MASS J15 031 961+2 525 196	4, 7
T6	1 001	15.22	15.56	15.77	SDSS J1642 414.37+002 915.6	4, 7
T7	820	15.54	15.97	16.01	2MASS J07 271 824+1 710 012	4, 7
T8	638	16.43	16.82	16.93	2MASS J04 151 954−0 935 066	4, 8
T9	565	18.39	18.77	18.89	UGPS J072 227.51−054 031.2	5, 8
Y0	371	20.09	20.60	20.70	WISE J173 835.52+273 258.9	5, 8
Y1					WISE J035 000.32−565 830.2	6

References. First reference is to adoption of the spectral standard, and the second reference is to the source of the mean absolute magitudes.
1. Kirkpatrick et al. (1991), 2. Kirkpatrick et al. (1999), 3. Kirkpatrick et al. (2010) 4. Burgasser et al. (2006a), 5. Cushing et al. (2011), 6. Kirkpatrick et al. (2012), 7. Dupuy & Liu (2012), 8. Dupuy & Kraus (2013)
Notes.
Mean effective temperatures are from the data of Figure 6. Spectral standards are those adopted for optical classification up to spectral class L8, and for near-IR classification for L9 and later. Near-IR spectral standards for earlier types can be found in Kirkpatrick et al. (2010). Spectral data is available for download for most of these objects (and other late-type dwarfs) at:
SpeX Prism Spectral Libraries (A. Burgasser)
— http://pono.ucsd.edu/~adam/browndwarfs/spexprism/
IRTF Spectral library (M.R. Cushing)
— http://irtfweb.ifa.hawaii.edu/~spex/IRTF_Spectral_Library/
L and T dwarf data archive (S.K. Leggett)
— http://staff.gemini.edu/~sleggett/LTdata.html
NIRSPEC Brown Dwarf Spectroscopic Survey (I.S. McLean)
— http://www.astro.ucla.edu/~mclean/BDSSarchive
Keck LRIS specra of late-M, L and T dwarfs (I.N. Reid)
— http://www.stsci.edu/~inr/ultracool.html

of NH_3 absorption, the condensation of H_2O clouds, and the development of redder near-IR colours reversing the trend in T dwarfs. A number of of very cool dwarfs were found in the CFBDS and UKIDSS surveys (Warren et al. 2007; Delorme et al. 2008b; Burningham et al. 2008). Lucas et al. (2010) reported the discovery of an even cooler object UGPS 0722−05 which they suggested should be classified as T10, and could in the future be regarded as the first example of a new spectral type.

In 2011, Cushing et al. (2011) reported the 'Discovery of Y-dwarfs'. Several objects identified using the WISE satellite were found to be of later spectral types than UGPS 0722−05. They reclassified UGPS 0722−05 as the T9 spectral standard, and classified six new objects as Y dwarfs with WISE 1738+27 as the Y0 standard. Kirkpatrick et al. (2012) report several more Y dwarfs and added a spectral standard for the Y1 class (see Table 1). Other reported Y dwarfs are WISE J1639−68 (Tinney et al. 2012) and the white dwarf companion WD 0806−661 B (Luhman, Burgasser, & Bochanski 2011; Luhman et al. 2012). The high proper motion object WISE J085 510.83−071 442.5 (Luhman 2014) has absolute magnitude and colours suggesting it is the coolest known Y dwarf with an effective temperature of 225 – 260 K.

All Y dwarfs are very faint objects (J mag of 19 or fainter) and so the quality of available spectra are limited. They resemble the late T dwarfs, but the 'window' features (particularly that at 1.27 μm) become increasingly narrow with later spectral types. The NH_3 absorptions expected at ∼1.53 and ∼1.03 μm are not seen at

the levels predicted by equilibrium chemistry (Leggett et al. 2013).

2.3 Photometry

Photometric data on ultracool dwarfs in the near-IR is available for a large number of objects. The database of L, T and Y dwarfs at DwarfArchives.org, for example, lists 1 281 objects most of which have JHK magnitudes. When interpreting photometric data at JHK it is important to note that there are several different JHK systems in use. In particular the 2MASS (Carpenter 2001) and MKO (Simons & Tokunaga 2002) systems are both widely used in brown dwarf research. The 2MASS system uses a significantly shorter wavelength and narrower K_s band compared to the K band of the MKO system. Transformations between the systems derived from data on stars (Carpenter 2001) are unlikely to be valid for the unusual energy distributions seen particularly in the T dwarfs. Stephens & Leggett (2004) provide a set of transformations between photometric systems specifically for L and T dwarfs that can be used if the spectral type is known.

Much of the energy in ultracool dwarfs is in the mid infrared, and photometry for these wavelengths has become increasingly available from Spitzer/IRAC (Patten et al. 2006; Leggett et al. 2007, 2010) and the WISE all sky catalog (Wright et al. 2010).

These objects are relatively nearby and so parallax measurements of good quality are generally feasible allowing absolute magnitudes to be derived. Conventional CCD parallax methods can be used for the earlier type objects (e.g. Dahn et al. 2002; Vrba et al. 2004; Andrei et al. 2011). Infrared parallaxes can be measured for the latest type objects (Tinney, Burgasser, & Kirkpatrick 2003; Dupuy & Liu 2012; Marsh et al. 2013). The recent compilation by Dupuy & Liu (2012) includes absolute magnitudes in the near and mid infrared for 314 objects with known parallaxes. Mean absolute magnitudes from this compilation in the MKO JHK systems are given in Table 1 supplemented by those of Dupuy & Kraus (2013) for the latest spectral types.

Figure 5 shows the J−K against M_K colour magnitude diagram for M to Y dwarfs. A distinctive feature of the diagram is the behaviour at the L/T transition. Generally the J−K colour becomes slowly redder with later spectral types through M and L, but then rapidly turn bluer through the early T spectral types. The limited photometry available for Y dwarfs suggests a turn back to redder colours.

In the J band a significant brightening with later spectral type can be seen (Dahn et al. 2002; Tinney, Burgasser, & Kirkpatrick 2003). In the mean data of Table 1 it can be seen that types L9 to T2 are all brighter at J than L6 and L7. Tsuji & Nakajima (2003) suggested that this may be an artifact of observing objects with different masses and ages, and not a feature seen in a single cooling track. Studies of binary brown dwarfs whose components straddle the L/T boundary, however, show 'flux reversals' where the cooler component is brighter in the 1 – 1.3 μm region (Burgasser et al. 2006b; Liu et al. 2006; Looper et al. 2008) showing that the effect is a real intrinsic features of the L/T transition.

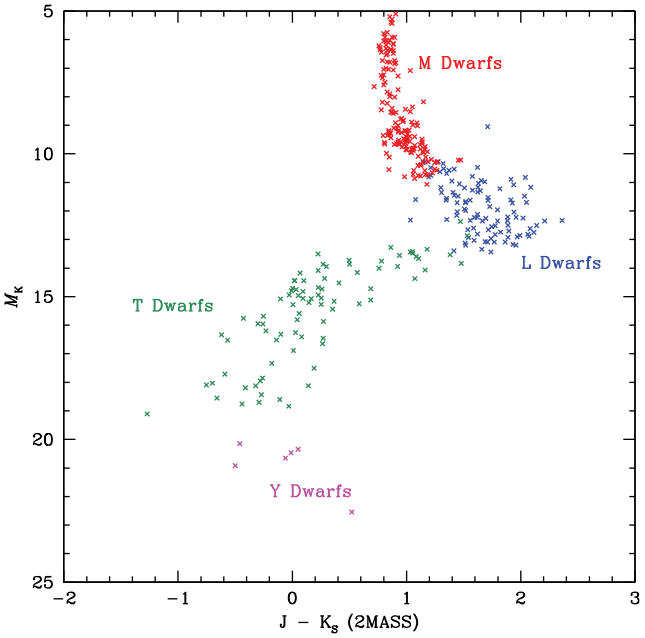

Figure 5. Colour magnitude diagram (J−K against M_K) for late type dwarfs. Most of the data is taken from Dupuy & Liu (2012). Data on late T and Y dwarfs is from Dupuy & Kraus (2013) and has been roughly converted to the 2MASS system according to Stephens & Leggett (2004). Additional data on earlier type M dwarfs has been added from the compilation of Reid (http://www.stsci.edu/~lnr/cmd.html) based on photometry from Leggett (1992) and converted to the 2MASS system using relations in Carpenter (2001).

2.4 Effective temperatures

The effective temperature of ultracool dwarfs can be determined by two main methods. The first way is to use photometry and parallax measurements to determine the bolometric luminosity. A temperature can then be derived if the radius is known. We don't have direct radius measurements for most of these objects, but as shown in Figure 2, models predict that the radius of brown dwarfs varies little with mass and age, so model based radius constraints can be used to determine effective temperature.

The other way to determine effective temperatures is to fit observed spectra to those predicted by model atmospheres. This is likely to be most reliable if the observations cover a large wavelength range that includes a substantial fraction of the luminosity, and for brown dwarfs this means including the mid-IR as well as the near-IR (e.g. Stephens et al. 2009).

Figure 6 is a compilation of effective temperature measurements from the literature using both of these methods. It shows reasonable agreement betwee the various determinations. A feature of this diagram is that, while the general trend is decreasing temperature with later spectral type, the

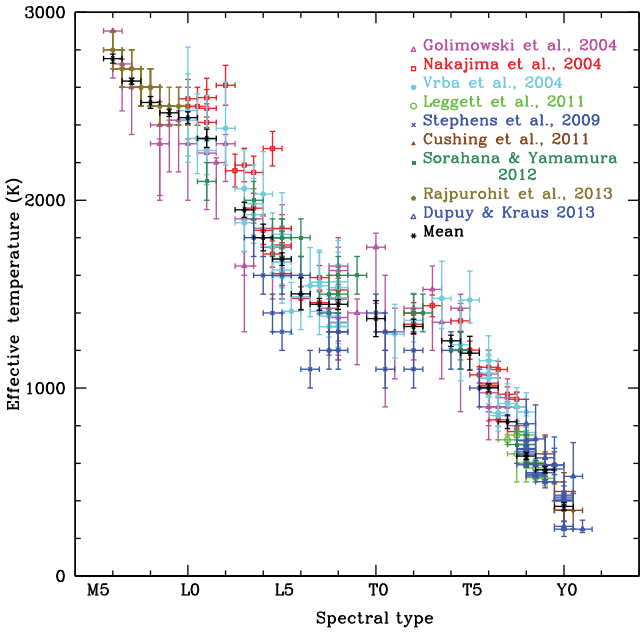

Figure 6. Effective temperatures plotted against spectral type. The effective temperatures are determined from bolometric luminosities (Vrba et al. 2004; Golimowski et al. 2004; Nakajima, Tsuji, & Yanagisawa 2004; Dupuy & Kraus 2013) or from fitting models to observed spectra (Stephens et al. 2009; Leggett et al. 2011; Cushing et al. 2011; Sorahana & Yamamura 2012; Rajpurohit et al. 2013). Optical spectral types are used up to L8, and infrared spectral types for L9 and later. Late T and Y dwarf spectral types are from Kirkpatrick et al. (2012). Spectral types are shown with error bars of ±0.5 subtypes. Mean values are given for spectral types that had more than 3 measurements. Where no error estimate was given in the original publication an error bar of ±100 K has been shown.

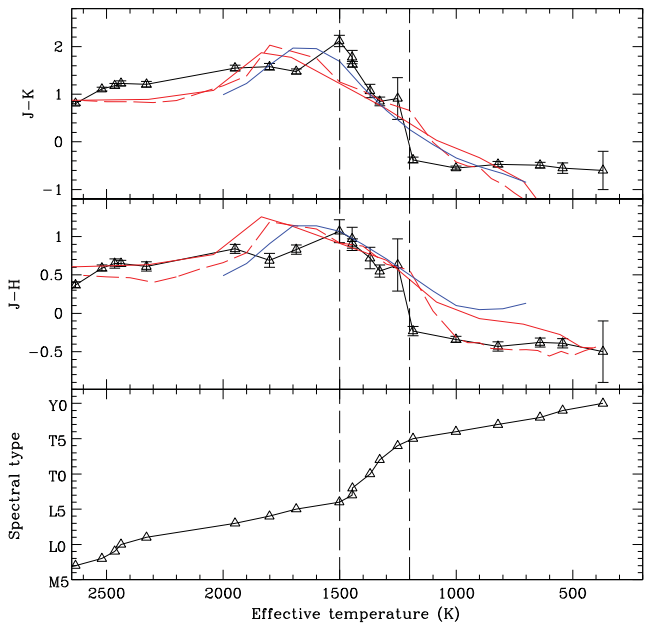

Figure 7. The L/T Transition. Over the small range of effective temperature from 1200–1500 K the observed colours and spectral types of ultracool dwarfs (black) vary through a large range. Models (red and blue lines, see section 4.4) show much more gradual changes. The data for this plot are that of Table 1. Model results are from the BT-Settl models (Allard et al. 2007, 2012) for $\log g = 5$ (solid red line) and for a 3 Gyr isochrone (red dashed line), and the Unified Cloudy Model (Tsuji 2002, 2005) for $\log g = 5$ and $T_{cr} = 1800$ K (blue line).

temperature actually changes little over the L/T transition from about L6 to T4. This suggests that the spectral changes seen over this range are due to the clearing of dust rather than to the direct effect of changing temperatures.

The mean effective temperatures for each spectral type from the data of Figure 6 have been included in Table 1.

The L/T transition shows up particularly clearly when the near-IR colours and spectral types are plotted against effective temperature using the mean values given in Table 1. The J−K and J−H colours and the spectral type all vary dramatically over the effective temperature range from 1200–1500 K, and show much less variability at other temperatures as shown in Figure 7. The changes are thought to be mostly due to the disappearance of dust clouds as the atmospheres cool, but it is not clear why this should appear as such a sharp transition. Cloud models (to be described in Section 4.4 — the red and blue lines) show much more gradual changes than those observed.

2.5 Variability

Variability has been reported in a number of L dwarfs (Clarke, Tinney, & Covey 2002; Koen 2006; Lane et al. 2007; Heinze et al. 2013). The amplitudes are typically ∼1% and the variations are quasi-periodic with periods of a few hours. The variability is generally attributed to rotational modulation either due to patchy clouds, or magnetic spots.

Two early T dwarfs have been observed to show larger amplitude variability (Artigau et al. 2009; Radigan et al. 2012). In the case of the T2.5 dwarf 2MASS 2139+02 an amplitude of up to 26% was observed with a period of 7.72 hours. The large amplitude in these early T objects is suggested to be indicative of patchy cloud regions arising during the clearing of clouds associated with the L/T transition as suggested by Marley, Saumon, & Goldblatt (2010). A further example reported recently (Gillon et al. 2013) is variability in the cooler component of the 2 pc binary brown dwarf WISE J1049−53 (Luhman 16).

Buenzli et al. (2012) have reported Spitzer and HST observations of variability with a 1.4 hr period in the T6.5 dwarf 2MASS 2228−43, confirming a ground-based detection of this period by Clarke et al. (2008). They find phase shifts between variations at different wavelengths which can provide a probe of the vertical atmospheric structure.

Recently Crossfield et al. (2014) have used time resolved near-infrared spectroscopy around the rotation period to derive a global 2D map of the brightness distribution of Luhman 16B using Doppler imaging techniques. The map reveals structure that may be due to patchy clouds.

3 EXOPLANETS

3.1 History and properties

Since the discovery of the first planets orbiting normal stars (Mayor & Queloz 1995; Marcy et al. 1997) the rate of discovery has steadily increased to more than 1 800 confirmed planets according to The Extrasolar Planets Encyclopedia (exoplanet.eu — Schneider et al 2011) as at July 2014. In addition more than 3 000 planet candidates have now been found by the Kepler mission (Batalha et al. 2013). The latter are not yet confirmed planets, but it is estimated that the false positive rate for Kepler planet candidates is likely to be ∼10% (Morton & Johnson 2011; Fressin et al. 2013).

While there are a large number of planets, observations of their atmospheres are much more difficult than for the brown dwarfs just considered. The vast majority of planet detections and observations are by indirect methods, such as radial velocity measurements of the host star, and transit measurements. These provide information on the orbit, mass and radius (for transitting planets). However, apart from a small number of directly imaged planets, we don't yet have the capability to resolve planets from their stars in order to measure their spectra. At present most of our data on the spectra of exoplanets comes from analysis of unresolved planets that require extracting signals that are a small fraction of that from the host star.

A recent review of exoplanet detection methods is given by Wright & Gaudi (2013). All methods currently used are subject to biases. The radial velocity (RV) technique that has been used for the majority of exoplanet discoveries favours the detection of massive planets and short period orbits. The majority of RV detected planets are therefore giant planets, but at short periods this method can detect planets down to a few Earth masses. When corrections are made for incompleteness the statistics show that planet frequency increases for decreasing mass (Howard et al. 2010; Wittenmyer et al. 2011). This is consistent with the increasing planet frequency at small sizes shown by analysis of the Kepler planet candidates (Howard et al. 2012). Ground-based transit searches (e.g. Bakos et al. 2004; Pollacco et al. 2006) are strongly biased toward finding large short period planets (i.e. hot Jupiters).

Our current ability to characterise exoplanet atmospheres is largely limited limited to giant planets and to planets with high temperatures (T > ∼1 000 K). In most cases these are hot Jupiters, i.e. massive planets that are hot because they are close to their star, or are directly imaged massive planets that are hot because they are young planets still cooling. There are a few cases of lower mass planets, for example Neptune/Uranus mass planets such as GJ 3470b and GJ 436b and two examples of transiting super-Earths, GJ 1214b (Charbonneau et al. 2009) and HD 97658b for which characterisation observations have been made.

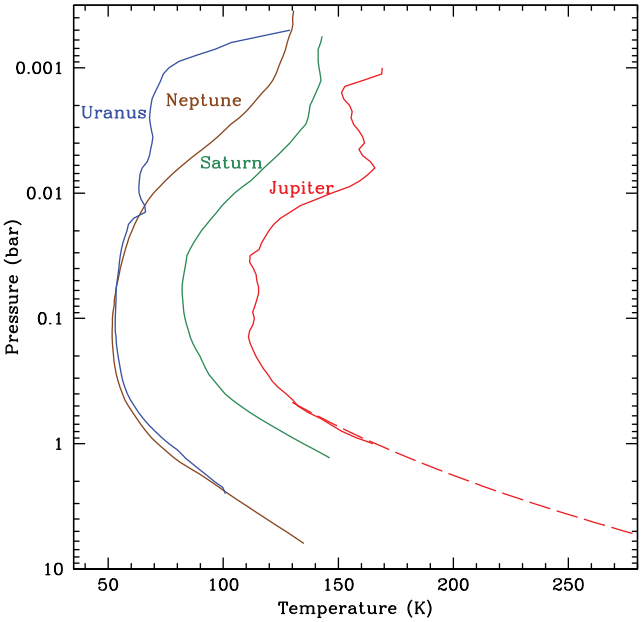

Figure 8. Temperature profiles of the Solar system giant planet atmospheres from Voyager radio occultation measurements (Lindal 1992), and from the Galileo probe for Jupiter (dashed line – Seiff et al. 1998).

3.2 Solar system giant planets

We do, however, know of several giant planets that have been studied in considerable detail, the giant planets in our own Solar system. It is useful to briefly review their properties. All the giant planets have atmospheres composed of hydrogen and helium and are enriched in heavy elements with respect to the solar composition. In the case of Jupiter measurements with the Galileo probe show C, N, S, Ar, Kr, and Xe enriched by factors of 2 to 4 relative to solar abundances (Owen et al. 1999; Wong et al. 2004). Carbon is enriched relative to its solar value by 7 times in Saturn (Flasar et al. 2005) and by 30–40 times in Uranus and Neptune (Lodders & Fegley 1994).

All the Solar system giant planet atmospheres have directly measured temperature structures from radio occultation measurements (Lindal 1992), and from the Galileo probe (Seiff et al. 1998) in the case of Jupiter (see Figure 8). All the planets have clouds with the main cloud deck at about 0.75 bar in Jupiter (Banfield et al. 1998; Kedziora-Chudczer & Bailey 2011), 2.5 bar in Saturn (Fletcher et al. 2011) and ∼2 bar in Uranus and Neptune (Irwin, Teanby, & Davis 2010).

Near-IR spectra of the giant planets are shown in Figure 9. All of these are dominated by absorption band systems due to methane (CH_4) centred around 1.15, 1.4, 1.7 and 2.3 μm, and are bright in the window regions between these absorptions. In this respect the spectra resemble those of late T dwarfs, and the T9 dwarf UGPS 0722-05 is shown in Figure 9 for comparison. Jupiter also show absorption due to NH_3 at around 1.55 μm. All the planets also show collision induced absorption due to H_2 – H_2 pairs, which at these low temperatures shows up as a distinctive broad feature at around 2.12 μm.

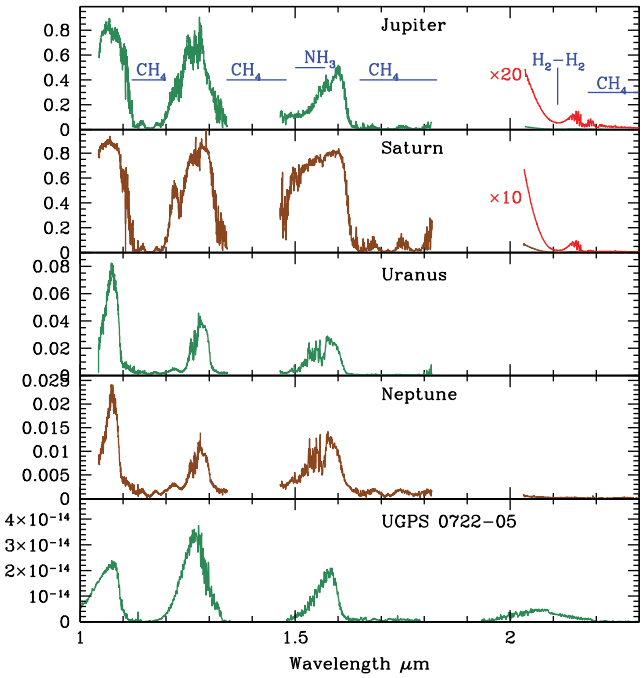

Figure 9. Near-IR reflected light spectra of the Solar system giant planets Jupiter, Saturn, Uranus and Neptune (plotted as radiance factor I/F). The data are from IRIS2 on the Anglo-Australian Telescope as described by Kedziora-Chudczer & Bailey (2011). The red curves show the weak K-band spectra of Jupiter and Saturn scaled up by factors of 10 and 20. The spectrum of the T9 dwarf UGPS 0722-05 is shown for comparison using data from Bochanski et al. (2011).

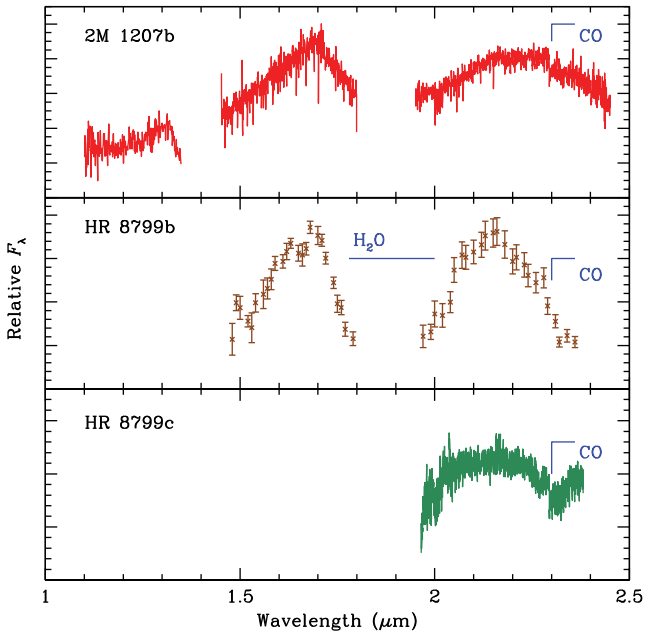

Figure 10. Spectra of the direct imaged planets (or planetary mass objects) 2M 1207b (Patience et al. 2010), HR 8799b (Barman et al. 2011a) and HR 8799c (Konopacky et al. 2013). The CO bandhead at 2.3 μm is apparent in all three objects as well as H_2O absorption at ∼1.9 and ∼1.4 μm.

This depresses the brightness in the methane window that would otherwise be present at around 2 μm, and makes all the planets quite faint in the K-band compared with the J and H bands.

Other species present in the atmospheres at trace levels and detected in longer wavelength spectra include PH_3 and AsH_3 in Jupiter and Saturn (Fletcher et al. 2011), and hydrocarbons such as C_2H_2 and C_2H_6 in the stratospheres (Hesman et al. 2009; Greathouse et al. 2011).

3.3 Observing exoplanet atmospheres

3.3.1 Direct spectroscopy of resolved planets

A number of 'planets' have been discovered through direct imaging of young objects using ground-based adaptive optics or the Hubble Space Telescope. These include the companion of the brown dwarf 2MASSW J1207 334−393 254 (usually referred to as 2M 1207b — Chauvin et al. 2005), and the four planets of HR 8799 (Marois et al. 2008, 2010).

The classification of some of these objects as planets is controversial. Although 2M 1207b was announced as the first directly imaged extrasolar planet by its discoverers, it can be argued that it is not a planet because it orbits a brown dwarf, not a star, or because it is unlikely that it formed through the normally understood planet formation process from a disk around its primary object (Soter 2006). 2M 1207b is usually referred to as a 'planetary mass object' in recent literature.

The classification of such objects as planets also depends on the masses determined by application of evolutionary models, and this critically depends on the age. Marois et al. (2010) use age ranges from 20 – 160 Myr for HR8799 to derive masses for the planets in the range 5 – 13 M_{Jup} placing them most likely below the deuterium burning limit. However, an age as high as ∼1 Gyr is suggested by asteroseismology methods (Moya et al. 2010) which would make the objects brown dwarfs rather than planets. A number of recent studies based on dynamics (Moro-Martín, Rieke, & Su 2010; Sudol & Haghighipour 2012) and a direct radius determination for HR 8799 (Baines et al. 2012) favour a young age and planetary masses for the companions.

Near-IR spectra have been obtained for 2M 1207b (Mohanty et al. 2007; Patience et al. 2010), the HR 8799 planets (Bowler et al. 2010; Barman et al. 2011a; Oppenheimer et al. 2013; Konopacky et al. 2013) and β Pic b (Chilcote et al. 2014). Spectra of 2M 1207b and HR 8799 b and c are shown in Figure 10. The spectra show the CO bandhead at 2.3 μm, and H_2O absorption at 1.4 and 1.9 μm (deepest in HR 8799b). CH_4 absorption is either absent or possibly weakly present in HR 8799b. The spectral features are similar to those of mid to late L dwarfs, which would imply objects of T_{eff} ∼1400–1600 K.

However, photometry of 2M 1207b shows it to be very red in J−K and underluminous compared with L dwarfs (Figure 11). This led Mohanty et al. (2007) to suggest that grey extinction by an edge-on disk may be the cause of the

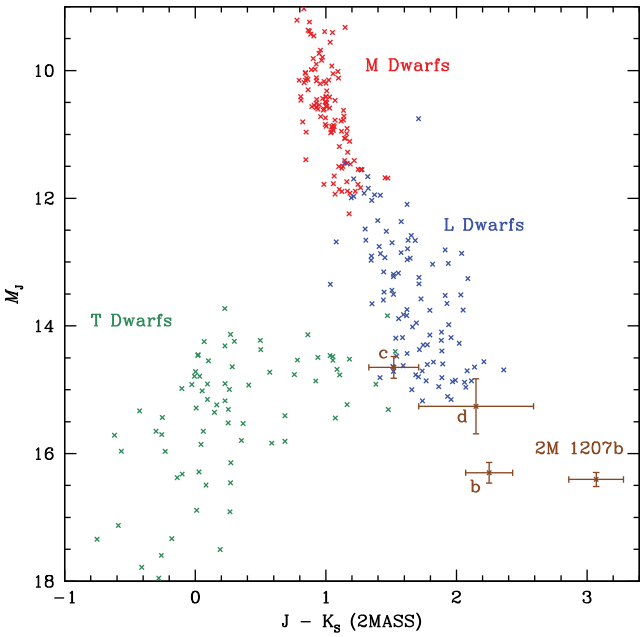

Figure 11. Colour magnitude diagram for 2M 1207b and the b, c and d planets of HR 8799 (photometry from Chauvin et al. 2005; Marois et al. 2008; Mohanty et al. 2007) compared with field M, L and T dwarfs (from the same data sources as Figure 5).

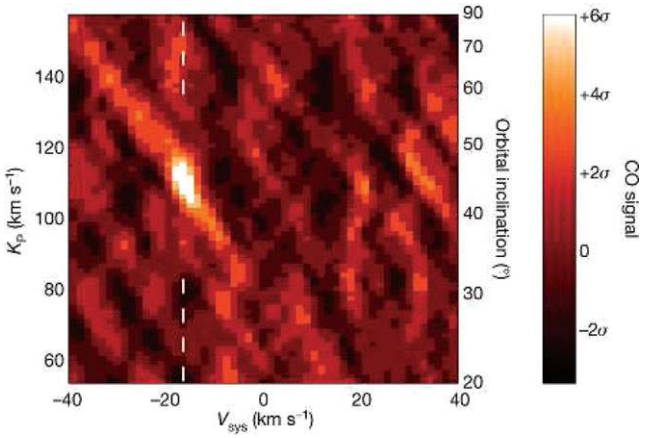

Figure 12. Carbon monoxide cross correlation signal for τ Boo b (Brogi et al. 2012) as a function of systemic velocity (V_{sys}) and radial velocity amplitude of the planet (K_P). A 6.2σ signal is seen at $K_P = 110 \pm 3.2$ km s^{-1} corresponding to an inclination $i = 44.5° \pm 1.5$ and a planet mass $M_P = 5.95 \pm 0.28 M_{Jup}$ — Reprinted by permission from Macmillan Publishers Ltd: *Nature*, 486, 502–504, © (2012).

underluminosity. Photometry of HR 8799b show that it is similarly underluminous. Barman et al. (2011b) have shown that it is possible to model the spectrum of 2M 1207b with a cool (T_{eff} ~1 000 K) model by including clouds and a departure from chemical equilibrium due to vertical mixing that inhibits the formation of methane. Similar models have been fitted to the spectra of HR 8799b (Barman et al. 2011a) and c (Konopacky et al. 2013).

Spectroscopy of β Pic b in the H band (Chilcote et al. 2014) taken with the Gemini Planet Imager shows spectral structure indicating H_2O absorption and atmospheric model fits give $T_{eff} = 1\,650 \pm 50$ K and $\log g = 4.0 \pm 0.25$.

A detection of methane (Janson et al. 2013) has been reported in the planetary mass companion GJ 504b (Kuzuhara 2013). This was achieved using Spectral Differential Imaging with the HiCAIO adaptive optics camera on the Subaru telescope. The companion was found to be much fainter in the CH_4 absorption band at ~1.7 μm than in other bands indicating a deep methane absorption comparable to that in late T dwarfs.

3.3.2 High resolution cross correlation techniques

Spectral features due to an unresolved extrasolar planet can be detected using high-resolution spectroscopy, and cross correlation techniques to pick out the faint signal due to the planet from the much brighter contribution of the host star. The technique was first used to attempt to detect the reflected light signal in high-resolution optical spectra of hot Jupiters. A possible detection of a planetary signal in τ Boo was reported (Collier Cameron et al. 1999) but was not confirmed (Charbonneau et al. 1999; Leigh et al. 2003a) and is inconsistent with the subsequent infrared detections by Brogi et al. (2012) and Rodler, Lopez-Morales, & Ribas (2012). These studies set upper limits on the geometric albedo of τ Boo b of 0.3 at 480 nm (Charbonneau et al. 1999) and 0.39 over 400–650 nm (Leigh et al. 2003a). Other reflected light studies for a number of the brighter hot Jupiter systems (Collier Cameron et al. 2002; Leigh et al. 2003b; Rodler, Kurster, & Henning 2008, 2010; Langford et al. 2011) result in similar upper limits on geometric albedo.

Much more successful have been similar studies in the near-IR where it is possible to search for specific molecular absorption features either in the transmission spectrum during transit (Snellen et al. 2010a) or in the thermal emission from the planet (which does not require a transiting planet). In these studies the telluric and stellar absorption features are removed as best as possible and the remaining signal is cross correlated with a template spectrum. The large radial velocity amplitude of the planet causes the absorption features to shift with orbital phase, so that a cross correlation peak can be searched for as a function of radial velocity amplitude (K_P) and systemic velocity (V_{sys}) as shown in Figure 12 (Brogi et al. 2012).

The method determines K_P and thus provides a direct measurement of the planet's mass and the orbital inclination, removing the sin i uncertainty for non-transiting planets. If the planet is transiting the results can be checked against those determined from transit analysis. The systemic velocity is also determined and should agree with that measured for the host star. Table 2 list the detections reported. For two objects (τ Boo b and HD 189733b) there are independent results from two studies that are in good agreement.

Most of the objects observed in this way are hot Jupiters, but essentially the same method has also been applied to the

Table 2. High-Resolution Cross Correlation Detections

Planet	Species Detected	K_P (km s^{-1})	M_P (M_{Jup})	Reference
HD 209458b[a]	CO 5.6σ	140 ± 10	0.64 ± 0.09	Snellen et al. (2010a)
τ Boo b	CO 6.2σ	110 ± 3.2	5.95 ± 0.28	Brogi et al. (2012)
τ Boo b	CO 3.4σ	115 ± 11	5.6 ± 0.7	Rodler et al. (2012)
τ Boo b	H_2O 6σ	111 ± 5	$5.9^{+0.35}_{-0.20}$	Lockwood et al. (2014)
51 Peg b	CO/H_2O 5.9σ	134.1 ± 1.8	0.46 ± 0.02	Brogi et al. (2013)
HD 189733b	CO 5.0σ	154^{+4}_{-3}	$1.162^{+0.058}_{-0.039}$	de Kok et al. (2013)
HD 189733b	H_2O 4.8σ	154^{+14}_{-10}		Birkby et al. (2013)
HD 189733b	CO 3.4σ	154		Rodler, Kürster, & Barnes (2013)
HD 179949b	CO/H_2O 6.3σ	142.8 ± 3.4	0.98 ± 0.04	Brogi et al. (2014)
β Pic b	CO 6.4σ			Snellen et al. (2014)

[a]Transmission spectrum during transit. All others are dayside emission detections.

directly imaged exoplanet β Pic b (Snellen et al. 2014). In this case it was possible to detect rotational broadening of about 25 kms^{-1} in the CO cross correlation signal indicating a rapid rotation for the planet.

All detections so far are either for carbon monoxide or water. In HD189733b (de Kok et al. 2013) CO_2, CH_4 and H_2O were searched for in the 2 μm region but not detected. However, H_2O was detected in HD 189733b using longer wavelength (3.2 μm) observations (Birkby et al. 2013). While CO is expected to be strong feature in these planets, part of the reason it is most easily detected may be that as a diatomic molecule it has a simpler spectrum and better quality line lists. Difficulty in detecting other species may, in part, be due to errors in the template spectra due to problems with the line lists, such as errors in line positions (see discussion in Barnes et al. 2010) and incompleteness. Methane line lists used for atmospheric modelling are known to be missing many hot bands that are needed at the high temperatures of these objects.

3.3.3 Secondary eclipse photometry and spectroscopy

The secondary eclipse (or occultation[2]) occurs when a planet passes behind the star. If the planet is sufficiently bright a measurable dip in the light curve is seen, and the fractional depth of the dip is a direct measurement of the flux from the planet as a fraction of that from the star. In most cases such measurements detect thermal emission from the dayside of the planet, and so contrasts are greatest at infrared wavelengths.

The first detection of a secondary eclipse was made at 24 μm for HD 209458b using the Spitzer Space Telescope (Deming et al. 2005). Since then a substantial number of mostly hot Jupiter type systems have had their secondary eclipse depth measured in the Spitzer/IRAC bands (3.6 μm, 4.5 μm, 5.8 μm and 8.0 μm). There are also a number of measurements at shorter wavelengths from ground-based telescopes. The broad band eclipse depth results are summarised in Table 3. This lists secondary eclipse depths measured in the four Spitzer/IRAC bands and in the K_s band (2.15 μm). Where there are multiple measurements in a band the one with the smaller quoted error is listed, but references to all measurements are given. The 'Other' column lists other bands in which eclipse depths have been measured and the references to these are also given.

For a few of the brighter systems it is possible to go further and obtain spectra of the dayside emission using the secondary eclipse depth. Such results are listed in Table 4. Figure 13 shows the combined data from broad band and spectroscopic observations for some of the best studied cases.

With secondary eclipse data of sufficient quality it is possible to map the brightness distribution across the disk of the planet (Williams et al. 2006). This has been attempted for HD 189733b by Majeau, Agol, & Cowan (2012) and de Wit et al. (2012). The results show a bright spot shifted east from the subsolar point in agreement with results from the full phase light curve (Knutson et al. 2007a)

While the infrared secondary eclipse shows the thermal emission from the planet, observations of the secondary eclipse at visible wavelengths can show the planet through light reflected from its star. However, if the planet is very hot, thermal emission may still be present even at visible wavelengths. Table 5 summarises measurements so far, mostly from observations with Kepler, in a broad band covering 400–850 nm. These observations provide a measure of the geometric albedo of the planet, and show that some of these planets are quite dark, while others have geometric albedos up to ∼0.4. In the case of HD 189733b observations have been made with STIS showing the planet to be dark at 450–570 nm, but with an albedo of 0.4 at 290–450 nm, the blue colour being indicative of a Rayleigh scattering haze (Evans

[2]Referring to this event as the secondary eclipse is consistent with standard terminology for eclipsing binary systems. The term occultation for this event is suggested by terminology used in the Solar system for e.g. the phenomena of Jupiter's satellites, where eclipses, occultations and transits all occur, and eclipse is reserved for the case where a satellite passes into the shadow of the planet. Both terms are used in the exoplanet literature with secondary eclipse being more common.

Table 3. Secondary eclipse depth broadband measurements (%)

Planet	K_s	3.6μm	4.5μm	5.8 μm	8.0 μm	Other	References
CoRoT-1b	0.336±.042	0.415±.042	0.482±.042			0.71 μm	1,2,3,4
CoRoT-2b		0.355±.020	0.500±.020		0.510±.059	0.71 μm	5,6,7
GJ436b		0.041±.003	<0.010	0.033±.014	0.054±.008	16, 24 μm	8,58
HD 149026b		0.040±.003	0.034±.006	0.044±.010	0.052±.006	16 μm	9
HD 189733b		0.147±.004	0.179±.004	0.310±.034	0.344±.004	16, 24 μm	10,11,12,59
HD 209458b		0.094±.009	0.139±.007	0.301±.043	0.240±.026	24 μm	13,14,15,62
HAT-P-1b	0.109±.025	0.080±.008	0.135±.022	0.203±.031	0.238±.040		16,17
HAT-P-3b		$0.112^{+.015}_{-.030}$	$0.094^{+.016}_{-.009}$				18
HAT-P-4b		$0.142^{+.014}_{-.016}$	$0.122^{+.012}_{-.014}$				18
HAT-P-6b		0.117±.008	0.106±.006				19
HAT-P-7b		0.098±.017	0.159±.022	0.245±.031	0.225±.052		20
HAT-P-8b		$0.131^{+.007}_{-.010}$	$0.111^{+.008}_{-.007}$				19
HAT-P-23b	0.234±.046	0.248±.019	0.309±.026				60
Kepler-5b		0.103±.017	0.107±.015				21
Kepler-6b		0.069±.027	0.151±.019				21
Kepler-12b		0.137±.020	0.116±.031				22
TrES-1b			0.066±.013		0.225±.036		23
TrES-2b	$0.062^{+.013}_{-.011}$	0.127±.021	0.230±.024	0.199±.054	0.359±.060		24,25
TrES-3b	$0.133^{+0.018}_{-0.016}$	0.346±.035	0.372±.054	0.449±.097	0.475±.046		26,27,28
TrES-4b		0.137±.011	0.148±.016	0.261±.059	0.318±.044		29
WASP-3b	0.181±.020	$0.209^{+0.040}_{-0.028}$	0.282±0.012		$0.328^{+0.086}_{-0.055}$		30,64
WASP-4b	$0.182^{+.014}_{-.013}$	0.319±.031	0.343±.027				31,32
WASP-5b	0.269±.062	0.197±.028	0.227±.025			H	33,63
WASP-8b		0.113±.018	0.069±.007	0.093±.023			34
WASP-12b	0.339±.014[a]	0.419±.014[b]	0.424±.021[b]	0.694±.057[b]	0.701±.074[b]	z, J, H, 2.3 μm	35,36,37,38,39,40
WASP-14b		0.19±0.01	0.224±.018		0.181±0.022		61
WASP-17b			0.229±.013	0.237±.039			41
WASP-18b		0.304±.017	0.379±.008	0.37±.03	0.41±.02		42,43
WASP-19b	0.287±.020	0.483±.025	0.572±.030	0.65±.11	0.73±.12	z, H	44,45,46,47,57,67
WASP-24b		0.159±.013	0.202±.018				48
WASP-26b		0.126±.013	0.149±.016				49
WASP-33b	$0.244^{+.027}_{-.020}$	0.26±.05	0.41±.02			z	50,51,52
WASP-43b	0.181±.027	0.346±.013	0.382±.015				53,66,67
WASP-46b	$0.253^{+.063}_{-.060}$						65
WASP-48b	0.109±.027	0.176±.013	0.214±.020				60
XO-1b		0.086±.007	0.122±.009	0.261±.031	0.210±.029		54
XO-2b		0.081±.017	0.098±.020	0.167±.036	0.133±.049		55
XO-3b		0.101±.004	0.143±.006	0.134±.049	0.150±.036		56
XO-4b		$0.056^{+.012}_{-.006}$	$0.135^{+.010}_{-.007}$				19

[a]Value from Croll et al. (2011) as corrected by Crossfield et al. (2012b)
[b]Values from Campo et al. (2011) as corrected by Crossfield et al. (2012b)

References 1. Deming et al. (2011), 2. Gillon et al. (2009), 3. Rogers et al. (2009), 4. Snellen et al. (2009), 5. Deming et al. (2011), 6. Gillon et al. (2010), 7. Snellen et al. (2010b), 8. Deming et al. (2007), 9. Stevenson et al. (2012), 10. Charbonneau et al. (2008), 11. Knutson et al. (2012), 12. Deming et al. (2006), 13. Deming et al. (2005), 14. Knutson et al. (2008), 15. Crossfield et al. (2012a), 16. Todorov et al. (2010), 17. de Mooij et al. (2011), 18. Todorov et al. (2013), 19. Todorov et al. (2012), 20 Christiansen et al. (2010), 21. Désert et al. (2011a), 22. Fortney et al. (2011), 23. Charbonneau et al. (2005), 24. O'Donovan et al. (2010), 25. Croll et al. (2010a), 26. Fressin et al. (2010), 27. de Mooij & Snellen (2009), 28. Croll et al. (2010b), 29. Knutson et al. (2009a), 30. Zhao et al. (2012a), 31. Beerer et al. (2011), 32. Cáceres et al. (2011), 33. Baskin et al. (2013), 34. Cubillas et al. (2013), 35. Campo et al. (2011), 36. Croll et al. (2011), 37. Crossfield et al. (2012b), 38. Zhao et al. (2012b), 39. Cowan et al. (2012b), 40. López-Morales et al. (2010), 41. Anderson et al. (2011), 42. Nyemeyer et al. (2011), 43. Maxted et al. (2013), 44. Anderson et al. (2013), 45. Gibson et al. (2010), 46. Lendl et al. (2013), 47. Burton et al. (2012), 48. Smith et al. (2012), 49. Mahtani et al. (2013), 50. Deming et al. (2012), 51. de Mooij et al. (2013), 52. Smith et al. (2011), 53. Blecic et al. (2014), 54. Machalek et al. (2008), 55. Machalek et al. (2009), 56. Machalek et al. (2010), 57. Zhou et al. (2013), 58. Stevenson et al. (2010), 59. Agol et al. (2010), 60. O'Rourke et al. (2014), 61. Blecic et al. (2013), 62. Zellem et al. (2014), 63. Chen et al. (2014a), 64. Rostron et al. (2014), 65. Chen et al. (2014b), 66. Wang et al. (2013), 67. Zhou et al. (2014)

et al. 2013). Low albedos in the visible are to be expected for clear atmospheres due to the broad sodium and absorption lines, whereas higher albedos can result if clouds are present (Sudarsky, Burrows, & Pinto 2000).

3.3.4 Transit spectroscopy

Observations during transit (or primary eclipse, when the planet passes in front of the star) also provide information on the atmospheres. The depth of the primary eclipse is a

Table 4. Dayside emission spectroscopy from secondary eclipses.

Planet	Wavelengths	Instrument	Features Reported	Reference
CoRoT-2b	1.1–1.7 μm	HST/WFC3		Wilkins et al. (2014)
HD 189733b	5–14 μm	Spitzer/IRS	H_2O	Grillmair et al. (2008)
	1.5–2.5 μm	HST/NICMOS	H_2O, CO, CO_2	Swain et al. (2009a)
	2.0–4.1 μm	IRTF/SpeX	Emission feature at 3.3 μm	Swain et al. (2010)
	3.27–3.31 μm	Keck/NIRSPEC	No emission feature at 3.3 μm	Mandell et al. (2011)
	2.0–4.1 μm	IRTF/SpeX	Confirm emission at 3.3 μm	Waldmann et al. (2012)
	1.1–1.7 μm	HST/WFC3	H_2O	Crouzet et al. (2014)
HD 209458b	7.5–13.2 μm	Spitzer/IRS		Richardson et al. (2007)
	1.5–2.5 μm	HST/NICMOS	H_2O, CH_4, CO_2	Swain et al. (2009b)
TrES-3b	1.1–1.7 μm	HST/WFC3		Ranjan et al. (2014)
WASP-4b	1.1–1.7 μm	HST/WFC3		Ranjan et al. (2014)
WASP-12b	1–2.5 μm	IRTF/SpeX		Crossfield et al. (2012c)
	1.1–1.7 μm	HST/WFC3		Swain et al. (2013)
WASP-19b	1.25–2.35	Magellan/MMIRS		Bean et al. (2013)
WASP-43b	1.1–1.7 μm	HST/WFC3	H_2O	Kreidberg et al. (2014b)

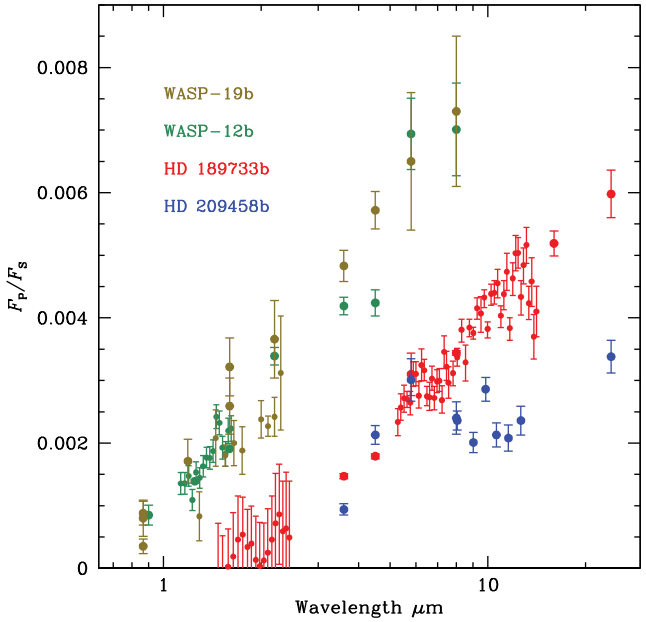

Figure 13. Dayside emission from WASP-12b, WASP-19b, HD189733b and HD209458b based on data listed in Tables 3 and 4. Large symbols are broad band measurements and smaller symbols are spectroscopic observations.

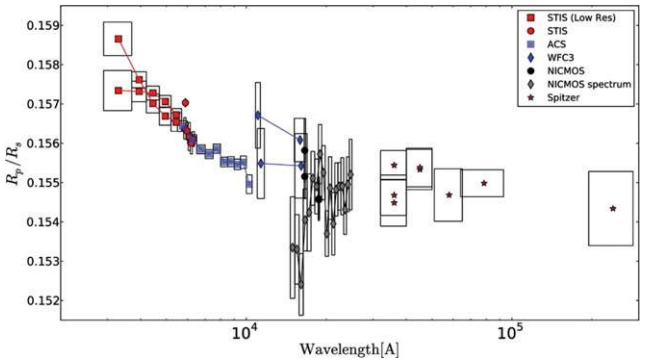

Figure 14. Transmission spectrum of HD 189733b from HST and Spitzer transit observations, showing increase to the blue interpreted as due to a Rayleigh scattering haze. — Figure 9 from 'The prevalence of dust on the exoplanet HD189733b from Hubble and Spitzer observations', Pont, F. et al., 2013, MNRAS, 432, 2917.

measure of the radius of the planet, and will be larger where absorption is strongest.

Spectroscopy during transits can reveal absorption features in the transmission spectrum of the planet's atmosphere. Transit spectroscopy samples the terminator of the planet and the long tangent path length means that it is sensitive to higher levels in the atmosphere than dayside emission spectroscopy from secondary eclipses.

The first detection of an exoplanet atmosphere was in observations of the transits of HD 209458 (Charbonneau et al. 2002) that showed absorption in the sodium doublet at 589.3 nm. Transit spectroscopy (other than studies of Na line absorption) studies are listed in Table 6. In addition to these spectroscopy observations there are numerous transit measurements in broad band filters, including measurements in the Spitzer/IRAC bands that extend coverage to longer wavelengths. HD 189733b is a particularly well studied system, and the various space observations have been combined by Pont et al. (2013) to give the transmission spectrum shown in Figure 14. It shows increasing absorption to the blue indicating the presence of a Rayleigh scattering haze. Wasp 12b (Sing et al. 2013) also shows a similar increase to the blue attributed to Rayleigh scattering from aerosols.

Transmission spectra in the near-IR for three systems are shown in Figure 15, showing water vapour absorption at $\sim$1.4 μm. As is conventional, these observations are plotted as R_P/R_S (i.e. the radius of the planet divided by the radius of the star as determined from the transit). This gives an inverted spectrum compared with conventional spectroscopy,

Table 5. Geometric albedo measurements from optical secondary eclipses.

Planet	Secondary eclipse depth (ppm)	Geometric albedo	Reference
HD 189733b (290–450 nm)	126^{+37}_{-36}	$0.40^{+0.12}_{-0.11}$	Evans et al. (2013)
HD 189733b (450–570 nm)	1^{+37}_{-30}	$0.00^{+0.12}_{-0.10}$	Evans et al. (2013)
HD 209458b	7 ± 9	0.038 ± 0.045	Rowe et al. (2008)
Kepler-5b	21 ± 6	0.12 ± 0.04	Désert et al. (2011a)
	19 ± 4	0.12 ± 0.02	Esteves et al. (2013)
	19.8 ± 3.65	0.16 ± 0.03	Angerhausen et al. (2014)
Kepler-6b	22 ± 7	0.11 ± 0.04	Désert et al. (2011a)
	8.9 ± 3.8	0.059 ± 0.025	Esteves et al. (2013)
	11.3 ± 4.2	0.07 ± 0.03	Angerhausen et al. (2014)
Kepler-7b	47 ± 14	0.38 ± 0.12	Kipping & Bakos (2011)
	42 ± 4	0.32 ± 0.03	Demory et al. (2011)
	48 ± 3	0.35 ± 0.02	Demory et al. (2013)
	46.6 ± 4.0	0.32 ± 0.03	Angerhausen et al. (2014)
Kepler-8b	26 ± 6	0.14 ± 0.03	Esteves et al. (2013)
	16.5 ± 4.45	0.11 ± 0.03	Angerhausen et al. (2014)
Kepler-12b	31 ± 7	0.14 ± 0.04	Fortney et al. (2011)
	18.7 ± 4.9	0.09 ± 0.02	Angerhausen et al. (2014)
Kepler-13Ab	173.7 ± 1.8	$0.33^{+0.04}_{-0.06}$	Shporer et al. (2014)
Kepler-17b	58 ± 10	0.10 ± 0.02	Désert et al. (2011b)
	43.7 ± 6.4	0.08 ± 0.01	Angerhausen et al. (2014)
Kepler-41b	64^{+10}_{-12}	0.30 ± 0.08	Santerne et al. (2011)
	60 ± 9	0.23 ± 0.05	Quintana et al. (2013)
	46.2 ± 8.7	0.18 ± 0.03	Angerhausen et al. (2014)
Kepler-43b	17.0 ± 5.3	0.06 ± 0.02	Angerhausen et al. (2014)
Kepler-76b	75.6 ± 5.6	0.22 ± 0.02	Angerhausen et al. (2014)
Kepler-412b	47.4 ± 7.4	0.094 ± 0.015	Deleuil et al. (2014)
	40.2 ± 9.0	0.11 ± 0.02	Angerhausen et al. (2014)
TrES-2b	6.5 ± 1.9	0.025 ± 0.007	Kipping & Spiegel (2011)
	7.5 ± 1.7	0.030 ± 0.007	Esteves et al. (2013)

All measurements are with Kepler (400–850 nm) except for HD 209458b observed with MOST (350–700 nm) and HD 189733b observed with HST/STIS.

since absorption features increase the apparent radius of the planet.

Measurements of the Sodium D-line absorption are listed in Table 7. Results are listed here where the absorption is detected at greater than the 3-sigma level. There are also a number of unsuccesful attempts at detections. Potassium absorption has been reported in XO-2b (Sing et al. 2011b).

Atomic and atomic ion species have also been detected in a number of transiting planets in the unbound portion of the atmosphere, or exosphere. The best studied case is HD 209458b where H I, C II, O I, and Si III have been observed (Vidal-Madjar et al. 2003, 2004; Linsky et al. 2010). Exosphere detections have also been reported in HD 189733b (Lecavelier Des Etangs et al. 2010; Jensen et al. 2012) and Wasp-12b (Fossati et al. 2010).

3.3.5 Full phase photometry

As well as observations of the transits and eclipses, information on a planet's atmosphere can be obtained from observations of the full phase light curve. In the infrared a hot Jupiter will show variations around the cycle due to the variation of temperature across its surface. In the optical where reflected light is seen, variations will occur due to the change in the illuminated fraction of the disk, as well as due to phase angle dependent scattering processes (Seager, Whitney, & Sasselov 2000). In some cases the light curves are complicated by ellipsoidal variations in the star (e.g. Welsh et al. 2010) or the planet (e.g. Cowan et al. 2012b). Systems with full phase light curves at infrared wavelengths showing significant variation around the cycle are listed in Table 8. In addition full phase light curves due to reflected light are observed in many of the systems listed in Table 5.

Analysis of these light curves has been used to derive maps of the temperature distribution of HD 189733b (Knutson et al. 2007a) showing a hot spot offset from the substellar point (consistent with models, see Section 4.1.3). In the case of Kepler-7b, the reflected light phase curve observed by Kepler is interpreted as showing the presence of patchy clouds (Demory et al. 2013).

3.3.6 Polarimetry

Reflected light from extrasolar planets will be polarised as a result of scattering from cloud and haze particles and from molecules. Normal stars are generally found to have very

Table 6. Transmission spectroscopy during transit.

Planet	Wavelengths	Instrument	Featues reported	Reference
CoRoT-1b	0.8–2.4 μm	IRTF/SpeX/MORIS	no TiO/VO	Schlawin et al. (2014)
	1.1–1.7 μm	HST/WFC3		Ranjan et al. (2014)
GJ 436b	1.1–1.7 μm	HST/WFC3		Knutson et al. (2014a)
GJ 1214b	0.78–1.00 μm	VLT/FORS1		Bean, Miller-Ricci Kempton, & Homeier (2010)
	2.1–2.4 μm	Keck/NIRSPEC		Crossfield et al. (2011)
	1.1–1.7 μm	HST/WFC3		Berta et al. (2012)
	1.1–1.7 μm	HST/WFC3	clouds	Kreidberg et al. (2014a)
GJ 3470b	2.09–2.36 μm	Keck/MOSFIRE		Crossfield et al. (2013)
	1.1–1.7 μm	HST/WFC3		Ehrenreich et al. (2014)
HD 97658b	1.1–1.7 μm	HST/WFC3		Knutson et al. (2014b)
HD 189733b	1.4–2.5 μm	HST/NICMOS	H_2O, CH_4	Swain et al. (2008)
	0.55–1.05 μm	HST/ACS	haze	Pont et al. (2008)
	1.66–1.87 μm	HST/NICMOS	haze, no H_2O	Sing et al. (2009)
	0.29–0.57 μm	HST/STIS	haze	Sing et al. (2011a)
	1.1–1.7 μm	HST/WFC3		Gibson et al. (2012)
	1.1–1.7 μm	HST/WFC3	H_2O	McCullough et al. (2014)
HD 209458b	0.3–1.0 μm	HST/STIS	H_2O[a]	Knutson et al. (2007b)
	1.1–1.7 μm	HST/WFC3	H_2O	Deming et al. (2013)
HAT-P-1b	1.1–1.7 μm	HST/WFC3	H_2O	Wakeford et al. (2013)
HAT-P-12b	1.1–1.7 μm	HST/WFC3	clouds	Line et al. (2013a)
	0.52–0.93 μm	Gemini/GMOS		Gibson et al. (2013a)
TrES-2b	1.1–1.7 μm	HST/WFC3		Ranjan et al. (2014)
TrES-4b	1.1–1.7 μm	HST/WFC3		Ranjan et al. (2014)
WASP-6b	0.48–0.86 μm	Baade/IMACS		Jordán et al. (2013)
WASP-12b	1.1–1.7 μm	HST/WFC3		Swain et al. (2013)
	0.7–1.0 μm	Gemini/GMOS		Stevenson et al. (2014)
	0.3–1.7 μm	HST/STIS+WFC3	aerosols, no TiO	Sing et al. (2013)
	1.1–1.7 μm	HST/WFC3		Mandell et al. (2013)
WASP-17b	1.1–1.7 μm	HST/WFC3		Mandell et al. (2013)
WASP-19b	1.25–2.35 μm	Magellan/MMIRS		Bean et al. (2013)
	0.29–1.69 μm	HST/STIS+WFC3	H_2O no TiO	Huitson et al. (2013)
	1.1–1.7 μm	HST/WFC3		Mandell et al. (2013)
WASP-29b	0.51–0.72 μm	Gemini/GMOS		Gibson et al. (2013b)
WASP-43b	0.52–1.04 μm	GTC/OSIRIS		Murgas et al. (2014)
	1.1–1.7 μm	HST/WFC3	H_2O	Kreidberg et al. (2014b)
XO-1b	1.2–1.8 μm	HST/NICMOS	H_2O, CO_2, CH_4	Tinetti et al. (2010)
	1.1–1.7 μm	HST/WFC3	H_2O	Deming et al. (2013)
XO-2b	1.1–1.7 μm	HST/NICMOS		Crouzet et al. (2012)

[a]According to reanalysis by Barman (2007).

Table 7. Sodium (589 nm) detections from transit spectroscopy.

Planet	Instrument	Line depth	Band	Reference
HD 189733b	HET/HRS	$6.72 \pm 2.07 \times 10^{-4}$	1.2 nm	Redfield et al. (2008)
	HET/HRS	$5.26 \pm 1.69 \times 10^{-4}$	1.2 nm	Jensen et al. (2011)
	HST/STIS	$9 \pm 1 \times 10^{-4}$	0.5 nm	Huitson et al. (2012)
HD 209458b	HST/STIS	$2.32 \pm 0.57 \times 10^{-4}$	1.2 nm	Charbonneau et al. (2002)
	HET/HRS	$2.63 \pm 0.81 \times 10^{-4}$	1.2 nm	Jensen et al. (2011)
	Subaru/HDS	$5.6 \pm 0.7^a \times 10^{-4}$	0.3 nm	Snellen et al. (2008)
	HST/STIS	11×10^{-4}	0.44 nm	Sing et al. (2008)
HAT-P-1b	HST/STIS	$9.8 \pm 3.0 \times 10^{-4}$	3.0 nm	Nikolov et al. (2014)
WASP-17b	VLT/GIRAFFE	$55 \pm 13 \times 10^{-4}$	0.15 nm	Wood et al. (2011)
	Magellan/MIKE	$58 \pm 13 \times 10^{-4}$	0.15 nm	Zhou & Bayliss (2012)
XO-2b	GTC/OSIRIS	$4.7 \pm 1.1 \times 10^{-4}$	5.0 nm	Sing et al. (2012)

[a]$7.0 \pm 1.1 \times 10^{-4}$ (0.15 nm band), $13.5 \pm 1.7 \times 10^{-4}$ (0.075 nm band)

Table 8. Full phase infrared photometry of exoplanets.

Planet	Wavelength	Amplitude (ppm)	Reference
CoRoT-1b	710 nm	126 ± 33	Snellen et al. (2007)
υ And b	24 μm	1300 ± 74	Crossfield et al. (2010)
HD 179949	8 μm	1 410 ± 330	Cowan, Agol, & Charbonneau (2007)
HD 149026b	8 μm	227 ± 66	Knutson et al. (2009c)
HD 189733b	3.6 μm	1 242 ± 61	Knutson et al. (2012)
	4.5 μm	982 ± 89	Knutson et al. (2012)
	8 μm	1 200 ± 200	Knutson et al. (2007a)
HD 209458b	4.5 μm	1 090 ± 120	Zellem et al. (2014)
HAT-P-7b	400–850 nm	63.7	Welsh et al. (2010)
WASP-18b	3.6 μm	2 960 ± 90	Maxted et al. (2013)
	4.5 μm	3 660 ± 70	Maxted et al. (2013)

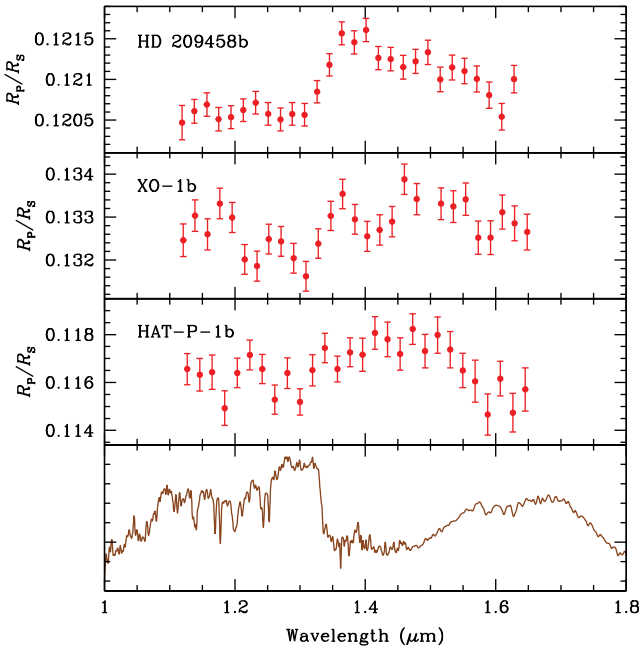

Figure 15. HST/WFC3 observations of the transmission spectra of HD209458b and XO-1b (Deming et al. 2013) and HAT-P-1b (Wakeford et al. 2013) showing absorption at ∼1.4 μm attributed to H_2O. The spectrum of the brown dwarf Kelu-1 showing the same absorption feature is shown for comparison in the bottom panel. The exoplanet spectra are inverted compared with the brown dwarf spectra since absorption features increase the radius of the planet as seen in transit observations.

low intrinsic polarisations (Kemp et al. 1987; Bailey, Lucas, & Hough 2010). In a hot Jupiter system the polarisation in the combined light of the unresolved star and planet is expected to be in the range 10^{-5}–10^{-6} (Seager, Whitney, & Sasselov 2000), and will vary around the orbital cycle with the changing phase angle.

While the expected polarisations are small, polarisation is a differential measurement that can be made to high sensitivity wth ground-based telescopes, and instruments capable of measuring stellar polarisation at the one part per million level have been developed (Hough et al. 2006; Wiktorowicz & Matthews 2008). Lucas et al. (2009) reported upper limits on the polarisation of τ Boo and 55 Cnc in a broad red band (590–920 nm) and set upper limits on the geometric albedo of τ Boo b and 55 Cnc e for Rayleigh scattering models.

Berdyugina et al. (2008) reported polarisation varying over the orbital cycle of HD 189733b with an amplitude of $\sim 2 \times 10^{-4}$ in the B band. Wiktorowicz (2009), however, found no polarisation variation in this system with a 99% confidence upper limit of 7.9×10^{-5} in a 400–675 nm wavelength range. Berdyugina et al. (2011) then reported further observations that confirmed a polarisation variation, but with a reduced amplitude of 10^{-4} in the U and B bands and much lower amplitude in the V band. They claim the data is consistent with that of Wiktorowicz (2009) when the different wavelengths are taken into account.

While HD 189733b is a system in which polarisation might be expected in view of the Rayleigh scattering haze seen in transmission spectroscopy (Pont et al. 2008, 2013), the reported polarisation amplitudes are too large to be easily explained. Berdyugina et al. (2011) report that the polarisation is consistent with a Rayleigh-Lambert model with a geometric albedo of ∼0.6 and 'scattered light maximally polarised' (i.e. 100%). However, in Rayleigh scattering models a layer sufficiently optically thick to produce a high geometric albedo has a maximum polarisation of only about 30% (Buenzli & Schmid 2009) as a result of depolarisation due to multiple scattering. Lucas et al. (2009) used Monte-Carlo scattering models to predict a maximum polarisation amplitude of 2.6×10^{-5} for HD 189733b.

3.4 Atmospheric structure

3.4.1 Inflated atmospheres

One result of transit observations is that many hot Jupiters are 'inflated', with radii significantly larger than predicted by models (Baraffe, Chabrier, & Barman 2008, 2010). This inflation is found to be correlated with the level of stellar irradiation, with inflation becoming apparent for planets receiving incident flux greater than 2×10^8 erg s^{-1} cm^{-2} (Miller & Fortney 2011; Demory & Seager 2011).

Weiss et al. (2013) have used data on 138 exoplanets to derive empirical relations between radius, mass and incident flux as follows:

$$R_P/R_\oplus = 1.78(M_P/M_\oplus)^{0.53}(F/\text{erg s}^{-1}\text{ cm}^{-2})^{-0.03} \quad (1)$$

for $M_P < 150M_\oplus$, and

$$R_P/R_\oplus = 2.45(M_P/M_\oplus)^{-0.039}(F/\text{erg s}^{-1}\text{ cm}^{-2})^{0.094} \quad (2)$$

for $M_P > 150M_\oplus$.

The reason for this inflation is still debated. Guillot & Showman (2002) showed that the inflated radii could be understood if ∼1% of the stellar flux received by the planet was transferred into the deep atmosphere below the photosphere. The observed relationships between inflated radii and incident flux appear consistent with this idea. However, it is unclear what is the mechanism for transferring energy into the interior. Mechanisms for inflated radii include downward transport of mechanical energy by atmospheric circulation (Showman & Guillot 2002), enhanced opacities that help to trap heat in the interior (Burrows et al. 2007a), dissipation of thermal tides (Arras & Socrates 2010), and tidal heating due to a non-zero eccentricity (Jackson et al. 2008; Ibgui, Burrows, & Spiegel 2010). The Ohmic dissipation model (Batygin & Stevenson 2010; Perna, Menou, & Rauscher 2010) uses the interaction of atmospheric winds and the planetary magnetic field to induce electric currents that heats the interior. Rauscher & Menou (2013) have modelled the process using a 3D model (see Section 4.1.3) and find that ohmic dissipation can explain the radius of HD 209458b for a planetary magnetic field of 3–10 G. However, Rogers & Showman (2014) used 3D magnetohydrodynamic simulations of the atmosphere of HD 209458b and found Ohmic dissipation rates orders of magntiude too small to explain the inflated radius.

3.4.2 Temperature structure

The dayside spectra of hot Jupiters as defined by the Spitzer IRAC colours (Table 3 and Figure 13) have been used to derive information on the atmospheric temperature structure. If temperature decreases with height then the spectrum shows absorption features due to its atmospheric molecules, but a temperature inversion can cause the same features to appear in emission. A constant temperature (isothermal) atmosphere would shown no spectral features.

The presence of a temperature inversion was first suggested in the infrared spectrum of HD 209458b (Knutson et al. 2008; Burrows et al. 2007a) where a bump in the spectrum at 4.5 and 5.8 μm can be understood as water vapour in emission. A number of other cases have been suggested based on Spitzer photometry. It has been suggested that inversions result from absorption of starlight by an absorber high in the atmosphere. Suggestions for the absorber include TiO and VO (Hubeny et al. 2003; Fortney et al. 2008) or photochemically produced sulfur compounds (Zahnle et al. 2009). However, observations have so far failed to detect the presence of TiO or VO in eclipse or transit spectroscopy in any of these systems.

Knutson, Howard, & Isaccson (2010) argue that the presence of an inversion correlates with the activity of the host star, with the temperature inversions being found for planets orbiting inactive stars, whereas the non-inverted atmospheres occur in planets orbiting chromospherically active stars.

However, Madhusudhan & Seager (2010) have investigated the degeneracies between thermal inversions and molecular abudnances, and find it is often possible to fit both inversion and non-inversion models given the limited data points available from Spitzer photometry.

3.5 Composition

3.5.1 Water vapour, carbon monoxide and methane

Analogy with brown dwarfs of similar temperatures discussed in Section 2 suggests that the most important species in the near-IR spectra should be H_2O, CO and CH_4. From the discussion in Section 3.3 and Tables 2– 6, it will be apparent that H_2O and CO are indeed detected in quite a number of giant exoplanet systems by a variety of different methods. Evidence for these molecules is found in spectroscopy of direct imaged planets (Section 3.3.1), from high resolution cross correlation methods (Section 3.3.2 and Table 2) and from secondary eclipse (Section 3.3.3, Table 4) and transit (Section 3.3.4 and Table 6) spectroscopy.

The data on CH_4 is less clear. Although it is reported, for example, in the NICMOS transmission spectrum of HD 189733b (Swain et al. 2008), high resolution cross correlation studies at the same wavelength do not detect it (de Kok et al. 2013), but do detect CO. This suggests a departure from equilibrium chemistry due to vertical mixing as also suggested by Knutson et al. (2012) based on Spitzer phase curves.

The spectra of directly imaged planets shown in Figure 10 also show CO, but at best very weak evidence for CH_4. These are all objects that are cool enough to be in the T dwarf range, but actually show spectra more like those of L dwarfs. The lack of CH_4 once again indicates non-equilibrium chemistry (Barman et al. 2011a, 2011b; Skemer et al. 2014; Zahnle & Marley 2014). Departures from equilibrium chemistry are discussed further in Section 4.2.2.

Recently, however, CH_4 has been detected photometrically in the very cool (∼600 K) planetary mass companion GJ 504b (Janson et al. 2013) as described in Section 3.3.1

3.5.2 Carbon dioxide

Up to a few years ago CO_2 was not considered to be an important species for exoplanet and brown dwarf atmospheres as its predicted equilibrium abundance is quite low. Then Swain et al. (2009a) reported an absorption feature at 2.0 μm in the NICMOS dayside emission spectrum of HD189733b that they identified as CO_2. This is a relatively weak CO_2 band. It has never been seen in brown dwarfs, for example,

whereas the much stronger CO_2 band at 4.2 μm has been seen (Yamamura, Tsuji, & Tanabé 2010; Sorahana & Yamamura 2012).

Fitting the NICMOS feature at 2.0 μm in HD189733b as a CO_2 band results in CO_2 mole fractions $\sim 10^{-3}$ (Madhusudhan & Seager 2009; Lee, Fletcher, & Irwin 2012; Line et al. 2012). This is several thousand times higher than the expected chemical equilibrium abundance for solar composition (Moses et al. 2011) or the observed CO_2 abundances in brown dwarfs (Tsuji, Yamamura, & Sorahana 2011). Inclusion of non-equilibrium processes such as photochemistry does not substantially increase CO_2 abundances (Zahnle et al. 2009; Moses et al. 2011). However, CO_2 abundances are sensitive to elemental composition increasing quadratically with increasing metallicity (Lodders 2002; Zahnle et al. 2009).

The high CO_2 abundance is not clearly seen in other observations of HD189733b. In particular the much stronger CO_2 bands at 4.2 μm and 15 μm are not apparent in the Spitzer secondary eclipse data. Fitting separately to the NICMOS and Spitzer data, Madhusudhan & Seager (2009) found a much lower CO_2 abundance from the Spitzer data consistent with equilibrium predictions. If a model is required to fit both the Spitzer and NICMOS data simultaneously, as in the retrieval analysis of Lee et al. (2012) the result is a very high CO_2 abundance to fit the NICMOS data, and then a tightly constrained isothermal temperature profile in the upper atmosphere, which hides the strong 4.2 μm and 15 μm CO_2 bands that would otherwise be present.

An alternative interpreation is to disregard the NICMOS 2 μm feature, the only evidence pointing to a high CO_2 abundance in HD 189733b. Gibson et al. (2011) have argued that NICMOS observations are too sensitive to the method of removing systematics to reliably detect molecular species. In that case it is possible to fit the remaining data on the transmission and dayside emission spectra of HD 189733b very well using equilibrium abundances as shown by Dobbs-Dixon & Agol (2013) who used the solar composition opacities from Sharp & Burrows (2007).

3.5.3 C/O ratios

A high C/O ratio was first suggested for the atmosphere of the highly irradiated hot Jupiter WASP-12b (Madhusudhan et al. 2011) and Madhusudhan (2012) has suggested that C/O ratio may be an important parameter for classifying exoplanet atmospheres. If C/O is greater than 1.0 (the solar value is about 0.5) the chemistry changes substantially for temperatures above about 1 500 K, since almost all the oxygen combines with carbon to form CO, and the abundances of other oxygen bearing species, including H_2O and TiO/VO are substantially reduced. The excess carbon also results in increased abundances of carbon species such as HCN and C_2H_2.

Reanalysis of the secondary eclipse data on WASP-12b by Crossfield et al. (2012b), with corrections for the effects of a contaminating star, concluded that the spectrum was well-approximated by a blackbody and that no constraints on its atmospheric abundances could be set. Other recent studies of the emission and transmission spectra of WASP-12b (Sing et al. 2013; Swain et al. 2013; Mandell et al. 2013) do not clearly detect any molecular species and do not significantly constrain the C/O ratio.

Line et al. (2013b) have investigated the ability to determine C/O ratios using retrieval models (see Section 4.1.2) and find that with limited data this is very difficult and the retrieved values are biased towards the solar value or a value of one.

3.6 Clouds and hazes

The best evidence for cloud or haze[3] in giant exoplanets comes from observations of the resolved planets (or planetary mass objects) HR 8799b, HR 8799c and 2M 1207b where photometry and spectroscopy point to cloudy atmospheres similar to those of L dwarfs as already discussed in Section 3.3.1. A recent analysis by Skemer et al. (2014) including mid-infrared data concluded that patchy clouds as well as non-equilibrium chemistry (to explain the weakness of the 3.3 μm CH_4 band) were needed to fit the data for the HR 8799 planets, whereas a thick cloud model fitted the 2M 1207b data.

HD 189733b has good evidence for a Rayleigh scattering haze that is visible in both the transmission spectrum observed during transit (Pont et al. 2013) and in the reflection spectrum from secondary eclipse (Evans et al. 2013). Rayleigh scattering (seen as an increase in radius to the blue) is also seen in the transmission spectrum of WASP-12b (Sing et al. 2013) and WASP-6b (Jordán et al. 2013).

Demory et al. (2013) use an analysis of the optical phase curve and secondary eclipse of Kepler-7b to conclude that clouds must be present and must have an inhomogenous distribution to explain the lack of symmetry in the phase curve.

The presence of clouds or hazes are suggested in some other systems by essentially featureless transmission spectra that lack features expected for a clear atmosphere such as Na or H_2O absorption (e.g. Line et al. 2013a; Gibson et al. 2013a).

4 ATMOSPHERIC MODELS

4.1 Types of models

Exoplanet and brown dwarf atmospheres occupy a temperature range extending from that of the Solar system planets to that of the coolest stars. Modelling techniques for these objects can thus adapt techniques both from traditional stellar atmosphere modelling (e.g. Gray 2005) and those developed

[3] In using the terms 'cloud' or 'haze' here I have followed the terminology used in the orignal reports. I am not aware of any accepted definition of the difference between these two terms, and in this context they likely refer to the same types of particles but haze is usually thinner than cloud and often occurs at higher altitude.

for modelling of the Earth and other Solar system planet atmospheres (e.g. Liou 2002). These two fields have developed largely independently and have significant difference in approach that are now becoming apparent, as methods from both fields are applied to the modelling of exoplanet atmospheres.

Howvever, the essentials of atmospheric modelling are the same for all such objects. The VSTAR modeeling code (Bailey & Kedziora-Chudczer 2012), for example, has been used successfully for objects ranging from terrestrial (Bailey 2009; Cotton et al. 2012) and giant planets (Kedziora-Chudczer & Bailey 2011) in the Solar system to exoplanets (Zhou et al. 2013, 2014), brown dwarfs and cool stars (Bailey & Kedziora-Chudczer 2012).

4.1.1 Stellar atmosphere type models

The traditional approach to stellar atmosphere modelling is typified by the ATLAS series of modelling codes (Kurucz 1970, 1993; Castelli & Kurucz 2004), and the MARCS models (Gustaffson et al. 2008). Normally with such models the starting point is an adopted effective temperature $T_{\rm eff}$, surface gravity (usually specified as $\log g$ in cgs units), and metallicity [M/H]. Grids of models can then be calculated for different values of these parameters. The essential stages in such models are:

1. Start with an initial estimate for the pressure temperature structure of the atmosphere specified at a number ($\sim$40–80) of layers.
2. For each layer calculate the composition of the layer. For hotter stars this primarily involves determining the distribution of ionisation states for each element using Saha's equation. For cooler stars some molecules become important and their concentrations are calculated assuming chemical equilibrium.
3. Calculate the opacity (extinction coefficient) of each layer at each required wavelength taking account of atomic absorption lines, molecular absorption lines and continuum opacity sources such as bound-free and free-free absorption, collision induced absorptions, Rayleigh and electron scattering. The wavelength range must cover all wavelengths at which significant energy transport occurs.
4. Solve the radiative transfer equation to determine the radiative energy flux through each layer.
5. Iteratively adjust the temperature structure of the model, repeating steps 2–4 as required until the model is in energy balance. The total flux through each layer, including convective energy flux which is normally determined using mixing length theory (Henyey, Vardya, & Bodenheimer 1965) must equal $\sigma T_{\rm eff}^4$.

The spectrum of the star can then be obtained, either from the last iteration of the model if opacities and radiative transfer are calculated with sufficient resolution, or from a separate spectral synthesis model.

Models based on essentially this procedure have been developed for brown dwarf and exoplanet atmospheres (e.g. Tsuji et al. 1996; Allard et al. 2001; Barman, Hauschildt, & Allard 2001; Marley et al. 2002; Burrows, Sudarsky, & Hubeny 2003). In order to model the atmospheres of these cooler objects a number of additional complications have to be dealt with.

At lower temperatures the composition becomes dominated by molecules (as shown in Figure 3), and the calculation of composition (or equation of state) becomes primarily a chemical model. Large numbers of chemical compounds are potentially important and hence large chemical models handling hundreds or in some case thousands of species have been developed (e.g Lodders & Fegley 2002). (see Section 4.2).

As well as gas phase species, at temperatures below about 2 000 K condensates start to form and both modify the gas phase chemistry, and can form clouds that contribute substantially to the opacity. As we have already seen clouds are important in understanding the behaviour of L dwarfs and the L/T transition, and are also probably important in giant exoplanets. (see Section 4.4).

Molecules and cloud particles contribute to scattering of light. Scattering is usually a relatively minor contribution to the opacity of stellar atmospheres and is usually treated using simplifying approximations such as that of isotropic scattering. In the cooler atmospheres of brown dwarfs and exoplanets scattering becomes more significant, and more rigorous treatments of scattering that accurately account for the non-isotropic phase functions may be needed (de Kok et al. 2011; Bailey & Kedziora-Chudczer 2012). (see Section 4.5).

4.1.2 Retrieval models

A different approach to modelling exoplanet atmospheres is shown in a number of recent studies (Madhusudhan & Seager 2009; Line et al. 2012; Lee et al. 2012; Benneke & Seager 2012; Line et al. 2013b; Benneke & Seager 2013) that adopt a retrieval approach. These approaches are similar to that used in remote sensing studies of the Earth atmosphere where temperature structure (e.g. Rozenkranz 2001) trace gas content (e.g. Buchwitz et al. 2005), and cloud properties (e.g. Garnier et al. 2012) are routinely retrieved from satellite observations, and similar techniques are used to study the atmospheres of other Solar system planets from orbiting spacecraft or Earth-based telescopes.

These models seek to retrieve the temperature structure and composition of the atmosphere directly from observations, rather than predict these using energy balance and chemical models as in the approach described above. Thus only steps 3 and 4 of the modelling procedure are needed in the forward model. A number of different approaches to the retrieval process have been used. Madhusudhan & Seager (2009) search in a large grid of models covering a wide parameter space. Lee et al. (2012) use an iterative optimal estimation procedure. Line et al. (2013b) investigate several

different approaches to retrieval (Optimal Estimation, Bootstrap Monte Carlo, and Differential Evolution Markov Chain Monte Carlo).

Benneke & Seager (2012, 2013) use a somewhat different approach where the temperature profile is not retrieved, but is determined by a self consistent model requiring radiative and hydrostatic equilibrium and allowing for convection. The model can therefore be described by a small number of parameters (planet-to-star radius ratio, cloud-top pressure and Bond albedo) as well as the mole fractions of molecular species. The models include cloud and haze layers and retrieval uses a Bayesian Nested Sampling Monte Carlo method.

4.1.3 3D models of hot Jupiters

All the models considered so far are 1D models that describe the structure of the atmosphere with a single one dimensional profile. Such models cannot represent dynamical effects and diurnal variations. For hot Jupiters which all receive strong irradiation from their star, the structure is expected to vary substantially around the planet and can be very different on the dayside and nightside.

A number of studies have looked at full 3D models of the atmospheric circulation (General Circulation Models or GCMs) for hot Jupiters. A GCM typically consists of a dynamical core (usually adpated from an Earth atmosphere model) that numerically solves the equations that govern atmospheric circulation over a three dimensional grid of points. These equations can either be the 'primitive equations' that include the approximations of vertical hydrostatic equilibrium and a shallow atmosphere as used by Showman et al. (2009) and Rauscher & Menou (2012) or the full equations that avoid these approximations as used by Dobbs-Dixon & Lin (2008) and Mayne et al (2014). Initially simplified schemes were used to represent the forcing from the illuminating star (e.g. Showman & Guillot 2002; Cooper & Showman 2005; Menou & Rauscher 2009) but more recent models include a radiative transfer model and are therfore coupled radiative-dynamical models.

Because of the need to perform radiative transfer solutions for each grid point and time step, radiative transfer methods for GCMs generally need to be simplified compared with those used in the 1D models described earlier. Dobbs-Dixon & Lin (2008) used a grey model described by a single mean opacity. Heng, Frierson, & Phillips (2011) and Rauscher & Menou (2012) use dual-band radiative transfer, dividing radiation into incoming shortwave radiation from the star, and outgoing longwave radiation from the planet. Showman et al. (2009) use the correlated-k method (see Section 4.3) with 30 wavelength bins. Dobbs-Dixon & Agol (2013) use a similar set of 30 bins but use band-averaged opacities rather than the correlated-k method. The radiative transfer in all these cases uses a two-stream approximation. Amundsen et al. (2014) has tested the accuracy of some of these approaches and find that correlated-k and two-stream methods give reasonable accuracy, but band-averaged opacities can lead to substantial errors.

A review of atmospheric circulation models for exoplanets is given by Showman, Cho, & Menou (2010). Features predicted by such models are the presence of a superrotating jet in the equatorial regions with wind velocities of 1–4 km/s. This can cause an eastward displacement of the hottest region from the substellar point which is consistent with observations of HD 189733b (Knutson et al. 2007a, 2009b).

Models that specifically aim to simulate the atmospheres of HD 189733b and HD 209458b have been given by Showman et al. (2009) and an example of the predicted temperature structure and winds is given in Figure 16 and show reasonable agreement with observed day-night phase variations in Spitzer photometry of HD 189733b (Knutson et al. 2007a, 2009b).

Dobbs-Dixon & Agol (2013) have used a 3D model of HD 189733b including wavelength dependent radiative transfer to make predictions of the transmission spectrum, dayside spectrum, and phase curves that are in good agreement with the observations.

4.1.4 3D models of brown dwarfs

Studies of atmospheric circulation in brown dwarfs have been made using 3D models and analytic theory (Showman & Kaspi 2013) and shallow water models (Zhang & Showman 2014). These show atmospheric circulation with horizontal wind speeds up to 300 m s^{-1}, and vertical mixing that could help to explain the disequilibrium chemistry and patchy clouds near the L/T transition (see Section 2.5).

4.2 Atmospheric chemistry

4.2.1 Equilibrim chemistry

Chemical models for brown dwarf and exoplanet atmospheres aim to predict the chemical composition in the atmosphere given the pressure, temperature and elemental abundances. Normally this is based on the assumption of chemical equilibrium. This can be achieved by solving a system of equations for the mass balance of each element and for the overall charge balance using the equilibrium constants of formation for each compound (e.g. Tsuji 1973; Allard et al. 2001; Lodders & Fegley 2002). An alternative, but equivalent, approach is that of minimisation of the total Gibbs free energy of the system (Sharp & Huebner 1990; Sharp & Burrows 2007).

In either case the required data is available in compilations such as the National Institute for Standards and Technology (NIST)-JANAF thermochemical Tables (Chase 1998) and similar Tables such as Barin (1995) and Robie & Hemingway (1995). These tables list the equilibrium constants of formation K_f and Gibbs free energy of formation $\Delta_f G^o$ for a large number of compounds as a function of temperature. The two are related through

$$\Delta_f G^o = -RT \ln K_f \quad (3)$$

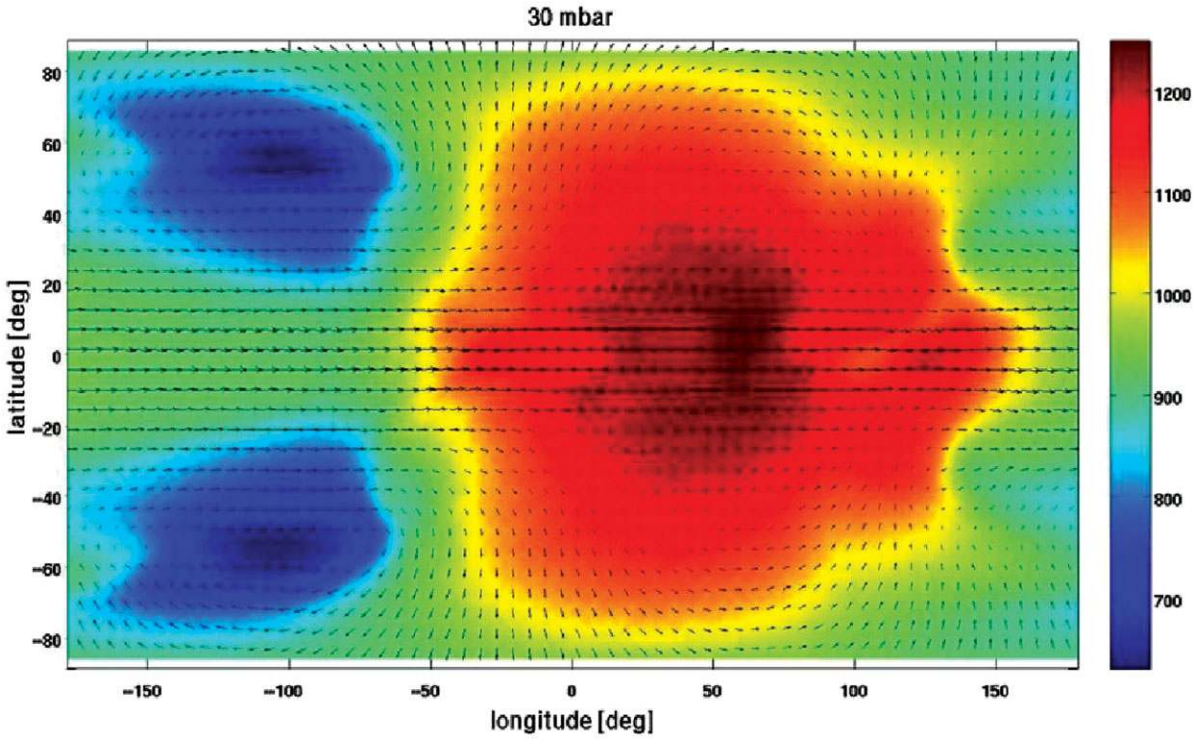

Figure 16. Temperature (colourscale in K) and winds (arrows) at the 30 mbar level for a 3D general circulation model simulation of the atmosphere of HD 189733b. (Figure 4, Showman, A.P. et al., Atmospheric Circulation of Hot Jupiters: Coupled Radiative-Dynamical General Circulation Model Simulations of HD 189733b and HD 209458b, The Astrophysical Journal, 699, 564. reproduced by permission of the AAS.)

Where R is the gas constant. The required thermochemical data for gas phase species can also be derived from spectroscopic constants.

Chemical models predict the abundances of gas phase species, ionised species and the formation of liquid and solid condensates. The thermochemical models can also predict quantities such as the mean molecular weight, the specific heat and the adiabatic gradient, the latter two quantities being needed for mixing length convection theory.

4.2.2 Departures from equilibrium

Departures from equlibrium chemistry can occur as a result of photochemistry or vertical mixing if these processes occur at a faster rate than the collisional processes that tend to restore equilibrium. A non-equilibrium correction to the equilibrium abundances of CH_4/CO and NH_3/N_2 due to vertical mixing (Saumon et al. 2003) has been adopted to explain the observations of these species in brown dwarfs. A similar nonequilibrium treatement is used by Barman et al. (2011a) to model the exoplanet HR8799b. Cooper & Showman (2006) have found that similar departures from CO/CH_4 equilibrium occur in tidally-locked hot-Jupiters.

Zahnle & Marley (2014) have explored the disequilibrium abundances of CH_4/CO and NH_3/N_2 in brown dwarfs and self-luminous giant planets using a chemical kinetic approach. They find that the low gravity of planets strongly discriminates against CH_4, and that in Jupiter mass planets CH_4 becomes more abundant than CO only for temperatures below about 400–600K depending on the effects of vertical mixing. Ammonia is also sensitive to gravity but insensitive to mixing making it a potetnial proxy for gravity.

Chemical models for hot Jupiter atmospheres using a chemical kinetic approach that can include the effects of photochemistry have been explored in a number of studies (e.g. Zahnle et al. 2009; Line, Liang, & Yung 2010; Line et al. 2011; Moses et al. 2011; Venot et al. 2012; Agúndez et al. 2014) (see also review by Moses 2014). There remain some differences between model predictions for species such as CH_4 and NH_3 due to uncertainties in reaction rates and transport parameters (see discussion in Moses 2014 and Agúndez et al. 2014), but generally these models show enhancements of a number of species in the upper atmosphere due to photochemical effects. Most of these models consider C, N and O containing species. The model by Zahnle et al. (2009) includes sulfur species and explores the photochemical production of HS (mercapto) and S_2 as possible absorbers that could contribute to stratospheric heating.

4.3 Spectral line absorption

Absorption lines due to rovibrational and electronic transitions of molecules are the most important features of the spectra of brown dwarfs and planets. Species that are important include H_2O, CO, CH_4, CO_2 and NH_3, metal oxides such

as TiO and VO, metal hydrides including FeH, CrH, MgH, CaH and TiH, and carbon species such as CH, CN, C_2, HCN and C_2H_2 (particularly in carbon rich atmospheres).

Large numbers of vibrational and rotational levels can be excited at the temperatures of a few thousand degrees encountered in ultracool dwarfs and hot Jupiters. This leads to a requirement for large line lists containing many millions of lines such as the BT2 (Barber et al. 2006) computed line list for H_2O.

The spectral line data are used in models to calculate the absorption in each atmospheric layer. This can be done using on-the-fly line-by-line calculations (Allard et al. 2001; Bailey & Kedziora-Chudczer 2012) which has the advantage of being the most accurate and flexible method and resulting in high-resolution model spectra. However it is also the most computationally intensive approach.

A faster approach is to precalcuate opacity tables (Sharp & Burrows 2007; Freedman, Marley, & Lodders 2008) that are then interpolated for the actual models. However, this can lead to inaccuracies if the wavelength bins are made too large. A widely used appoach in Earth atmosphere modelling is the correlated-k (or k-distribution) method (Goody et al. 1989), which allows the use of larger wavelength bins while retaining accuracy. Recently correlated-k techniques have been used in exoplanet retrieval models (Lee, Fletcher, & Irwin 2012) and in hot Jupiter GCMs (Showman et al. 2009).

Sources of spectral line data for the important species have been discussed in detail in a number of recent papers (Sharp & Burrows 2007; Freedman, Marley, & Lodders 2008; Bailey & Kedziora-Chudczer 2012; Tennyson & Yurchenko 2012). These also discuss related continuum absorption processes and the handling of line shapes. The reader is referred to these papers for detailed information, and the discussion here relates only to recent developments.

4.3.1 Carbon dioxide (CO_2)

The Carbon Dioxide Spectroscopic Databank (CDSD Tashkun et al. 2003) previously available in 296 K and 1 000 K versions is now available in a 4 000 K version[4] containing lines to an intensity of 10^{-27} cm molecule^{-1} at 4 000 K for four isotopologues over the range 226–8310 cm^{-1} (628 million lines).

New computed line lists for CO_2 and its isotopologues at 296K and 1 000K (the Ames-296K and Ames-1000K lists) have been described by Huang et al. (2013, 2014).

4.3.2 Ammonia (NH_3)

A computed line list for ammonia at temperatures up to 1 500 K and containing more than 1.1 billion lines for frequencies up to 12 000 cm^{-1} (the BYTe list) is described by Yurchenko, Barber, & Tennyson (2012).

Hargreaves, Li, & Bernath (2011, 2012a) have provided line lists based on laboratory measurements of NH_3 lines at temperatures from 300 °C to 1 400 °C over the wavelength range from 740–4 000 cm^{-1}.

4.3.3 Methane (CH_4)

Methane has been the most problematic of the important species in exoplanet and brown dwarf atmospheres as far as line data is concerned. Significant recent progress has been made with modelling (e.g. Rey, Nikitin, & Tyuterev 2013; Nikitin, Rey, & Tyuterev 2013b; Yurchenko et al. 2013) and a large computed line list for hot methane has very recently been developed (Yurchenko & Tennyson 2014)[5]. Yurchenko et al. (2014) have shown that using this line list it is possible to obtain good model fits to the methane bands in the near infrared spectra of brown dwarfs that could not be fitted with older line lists, such as those based on the Spherical Top Data System software (STDS Wenger & Champion 1998). Another computed line list for hot methane has been reported by Rey, Nikitin, & Tyuterev (2014) but is limited to wavelengths longer than 2 μm.

Much improved line lists for the 1.26–1.71 μm region at temperatures from 80–300 K have been developed recently from extensive laboratory measurements at cryogenic and room temperature (Wang et al. 2012; Campargue et al. 2012a, 2013). These lists, and earlier versions of them, have been used successfully for modelling the spectra of Titan (Bailey, Ahlsved, & Meadows 2011; de Bergh et al. 2012; Campargue et al. 2012b) and Uranus (Irwin et al. 2012; Bott, Kedziora-Chudczer, & Bailey 2013). An improved low temperature line list has also been developed for the 2 μm region (Daumont et al. 2013). These lists have been incorporated into the new 2012 edition of the HITRAN database[6] recently released.

Empirical line lists for methane measured at temperatures from 300–1 400 °C over the wavelength range from 2.0–10.4 μm have been provided by Hargreaves et al. (2012b).

4.3.4 SiO and HCN/HNC

New line lists for SiO (Barton, Yurchenko, & Tennyson 2013) and HCN/HNC (Barber et al. 2014) have recently been published by the ExoMol group.

4.3.5 Collision induced absorptions (CIA)

The collision induced absorption of H_2 - H_2 and H_2 - He pairs are important contributors to the opacity of brown dwarfs and planets. Updated data on these absorptions have recently been provided by Abel et al. (2011, 2012) as described in Saumon et al. (2012). This data as well as other CIA datasets have been recently made available in a new section of the HITRAN database (Richard et al. 2012).

[4] at ftp://ftp.iao.ru/pub

[5] available at http://www.exomol.com/data/molecules/CH4/12C-1H4

[6] www.cfa.harvard.edu/hitran

4.4 Condensates and clouds

Condensed phases (i.e. solids and liquids) begin to condense out of the gas when temperatures drop to around 2 000 K and lower. These condensates can form clouds that can significantly alter the opacity and hence the structure of the atmosphere. Chemical models (Section 4.2) can predict which species will condense (these include oxides, silicates and iron) and the amounts of condensed material produced. However, it is harder to predict what size particles will be produced and whether they will remain in place as clouds or fall under gravitation (precipitation, sedimentation or rain-out).

Lorenz-Mie scattering theory can be used to predict the optical properties of the cloud particles. In the general case these include the extinction coefficient, the single scattering albedo (the fraction of light that is scattered rather than absorbed) and the phase function that describes the angular distribution of scattered light. These are needed as inputs for solving the radiative transfer equation (Equations (4) and (5), Section 4.5).

4.4.1 Clouds in brown dwarfs

Two limiting cases were considered in the COND and DUSTY models of Allard et al. (2001). The COND models include condensate formation, which alters the chemistry by depleting elements from the gas, but did not include any contribution of the condensates to the opacity. In the DUSTY models the condensed material is assumed to remain in place in equilibrium with the gas phase and form clouds of small dust grains. The DUSTY models were found to be a good representation of late-M and early-L dwarfs, but at cooler temperatures they produce weakening of spectral features and increasingly red colours in disagreement with the observations of L-T transition objects.

The cloud-free COND models were found to be a fairly good representation of mid to late T dwarfs, indicating that gravitational settling has largely removed dust from the atmospheres in these cases. However, neither of these two models could account for the late-L to early T dwarfs. A number of cloud models have now been developed that aim to reproduce the behaviour of clouds through the full brown dwarf spectral sequence.

In the Unified Cloudy Model (Tsuji 2002, 2005), clouds are assumed to be restricted to a small range of temperatures between the condensation temperature T_{cond} and a critical temperature T_{cr}. Below the critical temperature it is assumed that grains will grow to such a size that they will rapidly precipitate under gravity. A fixed particle size ($r = 0.01$ μm) is used in the clouds. The critical temperature T_{cr} is an adjustable parameter, with values in the range 1 700–1 900 K providing a reasonable match to the observations.

Burrows, Sudarsky, & Hubeny (2006) describe a cloud model that similarly restricts the cloud extent but includes an exponential decay in cloud particle density at the upper and lower edges of the cloud. They investigate the effects of various cloud parameters and conclude that cloud particle sizes of 50–100 μm fit the data best. This is much larger than the grain sizes used in most other models which are around 1 μm or smaller.

Ackerman & Marley (2001) describe a cloud model based on a balance between turbulent diffusion and sedimentation in horizontally uniform cloud decks. The model involves a scaling factor f_{sed} that describes the efficiency of sedimentation and typically ranges from 1 to 5. Small f_{sed} values produce thicker clouds and match observations of L dwarfs and higher values are found for later type T dwarfs (Stephens et al. 2009).

The BT-Settl models (Allard et al. 2007, 2012) use a cloud treatment based on a model for cloud microphysics from analysis of solar system atmospheres (Rossow 1978) that predicts timescales for condensation, sedimentation and coagulation. These are compared with the turbulent mixing timescale to predict grain densities and sizes.

Woitke & Helling (2003, 2004) and Helling & Woitke (2006) have developed a kinetic (non-equilibrium) model for the nucleation, accretion, gravitational settling and evaporation of dust grains. A version of this cloud model has been integrated with the PHOENIX stellar atmosphere code (Hauschildt & Baron 1999) to provide the DRIFT-PHOENIX models for substellar atmospheres (Helling et al. 2008a).

A more detailed description of some of these different cloud models and a comparison of their predictions in test cases can be found in Helling et al. (2008b).

A specific aim of these models is to explain the changes that occur in brown dwarfs at the L/T transition as discussed in Section 2. Figure 17 shows that the BT-Settl model (and other cloud models make simiar predictions) can explain the general trend seen in the near-IR colour magnitude diagram of a swing from red to blue colours at the L/T transition. The models achieve this mostly because the cloud has a limited extent in temperature, and so for cooler models the clouds drop to layers below the photosphere where the effect on the spectra and colours become small.

However, all current models fail to match the details of the L/T transition. As can be seen in Figure 7 models fail to reproduce the sharpness of the transition as a function of effective temperature. Models also fail to reproduce the J-band brightening (see Section 2.3). The BT-Settl model also predicts J−K colours that continue to get bluer with lower effective temperatures, while observations show fairly constant J−K for mid to late T dwarfs (Figures 7 and 17).

Cloud species that condense at lower temperatures (including Cr, MnS, Na_2S, ZnS and KCl) are considered by Morley et al. (2012), and found to be helpful in explaining the colours and spectra of late-T and Y dwarfs (Leggett et al. 2013).

4.5 Radiative transfer

Atmospheric models can differ significantly in their handling of radiative transfer, particularly in regards to the treatment of scattering. Radiative transfer involves the flow of radiation

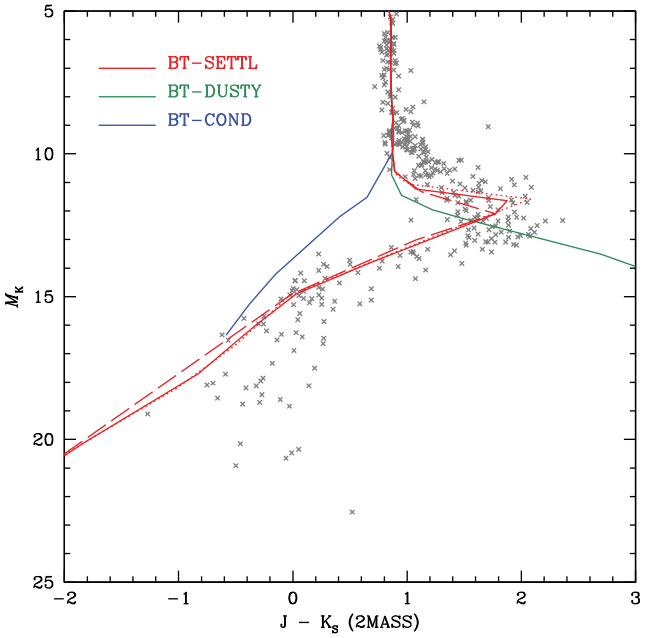

Figure 17. Colour magintude diagram using the same data as Figure 5 compared with the predictions of model atmospheres using different cloud models. The BT-COND and BT-DUSTY models are updated version of the COND and DUSTY models of Allard et al. (2001) with more modern opacities. The BT-SETTL model is described by Allard et al. (2007, 2012). The plotted lines are predicted synthetic magnitudes for the isochromes of Baraffe et al. (2003) and Chabrier et al. (2000a). For BT-SETTL 1, 3 and 5 Gyr isochrones are plotted as dotted, solid and dashed lines. For COND and DUSTY the 3 Gyr isochrone only is plotted.

through an atmosphere as determined by the processes of absorption, emission and scattering. The radiative transfer equation can be written as (Bailey & Kedziora-Chudczer 2012):

$$\mu \frac{dI_\nu(\tau,\mu,\phi)}{d\tau} = I_\nu(\tau,\mu,\phi) - S_\nu(\tau,\mu,\phi) \quad (4)$$

where I_ν is the monochromatic radiance (sometimes referred to as intensity or specific intensity) at frequency ν, and is a function of optical depth τ, and direction μ, ϕ, where μ is the cosine of the zenith angle, and ϕ is the azimuthal angle. The source function S_ν is given by:

$$\begin{aligned} S_\nu(\tau,\mu,\phi) = {} & \frac{\varpi(\tau)}{4\pi}\int_0^{2\pi}\int_{-1}^{1} P(\mu,\phi;\mu',\phi') I_\nu(\tau,\mu',\phi') d\mu' d\phi' \\ & + (1-\varpi) B_\nu(T) \\ & + \frac{\varpi F_\nu}{4\pi} P(\mu,\phi;\mu_0,\phi_0)\exp(-\tau/\mu_0) \end{aligned} \quad (5)$$

where the first term describes scattering of radiation into the beam from other directions according to single scattering albedo ϖ and phase function $P(\mu,\phi;\mu',\phi')$, the second term is thermal emission, with $B_\nu(T)$ being the Plank function and the third term is direct illumination of the atmosphere by an external source with flux $\mu_0 F_\nu$ and direction μ_0, ϕ_0 (e.g. the Sun or host star).

It is the first term in Equation (5) involving the double integral that significantly complicates radiative transfer. This term has the consequence that the radiance in any one direction is dependent on the radiance in all other directions (since any of these can potentially scatter into the line of sight). In general it is then only possible to solve for the full angular dependence of the radiation field in all directions.

To avoid this complication the handling of scattering is often simplified, in some cases by ignoring it entirely, or by using a simplified form for the phase function P such as the assumption of isotropic scattering, and/or a simplified form for the angular depedence of I_ν such as the two-stream approximation or the Eddington approximation. In stellar atmospheres approximate methods can be justified by the fact that scattering is generally of minor importance, and where it does become significant, in the form of Rayleigh scattering from molecules in cool stars, the phase functions are at least forward-backward symmetric.

Where clouds are present, however, the phase functions can be highly non-isotropic, and in the case of Solar system planet atmospheres, radiative transfer methods that more rigorously handle multiple scattering with non-isotropic phase functions are generally used. These include, in particular, versions of the discrete ordinate method originally due to Chandrasekhar (1960) which has been developed into robust and general radiative transfer solving codes such as DISORT (Stamnes et al. 1988), SHDOM (Evans 1998) and LIDORT (Spurr 2001). DISORT is used by Bailey & Kedziora-Chudczer (2012) in the VSTAR code to model brown dwarf spectra. Another appropriate method is the adding-doubling method (de Kok et al. 2011).

At present such methods are rarely used in exoplanet and brown dwarf atmospheric modelling, and this opens up the possibility of errors being introduced due to an oversimplified treatment of scattering. This was investgated by de Kok et al. (2011) for the thermal emission spectra of exoplanets who found that substantial errors can be introduced by neglecting scattering, or by using an isotropic scattering approximation where large particles are present.

4.6 Polarisation

Scattering processes polarise light, so a full treatment of radiative transfer should take account of polarisation. Light scattered from planetary atmospheres is expected to be polarised whereas the light of normal stars is mostly unpolarised (Bailey, Lucas, & Hough 2010), and this polarisation can potentially be used as a means of differentially detecting planets in imaging observations (Schmid et al. 2005; Keller 2006), and as a means of characterising extrasolar planet atmospheres by observing the phase variation of polarisation (Seager, Whitney, & Sasselov 2000; Bailey 2007). Polarisation has also been measured in some brown dwarfs (Ménard, Delfosse, & Monin 2002; Zapatero Osorio, Caballero, & Béjar 2005; Tata et al. 2009) and is thought to result from scattering in the dust clouds combined with either rotational

oblateness or a patchy cloud structure (Sengupta & Marley 2010).

Polarisation is particularly useful for determining the nature and size of cloud particles. A classic application of polarisation was the analysis of the polarisation phase curve of Venus by Hansen & Hovenier (1974) to determine that the clouds of Venus were composed of ∼1 μm radius sulfuric acid droplets.

Polarisation should also, ideally, be included in all radiative transfer modelling involving scattering, because even if we are not interested in observing polarisation, neglecting polarisation can alter the resulting fluxes. Stam & Hovenier (2005) investigated this for reflected light from extrasolar giant planets and found that errors in geometric albedo of up to 9% could arise as a result of neglecting polarisation. In practice, however, polarisation is normally ignored in radiative transfer calculations, because including polarisation would substantially slow down the computations.

Polarisation in Earth-like planet atmospheres will be discussed later in Section 5.4.

5 THE SEARCH FOR HABITABLE PLANETS AND LIFE

The main focus of this review has been on the study of planetary atmospheres for which we have observations, and so far this has been almost entirely giant planets. The only exceptions to this are the super-Earths GJ 1214b and HD 97658b. Transit spectroscopy of GJ 1214b has been obtained (Bean et al. 2010; Crossfield et al. 2011; Berta et al. 2012; Kreidberg et al. 2014a) showing a featureless spectrum indicating an atmosphere either rich in water vapour, or with high altitude clouds. Transit spectroscopy of HD 97658b (Knutson et al. 2014b) also shows a featureless spectrum inconsistent with a cloud-free solar metallicity atmosphere.

In this section the potential for characterisation of Earth-like planets in the habitable zone of their stars is briefly reviewed.

5.1 The habitable zone

The habitable zone is defined as the range of distances from its star at which a planet has suitable conditions for liquid water to be able to exist at its surface. In the absence of an atmosphere the average surface temperature T_{eq} of a planet is given by energy balance between radiation received from its star, and thermal radiation to space as:

$$(1-a)S/4 = \sigma T_{eq}^4 \quad (6)$$

Where S is the total incident flux (W m^{-2}) received from the star (in the case of the Earth this is the solar constant $S_0 = 1\ 361$ W m^{-2}), a is the Bond albedo of the planet and σ is the Stefan-Boltzmann constant. The factor of 4 comes from the fact that radiation received over an area of πr^2 is redistributed over the entire surface of the planet with area $4\pi r^2$. For Earth this calculation gives an equilibrium temperature of $T_{eq} \sim 255$ K currently, and lower in the past as the solar luminosity increases with time and was about 30% less early in the Sun's history (Bahcall, Pinsonnealt, & Basu 2001).

The global average temperature of the Earth is, of course, higher than this at about $T \sim 288$ K, with the difference being due to the operation of the greenhouse effect that traps some of the outgoing radiation and causes the outgoing flux to be less than σT_{eq}^4. In general, from observations of the orbit of a planet we can determine S, but in most cases we won't know the albedo a or the amount of the greenhouse effect, and so can't directly determine the surface temperature of a planet from observations. According to Selsis et al. (2007) T_{eq} must be less than 270 K for a planet to be habitable.

Estimates of the locations of the edges of the habitable zone have been made based on the assumption of an Earth-like planet with a CO_2/H_2O/N_2 atmosphere using cloud-free 1D radiative-convective models. Kasting, Whitmire, & Reynolds (1993) gave the extent of the habitable zone from 0.95 AU to 1.37 AU for our Solar system, with the inner edge being set by the onset of the moist greenhouse process (Kasting 1988) causing loss of water to space, and the outer edge being set by cooling due to the formation of CO_2 clouds. However Forget & Pierrehumbert (1997) showed that CO_2 clouds actually cause warming and allow a more extended habitable zone. An upadated calculation is given by Kopparapu et al. (2013) which sets the moist greenhouse inner edge at 0.99 AU, and the outer edge at 1.67 AU based on the maximum greenhouse criterion. On this basis the Earth is near the inner edge of the habitable zone.

These results can be scaled for other stars according to S/S_0, the flux received by the star as a fraction of the solar constant and the effective temperature of the star. A habitable zone calculator for this purpose based on the results of Kopparapu et al. (2013) is available[7]. The effects of different planet masses on the position of the habitable zone are considered by Kopparapu et al. (2014) who find that the inner edge moves so as to give a wider zone for higher mass planets.

Recent studies using 3D climate models, however, have found the inner edge of the habitable zone at ∼0.95 AU (Leconte et al. 2013) or ∼0.93 AU (Wold & Toon 2014), significantly smaller than the 1D models described above.

The results assume an Earth-like planet and could be different for other types of planets. Abe et al. (2011) have shown that a more extended habitable zone is possible for a desert planet with limited surface water, and Zsom et al. (2013) find a miminum inner edge for the habitable zone of 0.38 AU for hot desert worlds. Pierrehumbert & Gaidos (2011) have suggested that the greenhouse effect due to collision induced absorption in molecular hydrogen could allow habitable conditions to be maintained out to 10 AU from a G-type star.

[7] http://depts.washington.edu/naivpl/content/hz-calculator

Table 9. Low mass planets in or near the habitable zone.

	Star						
Planet	Type	Period T_{eff}	M sin *i* (days)	Radius $M_\oplus$	$R_\oplus$	S/S_0	Reference
τ Cet e	G8.5V	5 344	168.1	4.3		1.60	Tuomi et al. (2012)
HD 40307g	K2.5V	4 956	197.8	7.1		0.62	Tuomi et al. (2013)
HD 88512b	K5V	4 715	58.43	3.6		1.86	Pepe et al. (2011)
GJ 163c	M3.5		25.63	6.8		1.34	Bonfils et al. (2013)
GJ 667C c	M1.5V	3 350	28.14	3.8		0.90	Anglada-Escudé et al. (2012, 2013)
GJ 667C e	M1.5V	3 350	62.24	2.7		0.33	Anglada-Escudé et al. (2013)
GJ 667C f	M1.5V	3 350	39.03	2.7		0.58	Anglada-Escudé et al. (2013)
GJ 832c	M1.5V	3 472	35.68	5.4		0.87	Wittenmyer et al. (2014)
Kapteyn b	M1.0	3 570	48.616	4.8		0.4	Anglada-Escudé et al. (2014)
Kepler-22b	G5V	5 518	289.9		2.38	1.09	Borucki et al. (2012)
Kepler-61b	M0	4 017	59.88		2.15	1.26	Ballard et al. (2013)
Kepler-62e	K2V	4 925	122.4		1.61	1.2 ± 0.2	Borucki et al. (2013)
Kepler-62f	K2V	4 925	267.3		1.41	0.41 ± 0.05	Borucki et al. (2013)
Kepler-69c	G4V	5 638	242.5		1.71	1.91	Barclay et al. (2013); Kane et al. (2013)
Kepler-186f	M1V	3 788	129.9		1.11	$0.32^{+0.06}_{-0.04}$	Quintana et al. (2014)

5.2 Habitable zone planets

Table 9 lists planets that have been reported as being in or near the habitable zone with M sin $i < 10 M_\oplus$ or $R < 2.5 R_\oplus$. Note that the planet of τ Cet is only reported as a tentative detection (Tuomi et al. 2012) and the reality of some of the planets of GJ 667C have been disputed (Gregory 2012; Feroz & Hobson 2014). The reported habitable zone planets of GJ 581 (Mayor et al. 2009; Vogt et al. 2010) have been excluded from the table based on the analysis of Robertson et al. (2014).

Petigura, Howard, & Marcy (2013) have analysed Kepler data to find 10 planet candidates with radii of 1–2 $R_\oplus$ and within a habitable zone defined by $0.25 < S/S_0 < 4$. Allowing for incompleteness they estimate that Earth-size planets in the habitable zone occur in 22 ± 8 % of stars. With the narrower definition of the habitable zone discussed above (0.99–1.67 AU, Kopparapu et al. 2013) this becomes 8.6%.

5.3 Detecting and characterising earth-like planets

The direct detection and characterisation of Earth-like planets is far more challenging than for the giant planets discussed in Section 3. The contrast ratio between an Earth-like planet and its star is $\sim 10^{-10}$ at visible wavelengths and $\sim 10^{-7}$ in the thermal IR ($\sim 10 \mu$m).

One concept is that of an infrared interferometer in space as first suggested by Bracewell (1978). This was developed into the Darwin (Cockell et al. 2009) and Terrestrial Planet Finder Interferometer (TPF-I, Beichman, Woolf, & Lindensmith 1999) mission concepts. These involved several infrared telescopes flying in formation in space and combining their light to achieve nulling interferometry, so that the light of the star could be suppressed, and reveal the light of the planet. These missions would have aimed to both detect planets and obtain low resolution spectroscopy over the 6–20 μm range for atmospheric characterisation and biosignature detection.

An alternative concept was the Terrestrial Planet Finder Coronograph (TPF-C, Traub et al. 2006). This was envisaged as a space telescope with an 8 by 3.5 m elliptical mirror, using advanced coronographic techniques to suppress starlight at the 10^{-10} level. It operated at visible wavelengths and would be able to detect planets and carry out spectroscopic characterisation.

Both Terrestrial Planet Finder missions (TPF-I and TPF-C) have now been cancelled by NASA, and the ESA Darwin mission study ended in 2007.

A further concept for starlight suppression involves the use of an occulter (or starshade) placed in front of the telescope. The occulter must use a petal shaped design to suppress diffraction and be placed about 40 000 km in front of the telescope (Cash 2006). An occulter could be used in conjunction with the James Webb Space Telescope (Soummer 2009) and/or with a dedicated space telescope as in the New Worlds Observer (NWO, Turnbull et al. 2012) mission concept. NWO would use a 4m telescope and enable detection and spectroscopic characterisation of exoplanets with $R \sim 100$ over 0.3–1.6 μm. The mission aims to achieve a 95% probability of detecting and characterising at least one habitable zone Earth-like planet. A more recent starshade mission concept is the Exo-S mission described in Section 6.

Extreme adaptive optics systems on giant ground-based telescopes are another potential approach to the detection and characterisation of Earth-like exoplanets. However, a number of studies have concluded that such systems on currently planned extremely large telescopes fall well short of the required sensitivity (Stapelfeldt et al. 2005; Mountain et al. 2009). However, (Angel 2003) has suggested that detection

with a 20-m ground-based telescope and spectroscopic characterisation with a 100-m telescope should be feasible taking advantage of an Antarctic site.

Kaltenegger & Traub (2009) considered the feasibility of characterising Earth-like planets using transit spectroscopy from a 6.5-m telescope in space (e.g. the JWST). They found that the signal-to-noise values for all important spectral features were of the order of unity or less per transit.

The situation for transit observations is much improved if the Earth-like planet is assumed to be in the habitable zone of an M-dwarf rather than a solar type star. This leads to both a larger transit signal, since the star is smaller, and more frequent transits. Pallé, Zapatero Osorio, & García Muñoz (2011) conclude that detection of atmospheric features in transiting Earth-like planets could be possible in planets orbiting very cool stars or brown dwarfs with the proposed 42-m European Extremely Large Telescope.

Snellen et al. (2013) have suggested the use of high resolution cross correlation techniques (see Section 3.3.2) to detect oxygen absorption during the transit of an Earth-like planet across a red dwarf star. They suggest this should be feasible with a ground-based telescope with an effective aperture of ∼100 m and suggest this could be an array of low-cost 'flux collectors' which would not require high image quality.

5.4 Signatures of habitability

The presence of a planet within the habitable zone does not necessarily mean that it has habitable conditions on its surface. The best signature of habitability would be direct detection of the presence of liquid water. This is difficult to achieve using spectroscopy. While atmospheric water vapour can be detected through absorptions in the near-IR or thermal infrared, the presence of surface liquid water does not provide any clear spectroscopic signature.

A possible indicator of liquid water would be the presence of the 'glint' signal due to specular reflection from oceans. Williams & Gaidos (2008) modelled the light curves and polarisation phase depenence for Earth-like planets and showed that distinctive signals due to glint should be detectable for planets with surface oceans. Robinson, Meadows, & Crisp (2010) used an Earth simulation to show that glint increases the brigthness of the Earth by as much as 100% at crescent phases. Zugger et al. (2010, 2011) modelled glint effects including polarisation and found that the glint signal becomes diluted and more difficult to detect when clouds, aerosols and surface winds are included. Cowan, Abbott, & Voigt (2012a) show, however, that latitude dependent albedo variations produce a signal in the phase curve very similar to that from glint, and therefore the glint signal may not be a reliable indicator of the presence of oceans.

Another potential way of detecting the presence of oceans is to use rotational changes in the brightness and colours (Ford, Seager, & Turner 2001; Kawahara & Fujii 2010). Such observations can in principle determine the fraction of ocean and land coverage and even provide maps of the distribution. These ideas have been tested using observations of the integrated Earth from the EPOXI mission with the Deep Impact spacecraft (Cowan et al. 2009; Fujii et al. 2011; Cowan & Strait 2013). Langford, Wyithe, & Turner (2009) used lunar Earthshine measurements to detect photometric changes associated with the passage of the specular reflection glint spot from land to ocean.

Liquid water clouds in a planet's atmosphere could be detected through the presence of the primary rainbow which would appear as a peak in the phase curve at a phase angle of about 40 degrees. While the rainbow peak could be visible in the phase light curve, it is better defined, particularly for small cloud particles, in the polarisation phase curve (Bailey 2007; Karalidi et al. 2012). The size of the disk integrated rainbow polarisation signal for the Earth has not been measured, but in principle could be obtained from lunar earthshine polarisation measurements. Current data however does not have sufficient phase coverage (Sterzik, Bagnulo, & Palle 2012; Takahashi et al. 2013; Bazzon, Schmidt, & Gisler 2013).

5.5 Biosignatures

The ultimate aim of such studies is to make observations that would test for the presence of life on an exoplanet. A number of potential biosignatures have been suggested (e.g. Des Marais et al. 2002) and tests have been made to determine whether these are actually visible in observations of the integrated Earth using spacecraft (Livengood et al. 2011) or lunar Earthshine measurements (Woolf et al. 2002). Models of the integrated Earth spectrum have been presented by Tinetti et al. (2006) and Robinson et al. (2011).

The most important biosignature is generally considered to be atmospheric oxygen (O_2) or ozone (O_3). Oxygen is produced in the Earth atmosphere primarily by photosynthetic organisms. Possible abiotic sources of atmospheric oxygen that could lead to 'false positivies' have been discussed (Schindler & Kasting 2000; Selsis, Despois, & Parisot 2002; Segura et al. 2007) but such cases appear to be unlikely, or can be excluded on the basis of other observations. Atmospheric O_2 is detectable through a number of electronic absorption bands with the strongest being the A-band at around 760 nm. The longest wavelength O_2 band with significant strength is the a-X band at 1.27 μm. The lack of O_2 bands further into the infrared is a problem for life detection with instruments that work optimally at near-IR wavelengths (e.g. ground-based telescopes with extreme adaptive optics systems that work best at longer wavelenths). However, in the thermal infrared the band of ozone (O_3) at 9.7 μm can be used. This is also considered to be a good biosignature since O_3 is a photolytic by-product of O_2.

Methane (CH_4) is another potential biosignature. On Earth it originates largely from biological processes (methanogenic archaea), but there are also possible abiotic sources such as serpentenisation. The simultaneous presence of both oxygen and methane was suggested to be a good biosignature by Lovelock (1965) indicating chemical disequilibrium.

Methane has strong absorption bands at 7 and 3.3 μm and a series of weaker bands through the near-IR. Segura et al. (2005) have suggested that CH_4 and other reduced biogenic gases such as N_2O and CH_3Cl might be useful as biosignatures in planets around M dwarfs where these gases would have longer photochemical lifetimes than on Earth.

Another possible biosignature is the 'red edge', the sharp edge in the reflectance spectrum from vegetation at around 700-nm. This is a strong signal in light reflected directly from a vegetated area. However, in the integrated Earth, lunar Earthshine observations show a maximum effect of a few per cent (Hamdani et al. 2006; Arnold 2008). Kiang et al. (2007) suggested that spectral signatures could be different for photosynthetic pigments adapted for different stellar types, and Sanromá et al. (2014) investigate the spectra of the Archaean Earth when purple bacteria were widespread giving rise to a slightly longer wavelength signal.

6 THE FUTURE

The characterisation of exoplanet atmospheres has made substantial progress over the last few years and some aspects of their composition and structure are beginning to be resolved. However, there are still many uncertainties and controversies that remain. The major limitation is in the observational data which are, in most cases, extremely limited in spectral resolution and wavelength coverage. Data from space instruments have proved most valuable for studying the transmission and dayside emission spectra of transiting planets, and so the next major advance is likely to be the James Webb Space Telescope due for launch in 2018. Its NIRSpec and MIRI instruments should make possible spectra of transiting planets across the near-IR and mid-IR spectral regions (Shabram et al. 2011; Belu et al. 2011).

Another important mission is TESS (Ricker et al. 2014) that will carry out an all sky survey of bright stars for transiting planets. While it is not directly aimed at atmospheric characterisation, it may well find some of the best targets for more detailed studies. The ESA PLATO mission planned for 2024 launch (Rauer et al. 2013) is another mission that will search for planets transiting bright stars, and will target up to 1 000 000 stars. An exoplanet characterisation mission EChO (Tinetti et al. 2012) was also proposed for the same launch opportunitiy but was not selected.

NASA is currently studying three missions with relevance to exoplanet characterisation. The Wide-Field Infrared Survey Telescope - Astrophysics Focused Telescope Assets (WFIRST-AFTA) concept (Spergel et al. 2013) is a 2.4-m wide field near infrared (0.6–2.0 μm) telescope. It is mainly aimed at wide field surveys, but the design includes a coronograph that enables it do characterisation observations of exoplanets by direct imaging. Exo-C (Stapelfeldt et al. 2014) is a 1.5-m unobscured Cassegrain telescope with a coronograph providing imaging of exoplanets over the wavelength range 450–1 000 nm. Exo-S (Seager et al. 2014) is a 1.1-m telescope using the starshade concept (see Section 5.3) to provide imaging over the 400–1 000 nm range. Exo-S should have the capability to detect Earth-size planets in the habitable zones of about 20 Sun-like stars.

New facilities on ground-based telescopes include improved instruments for direct imaging such as the Gemini Planet Imager (GPI Macintosh et al. 2012) and SPHERE for the VLT (Bezuit et al. 2010). The new generation of extremely large telescopes now under development will open up new possibilities with planned instrument such as EPICS for the 42m E-ELT (Kasper et al. 2010) which will provide imaging, spectroscopy and polarimetry with a systematic contrast of 10^{-9} at 100 mas separation.

PASA, 31, e043 (2014)
doi:10.1017/pasa.2014.38

ACKNOWLEDGEMENTS

This research has benefitted from the M, L, T, and Y dwarf compendium housed at DwarfArchives.org. Use was also made of the L and T dwarf data archive of Sandy Leggett, the IRTF spectral library and the Database of Ultracool parallaxes maintained by Trent Dupuy. I thank Daniel Cotton and Brett Addison for valuable comments on the manuscript.

The work is supported by the Australian Research Council through Discovery grant DP110103167.

References

Abe, Y., Abe-Ouchi, A., Sleep, N. H., & Zahnle, K. 2011, AsBio, 11, 443
Abel, M., Frommhold, L., Li, X., & Hunt, K. L. C. 2011, JPCA, 115, 6805
Abel, M., Frommhold, L., Li, X., & Hunt, K. L. C. 2012, JChPh, 136, 044319
Ackerman, A. S., & Marley, M. S. 2001, ApJ, 556, 872
Agol, E., Cowan, N. B., Knutson, H. A., Deming, D., Steffen, J. H., Henry, G. W., & Charbonneau, D. 2010, ApJ, 721, 1861
Agúndez, M., Parmentier, V., Venot, O., Hersant, F., & Selsis, F. 2014, A&A, 564, A73
Albert, L., Artigau, E., Delorme, P., Reylé, C., Forveille, T., Delfosse, X., & Willott, C. J. 2011, AJ, 141, 203
Allard, F., Hauschildt, P. H., Alexander, D. R., Tamanai, A., & Schweitzer, A. 2001, ApJ, 556, 357
Allard, N. F., Allard, F., Hauschildt, P. H., Kielkopf, J. F., & Machin, L. 2003, A&A, 411, 473
Allard, F., Allard, N. F., Homeier, D., Kielkopf, J., McCaughrean, M. J., & Spiegelman, F. 2007, A&A, 474, L21
Allard, F., Homeier, D., Freytag, B., & Sharp, C. M. 2012, in Low-Mass Stars and the Transition Stars/Brown Dwarfs - Evry Schatzman School on Stellar Physics XXIII, ed. C. Reylé, C. Charbonnel, M. Schultheis, EAS Publications Series, 57, 3
Amundsen, D. S., Baraffe, I., Tremblin, P., Manners, J., Hayek, W., Mayne, N. J., & Acreman, D. M. 2014, A&A, 564, A59
Anderson, D. R., et al. 2011, MNRAS, 416, 2108
Anderson, D. R., et al. 2013, MNRAS, 430, 3422
Andrei, A. H., et al. 2011, AJ, 141, 54
Angel, R. 2003, in Proceedings of the Conference on Towards Other Earths: Darwin/TPF and the Search for Extrasolar Terrestrial Planets, ed. M. Fridlund, & T. Henning, ESA SP-539, 221 (Netherlands: ESA, Noordwijk)

Angerhausen, D., DeLarme, E., Morse, J. A. 2014, submitted to ApJ, arXiv:1404.4348
Anglada-Escudé, G., et al. 2012, ApJL, 751, L16
Anglada-Escudé, G., et al. 2013, A&A, 556, 126
Anglada-Escudé, G., et al. 2014, MNRAS, 443, L89
Arnold, L. 2008, SSRv, 135, 323
Arras, P., & Socrates, A. 2010, ApJ, 714, 1
Artigau, E., Bouchard, S., Doyon, R., & Lafrenière, D. 2009, ApJ, 701, 1534
Bailey, J. 2007, AsBio, 7, 320
Bailey, J. 2009, Icar, 201, 444
Bailey, J., & Kedziora-Chudczer, L. 2012, MNRAS, 419, 1913
Bailey, J., Lucas, P. W., & Hough, J. H. 2010, MNRAS, 405, 2570
Bailey, J., Ahlsved, L., & Meadows, V. S. 2011, Icar, 213, 218
Bahcall, J. N., Pinsonneault, M. H., & Basu, S. 2001, ApJ, 555, 990
Baines, E. K., et al. 2012, ApJ, 761, 57
Ballard, A., et al. 2013, ApJ, 773, 98
Bakos, G., Noyes, R. W., Kovács, G., Stanek, K. Z., Sasselov, D. D., & Domsa, I. 2004, PASP, 116, 266
Banfield, D., Gierasch, P. J., Bell, M., Ustinov, E., Ingersoll, A. P., Vasavada, A. R., West, R. A., & Belton, M. J. S. 1998, Icar, 135, 230
Baraffe, I., Chabrier, G., Allard, F., & Hauschildt, P. 2002, A&A, 382, 563
Baraffe, I., Chabrier, G., Barman, T. S., Allard, F., & Hauschildt, P. H. 2003, A&A, 402, 701
Baraffe, I., Chabrier, G., & Barman, T. 2008, A&A, 482, 315
Baraffe, I., Chabrier, G., & Barman, T. 2010, RPPh, 73, 016901
Barber, R. J., Tennyson, J., Harriss, G. J., & Tolchenov, R. N. 2006, MNRAS, 368, 1087
Barber, R. J., Strange, J. K., Hill, C., Polyansky, O. L., Mellau, G. Ch., Yurchenko, S. N., & Tennyson, J. 2014, MNRAS, 437, 1828
Barclay, T., et al. 2013, ApJ, 768, 101
Barin, I. 1995, Thermochemical Data of Pure Substances (3rd edn; Weinheim: VCH-Verlag)
Barman, T. 2007, ApJ, 661, L191
Barman, T. S., Hauschildt, P. H., & Allard, F. 2001, ApJ, 556, 885
Barman, T. S., Macintosh, B., Konopacky, Q. M., & Marois, C. 2011a, ApJ, 733, 65
Barman, T. S., Macintosh, B., Konopacky, Q. M., & Marois, C. 2011b, ApJL, 7335, L39
Barnes, J. R., et al. 2010, MNRAS, 401, 445
Barton, E. J., Yurchenko, S. N., & Tennyson, J. 2013, MNRAS, 434, 1469
Baskin, N. J., et al. 2013, ApJ, 773, 124
Basri, G., & Brown, M. E. 2006, Ann. Rev. Earth Planet. Sci., 34, 193
Basri, G., Marcy, G. W., & Graham, J. R. 1996, ApJ, 458, 600
Batalha, N. M., et al. 2013, ApJS, 204, 24
Batygin, K., & Stevenson, D. J. 2010, ApJL, 714, L238
Bazzon, A., Schmid, H. M., & Gisler, D. 2013, A&A, 556, A117
Bean, J. L., Miller-Ricci Kempton, E., & Homeier, D. 2010, Nature, 468, 669
Bean, J. L., Désert, J.-M., Seifahrt, A., Madhusudhan, N., Chilingarian, I., Homeier, D., & Szentgyorgyi, A. 2013, ApJ, 771, 108
Becklin, E. E., & Zuckerman, B. 1988, Nature, 336, 656
Beerer, I. M., et al. 2011, ApJ, 727, 23
Beichmann, C. A., Woolf, N. J., & Lindensmith, C. A., The Terrestrial Planet Finder (TPF): A NASA Origins Program to Search for Habitable Planets, JPL publication 99-3 (Pasadena: Jet Propulsion Laboratory)
Belu, A. R., Selsis, F., Morales, J.-C., Ribas, I., Cossou, C., & Rauer, H. 2011, A&A, 525, A83
Benneke, B., & Seager, S. 2012, ApJ, 753, 100
Benneke, B., & Seager, S. 2013, ApJ, 778, 153
Berdyugina, S. V., Berdyugin, A. V., Fluri, D. M., & Piirola, V. 2008, ApJ, 673, L83
Berdyugina, S. V., Berdyugin, A. V., Fluri, D. M., & Piirola, V. 2011, ApJL, 728, L6
Berta, Z. K., et al. 2012, ApJ, 747, 35
Bezuit, J.-L., et al. 2010, in Pathways Towards Habitable Planets, ASP Conf. Series Vol. 430, ed. Coudé, du Foresto, V., Gelino, D. M., & Ribas, I., 231
Birkby, J. L., de Kok, R. J., Brogi, M., de Mooij, E. J. W., Schwarz, H., Albrecht, S., & Snellen, I. A. G. 2013, MNRAS, 436, L35
Blecic, J., et al. 2014, ApJ, 781, 116
Blecic, J., et al. 2013, ApJ, 779, 5
Bochanski, J. J., Burgasser, A. J., Simcoe, R. A., & West, A. A. 2011, ApJ, 142, 169
Boeshaar, P. 1976, PhD thesis, Ohio State University
Boeshaar, P., & Tyson, J. A. 1985, AJ, 90, 817
Bonfils, X., et al. 2013, A&A, 556, A110
Borucki, W. J., et al. 2012, ApJ, 745, 120
Borucki, W. J., et al. 2013, Science, 340, 587
Borysow, A. 2002, A&A, 390, 779
Bott, K., Kedziora-Chudczer, L., & Bailey, J. 2013, in Proc. 12th Australian Space Science Conference, ed. W. Short & I. Cairns (Sydney: National Space Society of Australia, Sydney), 41
Bowler, B. P., Liu, M. C., Dupuy, T. J., & Cushing, M. C. 2010, ApJ, 723, 850
Boss, A., Basri, G., Kumar, S. S., Liebert, J., Martin, E. L., Reipurth, B., & Zinnecker, H. 2003, in Brown Dwarfs, IAU Symp., Vol. 211, ed. E. Martín, 529
Bracewell, R. N. 1978, Nature, 274, 780
Brogi, M., Snellen, I. A. G., de Kok, R. J., Albrecht, S., Birkby, J., & de Mooij, E. J. W. 2012, Nature, 486, 502
Brogi, M., Snellen, I. A. G., de Kok, R. J., Albrecht, S., Birkby, J. L., & de Mooij, E. J. W. 2013, ApJ, 767, 27
Brogi, M., de Kok, R. J., Birkby, J. L., Schwarz, H., Snellen, I. A. G. 2014, A&A, 565, A124
Buchwitz, M., et al. 2005, ACP, 5, 3313
Buenzli, E., & Schmid, H. M. 2009, A&A, 504, 259
Buenzli, E., et al. 2012, ApJL, 760, L31
Burgasser, A. J., et al. 2002, ApJ, 564, 421
Burgasser, A. J., Kirkpatrick, J. D., Liebert, J., & Burrows, A. 2003, ApJ, 594, 510
Burgasser, A., McElwain, M. W., Kirkpatrick, J. D., Cruz, K. L., Tinney, C. G., & Reid, I. N. 2004, AJ, 127, 2856
Burgasser, A. J., Geballe, T. R., Leggett, S. K., Kirkpatrick, J. D., & Golimowski, D. A. 2006, ApJ, 637, 1067
Burgasser, A. J., Kirkpatrick, J. D., Cruz, K. L., Reid, I. N., Leggett, S. K., Liebert, J., Burrows, A., & Brown, M. E. 2006b, ApJS, 166, 585
Burgasser, A. J., Sheppard, S. S., & Luhman, K. L. 2013, ApJ, 772, 129
Burningham, B., et al. 2008, MNRAS, 391, 320
Burningham, B., et al. 2010, MNRAS, 406, 1885
Burningham, B., et al. 2013, MNRAS, 433, 457

Burrows, A., & Sharp, C. M. 1999, ApJ, 512, 843
Burrows, A., & Volobuyev, M. 2003, ApJ, 583, 985
Burrows, A., et al. 1997, ApJ 491, 856
Burrows, A., Hubbard, W. B., Lunine, J. I., & Liebert, J. 2001, RvMP, 73, 719
Burrows, A., Sudarsky, D., & Hubeny, I. 2003, ApJ, 588, 1121
Burrows, A., Sudarsky, D., & Lunine, J. I. 2003, ApJ, 596, 587
Burrows, A., Sudarsky, D., & Hubeny, I. 2006, ApJ, 640, 1063
Burrows, A., Hubeny, I., Budaj, J., & Hubbard, W. B. 2007a, ApJ, 661, 502
Burrows, A., Hubeny, I., Budaj, J., Knutson, H. A., & Charbonneau, D. 2007b, ApJL, 668, L171
Burton, J. R., Watson, C. A., Littlefair, S. P., Dhillon, V. S., Gibson, N. P., Marsh, T. R., & Pollacco, D. 2012, ApJS, 201, 36
Cáceres, C., et al. 2011, A&A, 530, A5
Campargue, A., Leshchishina, O., Wang, L., Mondelain, D., Kassi, S., & Nikitin, A.V. 2012a, JQSRT, 113, 1855
Campargue, A., et al. 2012b, Icar, 219, 110
Campargue, A., Leshchishina, O., Wang, L., Mondelain, D., & Kassi, S. 2013, JMoSp, 291, 16
Campo, C. J., et al. 2011, ApJ, 727, 125
Cannon, A. J., & Pickering, E. C. 1901, Ann. Astron. Obs. Harvard Coll., 28(II), 131
Carpenter, J. M. 2001, AJ, 121, 2851
Cash, W. 2006, Nature, 442, 51
Castelli, F., & Kurucz, R. L. 2004, arXiv:astro-ph/0405087
Chabrier, G., & Baraffe, I. 1997, A&A, 327, 1039
Chabrier, G., Baraffe, I., Allard, F., & Hauschildt, P. H. 2000a, ApJ, 542, 464
Chabrier, G., Baraffe, I., Allard, F., & Hauschildt, P. 2000b, ApJ, 542, L119
Chandrasekhar, S. 1960, Radiative Transfer (New York: Dover)
Charbonneau, D., Noyes, R. W., Korzennik, S. G., Nisenson, P., Jha, S., Vogt, S. S., & Kilbrick, R. I. 1999, ApJ, 522, L145
Charbonneau, D., Brown, T. M., Noyes, R. W., & Gilliland, R. L. 2002, ApJ, 568, 377
Charbonneau, D., et al. 2005, ApJ, 626, 523
Charbonneau, D., Knutson, H. A., Barman, T., Allen, L. A., Mayor, M., Megeath, S. T., Queloz, D., & Udry, S. 2008, ApJ, 686, 1341
Charbonneau, D., et al. 2009, Nature, 462, 891
Chase, M.W. 1998, J. Phys. Cham. Ref. Data Mongraph No 9, NIST-JANAF Thermochemical Tables. American Chemical Society. Am. Inst. Phys., Woodbury
Chauvin, G., Lagrange, A.-M., Dumas, C., Zuckerman, B., Mouillet, D., Song, I., Beuzit, J.-L., & Lawrence, P. 2005, A&A, 438, L25
Chen, G., van Boekel, R., Madhusudhan, N., Wang, H., Nikolov, N., Seeman, U., & Henning, T. 2014a, A&A, 564, A6
Chen, G., van Boekel, R., Wang, H., Nikolov, N., Seemann, U., & Henning, Th. 2014b, A&A, 567, A8
Chilcote, J., et al. 2014, submitted to ApJL, arXiv:1407.4469
Christiansen, J. L., et al. 2010, ApJ, 710, 97
Clarke, F. J., Tinney, C. G., & Covey, K. R. 2002, MNRAS, 332, 361
Clarke, F. J., Hodgkin, S. T., Oppenheimer, B. R., Robertson, J., & Haubois, X. 2008, MNRAS, 386, 2009
Cockell, C. S., et al. 2009, AsBio, 9, 1
Collier Cameron, A., Horne, K., Penny, A., & James, D. 1999, Nature, 402, 751
Collier Cameron, A., Horne, K., Penny, A., & Leigh, C. 2002, MNRAS 330, 187
Cooper, C. S., & Showman, A. P. 2005, ApJ, 629, L45
Cooper, C. S., & Showman, A. P. 2006, ApJ, 649, 1048
Cotton, D. V., Bailey, J., Crisp, D., & Meadows, V. S. 2012, Icar, 217, 570
Cowan, N. B., Agol, E., & Charbonneau, D. 2007, MNRAS, 379, 641
Cowan, N. B., et al. 2009, ApJ, 700, 915
Cowan, N. B., Abbot, D. S., & Voigt, A. 2012a, ApJL, 752, L3
Cowan, N. B., Machalek, P., Croll, B., Shekhtman, L. M., Burrows, A., Deming, D., Greene, T., & Hora, J. L. 2012b, ApJ, 747, 82
Cowan, N. B., & Strait, T. E. 2013, ApJL, 765, L17
Croll, B., Jayawardhana, R., Fortney, J. J., Lafrenière, D., & Loic, A. 2010a, ApJ, 718, 920
Croll, B., Loic, A., Lafreniere, D., Jayawardhanan, R., & Fortney, J. J. 2010b, ApJ, 717, 1084
Croll, B., Lafreniere, D., Loic, A., Jayawardhana, R., Fortney, J., & Murray, N. 2011, AJ, 141, 30
Crossfield, I. J. M., Hansen, B. M. S., Harrington, J., Cho, J. Y.-K., Deming, D., Menou, K., & Seager, S. 2010, ApJ, 723, 1436
Crossfield, I. J. M., Barman, T., & Hansen, B. M. S. 2011, ApJ, 736, 132
Crossfield, I. J. M., Barman, T., Hansen, B. M. S., Ichi, T., & Kodama, T. 2012b, ApJ, 760, 140
Crossfield, I. J. M., Knutson, H., Fortney, J., Showman, A. P., Cowan, N. B., & Deming, D. 2012a, ApJ, 752, 81
Crossfield, I. J. M., Hansen, B. M. S., & Barman, T. 2012c, ApJ, 746, 46
Crossfield, I. J. M., Barman, T., Hansen, B. M. B., & Howard, A. W. 2013, A&A, 559, A33
Crossfield, I. J. M., et al. 2014, Nature, 505, 654
Crouzet, N., McCullough, P. R., Burke, C., & Long, D. 2012, ApJ, 761, 7
Crouzet, N., McCullough, P. R., Deming, D., & Madhusudhan, N. 2014, ApJ, in press, arXiv:1409.4000
Cubillas, P., et al. 2013, ApJ, 768, 42
Cushing, M. C., Rayner, J. T., & Vacca, W. D. 2005, ApJ, 623, 1115
Cushing, M. C., et al. 2011, ApJ, 743, 50
Dahn, C. C., et al. 2002, AJ, 124, 1170
Daumont, L., et al. 2013, JQSRT, 116, 101
de Bergh, C., et al. 2012, P&SS, 61, 85
de Kok, R. J., Helling, Ch., Stam, D. M., Woitke, P., & Witte, S. 2011, A&A, 531, A67
de Kok, R. J., Brogi, M., Snellen, I. A. G., Birkby, J., Albrecht, S., & de Mooij, E. W. J. 2013, A&A, 554, 82
de Mooij, E. J. W., & Snellen, I. A. G. 2009, A&A, 493, L35
de Mooij, E. J. W., de Kok, R. J., Nefs, S. V., & Snellen, I. A. G. 2011, A&A, 528, A49
de Mooij, E. J. W., Brogi, M., de Kok, R. J., Snellen, I. A. G., Kenworthy, M., & Karjaleinen, R. 2012, A&A, 550, A54
de Wit, J., Gillon, M., Demory, B.-O., & Seager, S. 2012, A&A, 548, A128
Delfosse, X., et al. 1997, A&A, 327, 25
Delorme, P., et al. 2008a, A&A, 484, 469
Delorme, P., et al. 2008b, A&A, 482, 961
Delorme, P., et al. 2012, A&A, 548, A26
Deleuil, M., et al. 2014, A&A, 564, A56

Deming, D., Seager, S., Richardson, L. J., & Harrington, J. 2005, Nature, 434, 740
Deming, D., Harrington, J., Seager, S., & Richardson, J. L. 2006, ApJ, 644, 560
Deming, D., Harrington, J., Laughlin, G., Seager, S., Navarro, S. B., Bowman, W. C., & Horning, K. 2007, ApJ, 667, L199
Deming, D., et al. 2011, ApJ, 726, 95
Deming, D., et al. 2012, ApJ, 754, 106
Deming, D., et al. 2013, ApJ, 774, 95
Demory, B.-O., & Seager, S. 2011, ApJS, 197, 12
Demory, B.-O., et al. 2011, ApJL, 735, L12
Demory, B.-O., et al. 2013, ApJL, 776, L25
Des Marais, D. J., et al. 2002, AsBio, 2, 153
Désert, J.-M., et al. 2011a, ApJS, 197, 11
Désert, J.-M., et al. 2011b, ApJS, 197, 14
Dobbs-Dixon, I., & Lin, D. N. C. 2008, ApJ, 673, 513
Dobbs-Dixon, I., & Agol, E. 2013, MNRAS, 435, 3159
Dupuy, T. J., & Liu, M. C. 2012, ApJS, 201, 19
Dupuy, T. J., & Kraus, A. L. 2013, Science, 341, 1492
Ehrenreich, D., et al. 2014, A&A, in press, arXiv:1405.1056
Esteves, L. J., de Mooij, E. J. W., & Jayawardhana, R. 2013, ApJ, 772, 51
Evans, K. F. 1998, JAtS, 55, 429
Evans, T. M., et al. 2013, ApJL, 772, L16
Fan, X. et al. 2000, AJ, 119, 928
Feroz, F., & Hobson, M. 2014, MNRAS, 437, 3540
Flasar, F. M., et al. 2005, Science, 307, 1247
Flectcher, L. N., Baines, K. H., Momary, T. W., Showman, A. P., Irwin, P. G. J., Orton, G. S., Roos-Serote, M., & Merlet, C. 2011, Icar, 214, 510
Freedman, R. S., Marley, M. S., & Lodders, K. 2008, ApJS, 174, 504
Fressin, F., Knutson, H. A., Charbonneau, D., O'Donovan, F. T., Burrows, A., Deming, D., Mandushev, G., & Spiegel, D. 2010, ApJ, 711, 374
Fressin, F., et al. 2013, ApJ, 766, 81
Ford, E. B., Seager, S., & Turner, E. L. 2001, Nature, 412, 885
Forget, F., & Pierrehumber, R. T. 1997, Science, 278, 1273
Fortney, J. J., Lodders, K., Marley, M. S., & Freedman, R. S. 2008, ApJ, 678, 1419
Fortney, J. J., et al. 2011, ApJS, 197, 9
Fossati, L., et al. 2010, ApJL, 714, L222
Fujii, Y., Kawahara, H., Yasushi, S., Fukuda, S., Nakajima, T., Livengood, T. A., & Turner, E. L. 2011, ApJ, 738, 184
Garnier, A., Pelon, J., Dubuisson, P. Faivre, M., Chomette, O., Pascal, N., & Kratz, D. P. 2012, JAMS, 51, 1407
Geballe, T. R., Saumon, D., Leggett, S. K., Knapp, G. R., Marley, M. S., & Lodders, K. 2001, ApJ, 556, 373
Geballe, T. R., et al. 2002, ApJ, 564, 466
Gibson, N. P., et al. 2010, MNRAS, 404, L114
Gibson, N. P., Pont, F., & Aigrain, S. 2011, MNRAS, 411, 2199
Gibson, N. P., et al. 2012, MNRAS, 422, 753
Gibson, N. P., Aigrain, S., Barstow, J. K., Evans, T. M., Fletcher, L. N., & Irwin, P. G. J. 2013a, MNRAS, 436, 2974
Gibson, N. P., Aigrain, S., Barstow, J. K., Evans, T. M., Fletcher, L. N., & Irwin, P. G. J. 2013b, MNRAS, 428, 3680
Gillon, M., et al. 2009, A&A, 506, 359
Gillon, M., et al. 2010, A&A, 511, A3
Gillon, M., Triaud, A. H. M. J., Jehin, E., Delrez, L., Opitom, C., Magain, P., Lendl, M., & Queloz, D. 2013, A&A, 555, L5
Golimowski, D. A., et al. 2004, ApJ, 127, 3516
Goody, R., West, R., Chen, L., & Crisp, D. 1989, JQSRT, 42, 539
Gray, D. F. 2005, The Observation and Analysis of Stellar Photospheres (3rd edn; Cambridge: Cambridge University Press)
Greathouse, T. K., Richter, M., Lacy, J., Moses, J., Orton, G., Encrenaz, T., Hammel, H. B., & Jaffe, D. 2011, Icar, 214, 606
Gregory, P. C. 2012, MNRAS, 415, 2523
Grevesse, N., Asplund, M., & Sauval, A. J. 2007, SSRv, 130, 15
Grillmair, C. J., et al. 2008, Nature, 457, 767
Guillot, T., & Showman, A. P. 2002, A&A, 385, 156
Gustaffson, B., Edvardsson, B., Eriksson, K., Jørgensen, U. G., Nordlund, A., & Plez, B. 2008, A&A, 486, 951
Hamdani, S., et al. 2006, A&A, 460, 617
Hansen, J. E., & Hovenier, J. W. 1974, JAtS, 31, 1137
Hargreaves, R. J., Hinkle, K. H., Bauschlicher, C. W., Wende, S., Seifahrt, A., & Bernath, P. F. 2010, AJ, 140, 919
Hargreaves, R. J., Li, G., & Bernath, P. F. 2011, ApJ, 735, 111
Hargreaves, R. J., Li, G., & Bernath, P. F. 2012a, JQSRT, 113, 670
Hargreaves, R. J., Beale, C. A., Michaux, L., Irfan, M., & Bernath, P. F. 2012b, ApJ, 757, 46
Hauschildt, P. H., & Baron, E. 1999, JCoAM, 109, 41
Hawley, S. L., et al. 2002, AJ, 123, 3049
Hayashi, C., & Nakano, T. 1963, PThPh, 30, 460
Heinze, A. N., et al. 2013, ApJ, 767, 173
Helling, Ch., & Woitke, P. 2006, A&A, 455, 325
Helling, Ch., Dehn, M., Woitke, P., & Hauschildt, P. H. 2008a, ApJL, 675, L105
Helling, Ch., et al. 2008b, MNRAS, 391, 1854
Heng, K., Frierson, D. M. W., & Phillips, P. J. 2011, MNRAS, 418, 2669
Henyey, L., Vardya, M. S., & Bodenheimer, P. 1965, ApJ, 142, 841
Hesman, B. E., et al. 2009, Icar, 202, 249
Hilico, J. C., Robert, O., Loete, M., Tuomi, S., Pine, A. S., & Brown, L. R. 2001, JMoSp, 208, 1
Hough, J. H., Lucas, P. W., Bailey, J. A., Tamura, M., Hirst, E., Harrison, D., & Bartholomew-Biggs, M. 2006, PASP, 118, 1302
Howard, A. W., et al. 2010, Science, 330, 653
Howard, A. W., et al. 2012, ApJS, 201, 15
Huang, X., Gamache, R. R., Freedman, R. S., Schwenke, D. W., & Lee, T. J. 2013, JQSRT, 130, 134
Huang, X., Freedman, R. S., Tashkun, S. A., Schwenke, D. W., & Lee, T. J. 2014, JQSRT, 147, 134
Hubeny, I., Burrows, A., & Sudarsky, D. 2003, ApJ, 594, 1011
Huitson, C. M., Sing, D. K., Vidal-Madjar, A., Ballester, G. E., Lecavelier des Etangs, A., Désert, J.-M., & Pont, F. 2012, MNRAS, 422, 2477
Huitson, C. M., et al. 2013, MNRAS, 434, 3252
Ibgui, L., Burrows, A., & Spiegel, D. S. 2010, ApJ, 713, 751
Irwin, P. G. J., Teanby, N. A., & Davis, G. R. 2010, Icar, 208, 913
Irwin, P. G. J., et al. 2012, Icar, 220, 369
Jackson, B., Greenberg, R., & Barnes, R. 2008, ApJ, 681, 1631
Janson, M., et al. 2013, ApJL, 778, L4
Jensen, A. G., Redfield, S., Endl, M., Cochran, W. D., Koesterke, L., & Barman, T. S. 2011, ApJ, 743, 203
Jensen, A. G., Redfield, S., Endl, M., Cochran, W. D., Koesterke, L., & Barman, T. S. 2012, ApJ, 751, 86
Jordán, A., et al. 2013, ApJ, 778, 184
Kaltenegger, L., & Traub, W. A. 2009, ApJ, 698, 519
Kane, S. R., Barclay, T., & Gelino, D. M. 2013, ApJL, 770, L20
Karalidi, T., Stam, D. M., & Hovenier, J. W. 2012, A&A, 548, A90

Kasper, M., et al. 2010, in Ground-based and Airborne Instrumentation for Astronomy III, Proc. SPIE, Vol. 7735, ed. I. S. McLean, S. K. Ramsay, & H. Takami, 77352E
Kasting, J. F. 1988, Icar, 74, 472
Kasting, J. F., Whitmire, D. P., & Reynolds, R. T. 1993, Icar, 101, 108
Kawahara, H., & Fujii, Y. 2010, ApJ, 720, 1333
Kedziora-Chudczer, L., & Bailey, J. 2011, MNRAS, 414, 1483
Keller, C. U. 2006, in Ground-based and Airborne Instrumentation for Astronomy, SPIE Proc. Vol. 6269, ed. I. S. MClean, & M. Iye (Bellingham: SPIE), 26
Kemp, J. C., Henson, G. D., Steiner, C. T., & Powell, E. R. 1987, Nature, 326, 270
Kiang, N. Y., et al. 2007, AsBio, 7, 252
Kipping, D., & Bakos, G. 2011, ApJ, 730, 50
Kipping, D., & Spiegel, D. S. 2011, MNRAS, 417, L88
Kirkpatrick, J. D., Henry, T. J., & McCarthy, D. W. 1991, ApJS, 77, 417
Kirkpatrick, J. D., et al. 1999, ApJ, 519, 802
Kirkpatrick, J. D., et al. 2000, AJ, 120, 447
Kirkpatrick, J. D., et al. 2010, ApJS, 190, 100
Kirkpatrick, J. D., et al. 2011, ApJS, 197, 19
Kirkpatrick, J. D., et al. 2012, ApJ, 753, 156
Kniazev, A. Y., et al. 2013, ApJ, 770, 124
Knutson, H. A., et al. 2007a, Nature, 447, 183
Knutson, H. A., Charbonneau, D., Noyes, R. W., Brown, T. M., & Gilliland, R. L. 2007b, ApJ, 655, 564
Knutson, H. A., Charbonneau, D., Allen, L. E., Burrows, A., & Megeath, S. T. 2008, ApJ, 673, 526
Knutson, H. A., Charbonneau, D., Burrows, A., O'Donovan, F. T., & Mandushev, G. 2009a, ApJ, 691, 866
Knutson, H. A., et al. 2009b, ApJ, 690, 822
Knutson, H. A., Charbonneau, D., Cowan, N. B., Fortney, J. J., Showman, A. P., Agol, E., & Henry, G. W. 2009c, ApJ, 703, 769
Knutson, H. A., Howard, A. W., & Isaacson, H. 2010, ApJ, 720, 1569
Knutson, H. A., et al. 2012, ApJ, 754, 22
Knutson, H. A., Benneke, B., Deming, D., & Homeier, D. 2014a, Nature, 505, 66
Knutson, H. A., et al. 2014b, submitted to ApJ, arXiv:1403.4602
Koen, C. 2006, MNRAS, 367, 1735
Konopacky, Q. M., Barman, T. S., Macintosh, B. A., & Marois, C. 2013, Sci, 339, 1398
Kopparapu, R. K., et al. 2013, ApJ, 765, 131
Kopparapu, R. K., Ramirez, R. M., SchottelKotte, J., Kasting, J. F., Domagal-Goldman, S., & Eymet, V. 2014, ApJ, 787, L29
Kreidberg, L., et al. 2014a, Nature, 505, 69
Kreidberg, L., et al. 2014b, ApJ, 793, L27
Kumar, S. S. 1963, ApJ, 137, 1121
Kurucz, R. 1970, SAO Special Report 309, Atlas: a Computer Program for Calculating Model Stellar Atmospheres (Cambridge, MA: Smithsonian Astrophysical Observatory)
Kurucz, R. 1993, PhST, T47, 110
Kuzuhara, M., et al. 2013, ApJ, 774, 11
Lane, C., et al. 2007, ApJ, 668, L163
Langford, S. V., Wyithe, J. S. B., & Turner, E. L. 2009, AsBio, 9, 305
Langford, S. V., Wyithe, J. S. B., Turner, E. L., Jenkins, E. B., Narita, N., Liu, X., Suto, Y., & Toru, Y. 2011, MNRAS, 415, 673
Lecavelier des Etangs, A., et al. 2010, A&A, 514, A72
Leconte, J., Forget, F., Charnay, B., Wordsworth, R., & Pottier, A. 2013, Nature, 504, 268
Lee, J.-M., Fletcher, L. N., & Irwin, P. G. J. 2012, MNRAS, 420, 170
Lendl, M., Gillon, M., Queloz, D., Alonso, R., Fumel, A., Jehin, E., & Naef, D. 2013, A&A, 552, 11
Leggett, S. K. 1992, ApJS, 82, 351
Leggett, S. K., et al. 2000, ApJ, 536, 35
Leggett, S. K., Allard, F., Geballe, T. R., Hauschildt, P. H., & Schweitzer, A. 2001, ApJ, 548, 908
Leggett, S. K., et al. 2002, ApJ, 564, 452
Leggett, S. K., Saumon, D., Marley, M. S., Geballe, T. R., Golimowski, D. A., Stephens, D., & Fan, X. 2007, ApJ, 655, 1079
Leggett, S. K., et al. 2010, ApJ, 710, 1627
Leggett, S. K., et al. 2011, in Astronomical Society of the Pacific Conference Series, 16th Cambridge Workshop on Cool Stars, Stellar Systems and the Sun, Vol. 448, ed. C. Johns-Krull, 913
Leggett, S. K., Morley, C. V., Marley, M. S., Saumon, D., Fortney, J. J., & Visscher, C. 2013, ApJ, 763, 130
Leigh, C., Collier Cameron, A., Horne, K., Penny, A., & James, D. 2003a, MNRAS, 344, 1271
Leigh, C., Collier Cameron, A., Udry, S., Donati, J.-F., Horne, K., James, D., & Penny, A. 2003b, MNRAS, 346, L16
Lindal, G. F. 1992, AJ, 103, 967
Line, M. R., Liang, M. C., & Yung, Y. 2010, ApJ, 717, 496
Line, M. R., Vasischt, G., Chen, P., Angerhausen, D., & Yung, Y. 2011, ApJ, 738, 32
Line, M. R., Zhang, X., Vasischt, G., Natraj, V., Chen, P., & Yung, Y. 2012, ApJ, 749, 93
Line, M. R., Knutson, H., Deming, D., Wilkins, A., & Desert, J.-M. 2013a, ApJ, 778, 183
Line, M. R., et al. 2013b, ApJ, 775, 137
Linsky, J. L., Yang, H., France, K., Froning, C. S., Green, J. C., Stocke, J. T., & Osterman, S. N. 2010, ApJ, 717, 1291
Liou, K. N. 2002, An Introduction to Atmospheric Radiation (Sab Diego: Academic Press)
Liu, M. C., Leggett, S. K., Golimowski, D. A., Chiu, K., Fan, X., Geballe, T. R., Schneider, D. P., & Brinkmann, J. 2006, ApJ, 647, 1393
Livengood, T. A., et al. 2011, AsBio, 11, 907
Lockwood, A. C., Johnson, J. A., Bender, C. F., Carr, J. S., Barman, T., Richert, A. J. W., & Blake, G. A. 2014, ApJL, 783, L29
Lodders, K. 2002, ApJ, 577, 974
Lodders, K., & Fegley, B. 1994, Icar, 112, 368
Lodders, K., & Fegley, B. 2002, Icar, 155, 393
Looper, D. L., Gelino, C. R., Burgasser, A. J., & Kirkpatrick, J. D. 2008, ApJ, 685, 1183
López-Morales, M., Coughlin, J. L., Sing, D. K., Burrows, A., Apai, D., Rogers, J. C., Spiegel, D. S., & Adams, E. R. 2010, ApJL, 716, L36
Lovelock, J. E. 1965, Nature, 207, 568
Lucas, P. W., & Roche, P. F. 2000, MNRAS, 314, 858
Lucas, P. W., Hough, J. H., Bailey, J. A., Tamura, M., Hirst, E., & Harrison, D. 2009, MNRAS, 393, 229
Lucas, P. W., et al. 2010, MNRAS, 408, L56
Luhman, K. L. 2013, ApJL, 767, L1
Luhman, K. L. 2014, ApJL, 768, L18
Luhman, K. L., Burgasser, A. J., & Bochanski, J. J. 2011, ApJL, 730, L9

Luhman, K. L., Burgasser, A. J., Labbé, I., Saumon, D., Marley, M. S., Bochanski, J. J., Monson, A. J., & Pearson, S. E. 2012, ApJ, 744, 135
Mace, G. N., et al. 2013, ApJS, 205, 6
Machalek, P., McCullough, P. R., Burke, C. J., Valenti, J. A., Burrows, A., & Hora, J. L. 2008, ApJ, 684, 1427
Machalek, P., McCullough, P. R., Burrows, A., Burke, C. J., Hora, J. L., & Johns-Crull, C. M. 2009, ApJ, 701, 514
Machalek, P., Greene, T., McCullough, P. R., Burrows, A., Burke, C. J., Hora, J. L., Johns-Krull, C. M., & Deming, D. 2010, ApJ, 711, 111
Macintosh, B. A., et al. 2012, in Ground-based and Airborne Instrumentation for Astronomy IV, Proc. SPIE, Vol. 8446, ed. I. S. McLean, S. K. Ramsay, & H. Takami, 84461U
Madhusudhan, N., & Seager, S. 2009, ApJ, 707, 24
Madhusudhan, N., & Seager, S. 2010, ApJ, 725, 261
Madhusudhan, N., et al. 2011, Nature, 469, 64
Madhusudhan, N. 2012, ApJ, 758, 36
Majeau, C., Agol, E., & Cowan, N. B. 2012, ApJL, 747, L20
Mandell, A. M., Deming, L. D., Blake, G. A., Knutson, H. A., Mumma, M. J., Villanueva, G. L., & Salyk, C. 2011, ApJ, 728, 18
Mandell, A. M., Haynes, K., Sinukoff, E., Madhusudhan, N., Burrows, A., & Deming, D. 2013, ApJ, 779, 128
Mahtani, D. P., et al. 2013, MNRAS, 432, 693
Marcy, G. W., Butler, R. P., Williams, E., Bildsten, L., Graham, J. R., Ghez, A. M., & Jernigan, J. G. 1997, ApJ, 481, 926
Marley, M. S., Seager, S., Saumon, D., Lodders, K., Ackerman, A. S., Freedman, R. S., & Fan, X. 2002, ApJ, 568, 335
Marley, M. S., Saumon, D., & Goldblatt, C. 2010, ApJL, 723, L117
Marsh, K. A., Wright, E. L., Kirkpatrick, J. D., Gelino, C. R., Cushing, M., Griffith, R. L., Skrutskie, M. F., & Eisenhardt, P. R. 2013, ApJ, 762, 119
Marois, C., Macintosh, B., Barman, T., Zuckerman, B., Song, I., Patience, J., Lafreniere, D., & Doyon, R. 2008, Sci, 322, 1348
Marois, C., Zuckerman, B., Konopacky, Q. M., Macintosh, B., & Barman, T. 2010, Nature, 468, 1080
Martín, E. L., Delfosse, X., & Guieu, S. 2004, AJ, 127, 449
Maxted, P. F. L., et al. 2013, MNRAS, 428, 2645
Mayne, N. J., et al. 2014, A&A, 561, A1
Mayor, M., & Queloz, D. 1995, Nature, 378, 355
Mayor, M., et al. 2009, A&A, 507, 487
McCullough, P., Crouzet, N., Deming, D., & Madhusudhan, N. 2014, ApJ, 791, 55
Ménard, F., Delfosse, X., & Monin, J.-L. 2002, A&A, 396, L35
Menou, K., & Rauscher, E. 2009, ApJ, 700, 887
Miller, N., & Fortney, J. J. 2011, ApJL, 736, L29
Mohanty, S., Jayawardhana, R., Huélamo, N., & Mamajek, E. 2007, ApJ, 657, 1064
Morley, C. V., Fortney, J. J., Marley, M. S., Channon, V., Saumon, D., & Leggett, S. K. 2012, ApJ, 756, 172
Moro-Martín, A., Reike, G. H., & Su, K. Y. L. 2010, ApJL, 721, L199
Morton, T. D., & Johnson, J. A. 2011, ApJ, 738, 170
Moses, J. I., et al. 2011, ApJ, 737, 15
Moses, J. I. 2014, PTRSL, 372, 20130073
Mountain, M., et al. 2009, Astro2010: the Astronomy and Astrophysics Decadal Survey, Technology Development Papers, no. 12
Moya, A., Amado, P. J., Barrado, D., García Hernández, A., Aberasturi, M., Montesinos, B., & Aceituno, F. 2010, MNRAS, 405, L81
Murgas, F., Pall'e, E., Zapatero Osorio, M. R., Nortmann, L., Hoyer, S., & Cabrera-Lavers, A. 2014, A&A, 563, A41
Nakajima, T., Oppenheimer, B. R., Kulkarni, S. R., Golinowski, D. A., Matthews, K., & Durrance, S. T. 1995, Nature, 378, 463
Nakajima, T., Tsuji, T., & Yanagisawa, K. 2004, ApJ, 607, 499
Nikitin, A., Boudon, V., Wenger, C., Albert, S., Brown, L., Baurecker, S., & Quack, M. 2013a, PCCP, 15, 10071
Nikitin, A. V., Rey, M., & Tyuterev, V. G. 2013b, CPL, 565, 5
Nikolov, N., et al. 2014, MNRAS, 437, 46
Noll, K. S., Geballe, T. R., Leggett, S. K., & Marley, M. S. 2000, ApJL, 541, L75
Nyemeyer, S., et al. 2011, ApJ, 742, 35
O'Donovan, F. T., Charbonneau, D., Harrington, J., Madhusudhan, N., Seager, S., Deming, D., & Knutson, H. A. 2010, ApJ, 710, 1551
O'Rourke, J. G., et al. 2014, ApJ, 781, 109
Oppenheimer, B. R., Kulkarni, S. R., Matthews, K., & Nakajima, T. 1995, Sci, 270, 1478
Oppenheimer, B. R., et al. 2013, ApJ, 768, 24
Owen, T., Mahaffy, P., Niemann, H. B., Atreya, S., Donahue, T., Bar-Nun, A., & de Pater, I. 1999, Nature, 402, 269
Pallé, E., Zapatero Osorio, M. R., García Muñoz, A. 2011, ApJ, 728, 19
Patience, J., King, R. R., de Rosa, R. J., & Marois, C. 2010, A&A, 517, A76
Patten, B. M., et al. 2006, ApJ, 651, 502
Perna, R., Menou, K., & Rauscher, E. 2010, ApJ, 724, 313
Pepe, F., et al. 2011, A&A, 534, A58
Petigura, E. A., Howard, A. W., & Marcy, G. W. 2013, PNAS, 110, 19273
Pierrehumbert, R., & Gaidos, E. 2011, ApJL, 734, L13
Pinfield, D. J., et al. 2008, MNRAS, 390, 304
Pollacco, D. L., et al. 2006, PASP, 118, 1407
Pont, F., Knutson, H., Gilliland, R. L., Moutou, C., & Charbonneau, D. 2008, MNRAS, 385, 109
Pont, F., Sing, D. K., Gibson, N. P., Aigrain, S., Henry, G., & Husnoo, N. 2013, MNRAS, 432, 2917
Quintana, E. V., et al. 2013, ApJ, 767, 137
Quintana, E. V., et al. 2014, Sci, 344, 277
Radigan, J., Jayawardhana, R., Lafreniere, D., Artigau, E., Marley, M., & Saumon, D. 2012, ApJ, 750, 105
Rajpurohit, A. S., Reylé, C., Allard, F., Homeier, D., Schultheis, M., Bessell, M. S., & Robin, A. C. 2013, A&A, 556, A15
Ranjan, S., Charbonneau, D., Désert, J.-M., Madhusudhan, N., Deming, D., Wilkins, A., & Mandell, A. V. 2014, 785, 148
Rauer, H., et al. 2013, submitted to ExA, arXiv:1310.0696
Rauscher, E., & Menou, K. 2012, ApJ, 750, 96
Rauscher, E., & Menou, K. 2013, ApJ, 764, 103
Rayner, J. T., Cushing, M. C., & Vacca, W. D. 2009, ApJS, 185, 289
Rebolo, R., Martín, E. L., & Magazzu, A. 1992, ApJ, 389, L83
Rebolo, R., Zapatero-Osorio, M. R., & Martin, E. L. 1995, Nature, 377, 129
Rebolo, R., Martín, E. L., Basri, G., Marcy, G. W., & Zapatero-Osorio, M. R. 1996, ApJ, 469, L53
Redfield, S., Endl, M., Cochran, W. D., & Koesterke, L. 2008, ApJL, 673, L87

Reid, I. N., Burgasser, A. J., Cruz, K. L., Kirkpatrick, J. D., & Gizis, J. E. 2001, AJ, 121, 1710
Rey, M., Nikitin, A. V., & Tyuterev, V. G. 2013, JMoSp, 291, 85
Rey, M., Nikitin, A. V., & Tyuterev, V. G. 2014, ApJ, 789, 2
Richard, C., et al. 2012, JQSRT, 113, 1276
Richardson, L. J., Deming, D., Horning, K., Seager, S., & Harrington, J. 2007, Nature, 445, 892
Ricker, G. R., et al. 2014, submitted to Proc. SPIE, arXiv:1406.0151
Robertson, P., Mahadevan, S., Endl, M., Roy, A. 2014, Sci, 345, 440
Robie, R. A., & Hemingway, B. S. 1995, UGSB, 2131
Robinson, T. D., Meadows, V. S., & Crisp, D. 2010, ApJL, 721, L67
Robinson, T. D., et al. 2011, AsBio, 11, 393
Rodler, F., Kurster, M., & Henning, T. 2008, A&A, 485, 859
Rodler, F., Kurster, M., & Henning, T. 2010, A&A, 514, A23
Rodler, F., Lopez-Morales, M., & Ribas, I. 2012, ApJL, 753, L25
Rodler, F., Kürster, M., & Barnes, J. R. 2013, MNRAS, 432, 1980
Rogers, J. C., Apai, D., López-Morales, M., Sing, D. K., & Burrows, A. 2009, ApJ, 707, 1707
Rogers, T. M., & Showman, A. P. 2014, ApJL, 782, L4
Rossow, W. 1978, Icar, 36, 1
Rostron, J. W., et al. 2014, MNRAS, 441, 36666
Rowe, J. F., et al. 2008, ApJ, 689, 1345
Rosenkranz, P. W. 2001, ITGRS, 39, 2429
Ruiz, M. T., Leggett, S. K., & Allard, F. 1997, ApJ, 491, 107
Sanromá, E., Pallé, E., Parenteau, M. N., Kiang, N. Y., Gutiérrez-Navarro, A. M., López, R., & Montañés-Rodríguez, P. 2014, ApJ, 780, 52
Santerne, A., Bonomo, A. S., Hébrard, G., Deleuil, M., Moutou, C., Almenara, J.-M., Bouchy, F., & Díaz, R. F. 2011, A&A, 536, A70
Saumon, D., Marley, M. S., Lodders, K., & Freedman, R. S. 2003, in Brown Dwarfs, Proc. IAU Symp. vol. 211, ed. E. Martín, 345
Saumon, D., & Marley, M. S. 2008, ApJ, 689, 1327
Saumon, D., Hubbard, W. B., Burrows, A., Guillot, T., Lunine, J. I., & Chabrier, G. 1996, ApJ, 460, 993
Saumon, D., Marley, M. S., Abel, M., Frommhold, L., & Freedman, R. S. 2012, 750, 74
Schindler, T. L., & Kasting, J. F. 2000, Icar, 145, 262
Schlawin, E., Zhao, M., Teske, J. K., Herter, T. 2014, ApJ, 783, 5
Schmid, H. M., et al. 2005, in Direct Imaging of Exoplanets: Science and Techniques, IAU Coll. Vol. 200, ed. C. Aime & F. Vakili (Cambridge: Cambridge University Press), 165
Schneider, J., Dedieu, C., Le Sidaner, P., Savalle, R., & Zolotukhin, I. 2011, A&A, 532, A79
Schweitzer, A., Gizis, J. E., Hauschildt, P. H., Allard, F., Howard, E. M., & Kirkpatrick, J. D. 2002, ApJ, 566, 435
Seager, S., Whitney, B. A., & Sasselov, D. D. 2000, ApJ, 540, 504
Seager, S., et al. 2014, Exo-S Science and Technology Development Team Interim Report (Pasadena: Jet Propulsion Laboratory)
Segura, A., et al. 2005, AsBio, 5, 706
Segura, A., Meadows, V. S., Kasting, J. F., Crisp, D., & Cohen, M. 2007, A&A, 472, 665
Seiff, A., et al. 1998, JGR, 103, E10, 22857
Selsis, F., Despois, D., & Parisot, J.-P. 2002, A&A, 388, 985
Selsis, F., Kasting, J. F., Levrard, B., Paillet, J., Ribas, I., & Delfosse, X. 2007, A&A, 476, 1373
Sengupta, S., & Marley, M. S. 2010, ApJL, 722, L142
Shabram, M., Fortney, J. J., Greene, T. P., & Freedman, R. S. 2011, ApJ, 727, 65
Sharp, C. M., & Huebner, W. F. 1990, ApJ, 72, 417
Sharp, C. M., & Burrows, A. 2007, ApJS, 168, 140
Showman, A. P., & Guillot, T. 2002, A&A, 385, 166
Showman, A. P., & Polvani, L. M. 2011, ApJ, 738, 71
Showman, A. P., Fortney, J. J., Lian, Y., Marley, M. S., Freedman, R. S., Knutson, H. A., & Charbonneau, D. 2009, ApJ, 699, 564
Showman, A. P., Cho, J. Y.-K., & Menou, K. 2010, in Exoplanets, ed. S. Seager (University Arizona Press), 471
Showman, A. P., & Kaspi, Y. 2013, ApJ, 776, 85
Shporer, A., et al. 2014, ApJ, 788, 92
Simons, D. A., & Tokunaga, A. 2002, PASP, 114, 169
Sing, D. K., Vidal-Madjar, A., Désert, J. M., Lecavelier des Etangs, A., & Ballester, G. 2008, ApJ, 686, 658
Sing, D. K., Désert, J.-M., Lecavelier des Etangs, A., Ballester, G. E., Vidal-Madjar, A., Parmentier, V., Hebrard, G., & Henry, G. W. 2009, A&A, 505, 891
Sing, D. K., et al. 2011a, MNRAS, 416, 1443
Sing, D. K., et al. 2011b, A&A, 527, A73
Sing, D. K., et al. 2012, MNRAS, 426, 1663
Sing, D. K., et al. 2013, MNRAS, 436, 2956
Skemer, A., et al. 2014, ApJ, 792, 17
Smith, A. M. S., Anderson, D. R., Skillen, I., Collier-Cameron, A., & Smalley, B. 2011, MNRAS, 416, 2096
Smith, A. M. S., et al. 2012, A&A, 545, 93
Snellen, I. A. G., de Mooij, E. J. W., & Albrecht, S. 2007, Nature, 459, 543
Snellen, I. A. G., Albrecht, S., de Mooij, E. J. W., & Le Poole, R. S. 2008, ApJ, 487, 357
Snellen, I. A. G., de Mooij, E. J. W., & Albrecht, S. 2009, Nature, 459, 543
Snellen, I. A. G., de Kok, R. J., de Mooij, E. J. W., & Albrecht, S. 2010a, Nature, 465, 1049
Snellen, I. A. G., de Mooij, E. J. W., & Burrows, A. 2010b, A&A, 513, A76
Snellen, I., de Kok, R., Le Poole, R., Brogi, M., & Birkby, J. 2013, ApJ, 764, 182
Snellen, I., Brandl, B. R., de Kok, R. J., Brogi, M., Birkby, J., & Schwarz, H. 2014, Nature, 509, 63
Sorahana, S., & Yamamura, I. 2012, ApJ, 760, 151
Soter, S. 2006, AJ, 132, 2513
Soummer, R., et al. 2009, in Techniques and Instrumentation for Detection of Exoplanets IV, Proc. SPIE Vol. 7440, ed. S. B. Shaklan, 74400A
Spergel, D., et al. 2013, WFIRST-AFTA Science Definition Team Final Report, IPAC, Pasadena
Spurr, R. J. D. 2001, JQSRT, 68, 689
Stam, D. M., & Hovenier, J. W. 2005, A&A, 444, 275
Stamnes, K., Tsay, S. C., Wiscombe, W., & Jayaweera, K. 1988, ApOpt, 27, 2502
Stapelfeldt, K. R. 2005, in Scientific Requirements for Extremely Large Telescopes, ed. P. Whitelock, M. Dennefeld, & B. Leibundgut, IAU Symp., No 232, 149
Stapelfeldt, K. 2014, Exo-C Science and Technology Definition Team Interim Report (Pasadena: Jet Propulsion Laboratory)
Stephens, D. C., & Leggett, S. K. 2004, PASP, 116, 9
Stephens, D. C., et al. 2009, ApJ, 702, 154
Sterzik, M. F., Bagnulo, S., & Palle, E. 2012, Nature, 483, 64
Stevenson, K. B., et al. 2010, Nature, 464, 1161
Stevenson, K. B., et al. 2012, ApJ, 754, 136

Stevenson, K. B., et al. 2014, AJ, 147, 161
Sudarsky, D., Burrows, A., & Pinto, P. 2000, ApJ, 538, 885
Swain, M. R., Vasisht, G., & Tinetti, G. 2008, Nature, 452, 329
Swain, M. R., Vasischt, G., Tinetti, G., Bouwman, J., Chen, P., Yung, Y., Deming, D., & Deroo, P. 2009a, ApJL, 690, L114
Swain, M. R., et al. 2009, ApJ, 704, 1616
Swain, M. R., et al. 2010, Nature, 463, 637
Swain, M. R., et al. 2013, Icar, 225, 432
Sudol, J. J., & Haghighipour, N. 2012, ApJ, 755, 38
Takahashi, J., Itoh, Y., Akitaya, H., Okazaki, A., Kawabata, K., Oasa, Y., & Isogai, M. 2013, PASJ, 65, 38
Tarter, J. 1975, PhD thesis, California University, Berkeley
Tashkun, S. A., Perevalov, V. I., Teffo, J. -L., Bykov, A. D., & Lavrentieva, N. N. 2003, JQSRT, 82, 165
Tata, R., Martín, E. L., Sengupta, S., Phan-Bao, N., Zapatero Osorio, M. R., & Bouy, H. 2009, 508, 1423
Tennyson, J., & Yurchenko, S. N. 2012, MNRAS, 425, 21
Tinetti, G., Meadows, V. S., Crisp, D., Fong, W., Fishbein, E., Turnbull, M., & Bibring, J.-P. 2006, AsBio, 6, 34
Tinetti, G., et al. 2010, ApJL, 712, L139
Tinetti, G., et al. 2012, ExA, 34, 311
Tinney, C. G., Burgasser, A. J., & Kirkpatrick, J. D. 2005, AJ, 126, 975
Tinney, C. G., Faherty, J. K., Kirkpatrick, J. D., Wright, E. L., Gelino, C. R., Cushing, M. C., Griffith, R. L., & Salter, G. 2012, ApJ, 759, 60
Todorov, K. O., Deming, D., Harrington, J., Stevenson, K. B., Bowman, W. C., Nymeyer, S., Fortney, J. J., & Bakos, G. A. 2010, ApJ, 708, 498
Todorov, K. O., et al. 2012, ApJ, 746, 111
Todorov, K. O., et al. 2013, ApJ, 770, 102
Traub, W. A., et al. 2006, in Advances in Stellar Interferometry, Proc. SPIE, Vol. 6268, ed. J. D. Monnier, M. Scholler, & W. C. Danchi, 62680T
Tsuji, T. 1973, A&A, 23, 411
Tsuji, T. 2002, ApJ, 575, 264
Tsuji, T. 2005, ApJ, 621, 1033
Tsuji, T., & Nakajima, T. 2003, ApJ, 585, L151
Tsuji, T., Yamamura, I., & Sorahana, S. 2011, ApJ, 734, 73
Tsuji, T., Ohnaka, K., Aoki, W., & Nakajima, T. 1996, A&A, 308, L29
Tuomi, M., et al. 2012, A&A, 551, A79
Tuomi, M., et al. 2013, A&A, 549, A48
Turnbull, M. C., et al. 2012, PASP, 124, 418
Venot, O., Hébrard, E., Agúndez, M., Dobrijevic, M., Selsis, F, Hersant, F, Iro, N., Bounaceur, R. 2012, A&A, 546, A43
Vidal-Madjar, A., Lecavelier des Etangs, A., Désert, J.-M., Ballester, G. E., Ferlet, R., Hébrard, G., & Mayor, M. 2003, Nature, 422, 143
Vidal-Madjar, A., et al. 2004, ApJL, 604, L69
Vogt, S. S., Butler, R. P., Rivera, E. J., Haghighipour, N., Henry, G. W., & Williamson, M. H. 2010, ApJ, 723, 954
Vrba, F. J., et al. 2004, ApJ 127, 2948
Wakeford, H. R., et al. 2013, MNRAS, 435, 3481
Waldmann, I. P., Tinetti, G., Drossart, P., Swain, M. R., Deroo, P., & Griffith, C. A. 2012, ApJ, 744, 35
Wang, L., Mondelain, D., Kassi, S., & Campargue, A. 2012, JQSRT, 113, 47
Wang, W., van Boekel, R., Madhusudhan, N., Chen, G., Zhao, G., & Henning, Th. 2013, ApJ, 770, 70
Warren, S. J., et al. 2007, MNRAS, 381, 1400
Weiss, L. M., et al. 2013, ApJ, 768, 14
Welsh, W. F., et al. 2010, ApJL, 713, L145
Wenger, C., & Champion, J. P. 1998, JQSRT, 59, 471
Wiktorowicz, S. J. 2009, ApJ, 696, 1116
Wiktorowicz, S. J., & Matthews, K. 2008, PASP, 120, 1282
Wilkins, A., Deming, D., Madhusushan, N., Burrows, A., Knutson, H., McCullough, P., & Ranjan, S. 2014, ApJ, 783, 113
Williams, D. M., & Gaidos, E. 2008, Icar, 195, 927
Williams, P. K. G., Charbonneau, D., Cooper, C. S., Showman, A. P., & Fortney, J. J. 2006, ApJ, 649, 1020
Wittenmyer, R. A., Tinney, C. G., Butler, R. P., O'Toole, S. J., Jones, H. R. A., Carter, B. D., Bailey, J., & Horner, J. 2011, ApJ, 738, 81
Wittenmyer, R. A., et al. 2014, ApJ, 791, 114
Woitke, P., & Helling, Ch. 2003, A&A, 399, 297
Woitke, P., & Helling, Ch. 2004, A&A, 414, 335
Wolf, E. T., & Toon, O. B. 2014, GeoRL, 41, 167
Wong, M. H., Mahaffy, P. R., Atreya, S. K., Niemann, H. B., & Owen, T. C. 2004, Icar, 171, 153
Wood, P. L., Maxted, P. F. L., Smalley, B., & Iro, N. 2011, MNRAS, 412, 2376
Woolf, N. J., Smith, P. S., Traub, W. A., & Jucks, K. W. 2002, ApJ, 574, 430
Wright, E. L., et al. 2010, AJ, 140, 1868
Wright, J. T., & Gaudi, B. S. 2013, in Planets, Stars and Stellar Systems, Solar and Stellar Planetary Systems, Vol. 3, ed. T. D. Oswalt, L. M. French, & P. Kalas, (Dordrecht: Springer), 489
Yamamura, I., Tsuji, T., & Tanabé, T. 2010, ApJ, 722, 682
Yurchenko, S. N., Barber, R. J., & Tennyson, J. 2012, MNRAS, 413, 1828
Yurchenko, S. N., Tennyson, J., Barber, R. J., & Thiel, W. 2013, JMoSp, 291, 69
Yurchenko, S. N., & Tennyson, J. 2014, MNRAS, 440, 1649
Yurchenko, S. N., Tennyson, J., Bailey, J., Hollis, M. D. J., Tinnetti, G. 2014, PNAS, 111, 9379
Zahnle, K., Marley, M. S., Freedman, R., Lodders, K., & Fortney, J. J. 2009, ApJL, 701, L20
Zahnle, K., & Marley, M. S. 2014, submitted to ApJ, arXiv:1408.6283
Zapatero Osorio, M. R., Caballero, J. A., & Béjar, V. J. S. 2005, ApJ, 621, 445
Zellem, R. T., et al. 2014, ApJ, 790, 53
Zhang, X., & Showman, A. P. 2014, ApJL, 788, L6
Zhao, M., Monnier, J. D., Swain, M. R., Barman, T., & Hinkley, S. 2012a, ApJ, 744, 122
Zhao, M., Milburn, J., Barman, T., Hinkley, S., Swain, M. R., Wright, J., & Monnier, J. D. 2012b, ApJL, 748, L8
Zhou, G., & Bayliss, D. R. 2012, ApJ, 426, 2483
Zhou, G., Kedziora-Chuczer, L., Bayliss, D. R., & Bailey, J. 2013, ApJ, 774, 9
Zhou, G., Bayliss, D. D. R., Kedziora-Chudczer, L., Salter, G., Tinney, C. G., & Bailey, J. 2014, MNRAS, in press, arXiv:1409.2775
Zsom, A., Seager, S., de Wit, J., & Stamenković, V. 2013, ApJ, 778, 109
Zugger, M. E., Kasting, J. F., Williams, D. M., Kane, T. J., & Philbrick, C. R. 2010, ApJ, 723, 1168
Zugger, M. E., Kasting, J. F., Williams, D. M., Kane, T. J., & Philbrick, C. R. 2011, ApJ, 739, 12